CANADIAN THESES
ON MICROFICHE

21008

THÈSES CANADIENNES
SUR MICROFICHE

AUTHOR/AUTEUR

FALK, M.V.

TITLE/TITRE

VIBRATIONAL SPECTRA OF SEVERAL
ISOTOPIC FORMS OF DIMETHYL ...

21008

NATIONAL LIBRARY
OTTAWA

BIBLIOTHÈQUE NATIONALE
OTTAWA

NAME OF AUTHOR... MICHAEL VICTOR FALK

TITLE OF THESIS... VIBRATIONAL SPECTRA OF SEVERAL ISOTOPIC FORMS OF ETHER-- HYDROGEN CHLORIDE AND ETHYLENE-SULPHIDE

UNIVERSITY.... UNIVERSITY OF ALBERTA

DEGREE FOR WHICH THESIS WAS PRESENTED.... Ph. D

YEAR THIS DEGREE GRANTED...... 1974

Permission is hereby granted to THE NATIONAL LIBRARY OF CANADA to microfilm this thesis and to lend or sell copies of the film.

The author reserves other publication rights, and neither the thesis nor extensive extracts from it may be printed or otherwise reproduced without the author's written permission.

(Signed)... MV Falk

PERMANENT ADDRESS:

#402-11007-83 AVE
EDMONTON, ALTA

DATED... Jan. 31 1974

NL-91 (10-68)

THE UNIVERSITY OF ALBERTA

VIBRATIONAL SPECTRA OF SEVERAL ISOTOPIC FORMS OF DIMETHYL ETHER--HYDROGEN CHLORIDE AND ETHYLENE SULPHIDE

by

© MICHAEL VICTOR FALK

A THESIS

SUBMITTED TO THE FACULTY OF GRADUATE STUDIES AND RESEARCH

IN PARTIAL FULFILMENT OF THE REQUIREMENTS FOR THE DEGREE

OF

DOCTOR OF PHILOSOPHY

DEPARTMENT OF CHEMISTRY

EDMONTON, ALBERTA

SPRING, 1974

THE UNIVERSITY OF ALBERTA

FACULTY OF GRADUATE STUDIES AND RESEARCH

The undersigned certify that they have read, and recommend to the Faculty of Graduate Studies and Research, for acceptance, a thesis entitled

"VIBRATIONAL SPECTRA OF SEVERAL ISOTOPIC FORMS OF DIMETHYL ETHER...HYDROGEN CHLORIDE AND ETHYLENE SULPHIDE"

submitted by MICHAEL VICTOR FALK in partial fulfilment of the requirements for the degree of Doctor of Philosophy.

....
Supervisor

....

Robert K. Brown
....

....

B. Kratochvil
....

Peter J. Krueger
....
External Examiner

January 17, 1974
....
Date

ABSTRACT

Infrared spectra of the gaseous, hydrogen-bonded molecule formed from dimethyl ether and hydrogen chloride, $(CH_3)_2O$---HCl, and its isotopic modifications $(CH_3)_2O$---DCl, $(CD_3)_2O$---HCl and $(CD_3)_2O$---DCl, have been studied in detail between 33 and 4000 cm^{-1}. The hydrogen bond stretching mode is assigned between 110 and 120 cm^{-1} for $(CH_3)_2O$---HCl, $(CH_3)_2O$---DCl and $(CD_3)_2O$---HCl. The two O---HCl deformation modes yield a broad, complex absorption centered at 470 cm^{-1}. It is interpreted in terms of sum and difference transitions involving the HCl wagging modes, which are deduced to be at 50 cm^{-1}. The O---DCl deformation modes yield a band centered at 360 cm^{-1}. Bands at 790 cm^{-1} and 600 cm^{-1} in the spectra of $(CH_3)_2O$---HCl and $(CD_3)_2O$---DCl are assigned to the overtones of the deformation modes. Many of the ethereal modes of $(CH_3)_2O$---HCl and $(CD_3)_2O$---HCl are assigned between 800 and 1500 cm^{-1}. The shape of the band assigned to the symmetric C-O stretching mode of $(CH_3)_2O$---HCl does not resemble band shapes calculated for this absorption using two possible geometries of the molecule and does not, therefore, indicate which geometry is correct. The effect of sample temperature on the shape of the band due to the HCl stretching mode indicates that the fundamental transition is at 2480 cm^{-1}, not at 2574 cm^{-1} as previously postulated. The band due to the DCl stretching

mode of $(CH_3)_2O$---DCl has a different shape to that of $(CD_3)_2O$---DCl. The differences are attributed to combination transitions involving the ethereal modes. It is suggested that combination transitions involving the DCl or HCl stretching modes and the DCl or HCl wagging modes cause shoulders 50 cm^{-1} away from the peak due to the DCl stretching mode and contribute to the general diffuseness of the band due to the HCl stretching mode. The relative intensities of all of the bands due to $(CH_3)_2O$---HCl are presented.

Infrared and Raman spectra of ethylene sulphide-h_4 and ethylene sulphide-d_4 and infrared spectra of cis and trans 1,2-dideuterioethylene sulphide have been recorded in this laboratory by D. A. Othen and are assigned in this work. Thirty-six frequencies from these spectra are assigned to fundamental vibrations and these frequencies are used in normal coordinate calculations. A force field containing sixteen force constants reproduces the thirty-six observed frequencies with an average error of 0.41%. The calculated frequencies allow many of the unassigned experimental frequencies to be assigned. The normal modes of each isotopic molecule are described in terms of the intramolecular displacements determined from the eigenvectors and potential energy distributions. Most of the methylenic modes of the dideuterated molecules cannot be described simply. The A_2 methylenic rock is calculated to be of a higher frequency than the A_2 methylenic twist for both ethylene sulphide-h_4 and ethylene sulphide-d_4.

PREFACE

This thesis deals with the vibrational spectra of two unrelated molecular systems. In the first three chapters, the infrared spectra of several isotopic forms of the hydrogen-bonded molecule dimethyl ether---hydrogen chloride are presented and discussed. In Chapter 4, the normal vibrations of four isotopic forms of ethylene sulphide are analyzed.

ACKNOWLEDGEMENTS

I wish to express my deepest gratitude to Dr. J. E. Bertie for the privilege of working under his direction and for his guidance and encouragement during the course of this work.

I also wish to express my appreciation to the other members of this department with whom I have discussed parts of this work and to the members of the machine shop, glass shops and electronics shop who constructed and maintained much of the equipment used in this research.

I also wish to express thanks to Dr. O. P. Strausz and members of his research group for supplying and purifying the various isotopic forms of ethylene sulphide and to Dr. D. A. Othen for recording the spectra of these molecules.

Financial support by the National Research Council of Canada and the University of Alberta is gratefully acknowledged.

TABLE OF CONTENTS

Page

CHAPTER 1

INTRODUCTION 1

1.1 General Introduction 1

1.2 Hydrogen Bonding. 1

1.3 The Infrared Spectra of Hydrogen-Bonded Molecules 5

1.4 Theories of Intensity Enhancement . . . 14

1.5 Theories of Band Broadening 17

1.6 Infrared Spectra of Gaseous Hydrogen-Bonded Molecules 27

1.7 Aims of this Work 32

CHAPTER 2

EXPERIMENTAL TECHNIQUES 34

2.1 Preparation and Purification of Chemicals 34

2.2 Vacuum Lines and the Infrared Cell. . . 35

2.3 Infrared Spectrophotometers 40

CHAPTER 3

RESULTS AND DISCUSSION 44

3.1 General 44

3.2 Far Infrared Region 46

3.3 Infrared Spectra Between 200 and 800 cm^{-1}. 53

3.4 Infrared Spectra Between 800 and 1500 cm^{-1}. 71

Page

3.5 Infrared Spectra Above 1500 cm^{-1} 84

3.6 Relative Intensities of the Bands . . . 99

3.7 Summary 102

CHAPTER 4

VIBRATIONAL ASSIGNMENT AND NORMAL COORDINATE CALCULATIONS FOR FOUR ISOTOPIC MODIFICATIONS OF ETHYLENE SULPHIDE 103

4.1 General Introduction 103

4.2 Structure, Symmetry and Vibrational Coordinates of Ethylene Sulphide . . . 104

4.3 Previous Studies of the Vibrations of Ethylene Sulphide 119

4.4 The Assignment of the Spectra of C_2H_4S, C_2D_4S, cis-$C_2D_2H_2S$ and trans-$C_2D_2H_2S$ 124

4.5 Computer Programs and the $\underset{\sim}{G}$ and $\underset{\sim}{F}$ Matrices 140

4.6 Development of the Force Field 144

4.7 Discussion 156

REFERENCES 169

APPENDIX I $\underset{\sim}{G}$ MATRICES 179

APPENDIX II EIGENVECTORS AND POTENTIAL ENERGY DISTRIBUTIONS 183

APPENDIX III POTENTIAL ENERGY DISTRIBUTIONS AMONG THE DIAGONAL ELEMENTS OF THE $\underset{\sim}{F}_s$ MATRICES. 191

APPENDIX IV INFRARED SPECTRA OF GASEOUS C_2D_4S, cis-$C_2D_2H_2S$ AND trans-$C_2D_2H_2S$ 196

LIST OF TABLES

Table		Page
1	Frequencies and Assignments of Absorption Between 800 and 1500 cm^{-1} by $(CH_3)_2O$---HCl, $(CD_3)_2O$---HCl and the Free Ethers	77
2	Frequencies and Relative Intensities of the Absorption Bands of $(CH_3)_2O$---HCl	100
3	Molecular Parameters of Ethylene Sulphide	107
4	Rotational Constants of Four Isotopic Forms of Ethylene Sulphide	108
5	Internal Coordinates for Ethylene Sulphide	110
6	Symmetry Coordinates for C_2H_4S and C_2D_4S	112
7	Symmetry Coordinates for cis-$C_2D_2H_2S$	114
8	Symmetry Coordinates for trans-$C_2D_2H_2S$	116
9	Previous Assignments of the Fundamental Frequencies of Liquid C_2H_4S	121
10	Previous Assignments of the Fundamental Frequencies of Gaseous C_2H_4S	122
11	Frequencies and Assignment of Features Observed in the Infrared and Raman Spectra of C_2H_4S	126
12	Frequencies and Assignment of Features Observed in the Infrared and Raman Spectra of C_2D_4S	127

Table		Page
13	Frequencies and Assignment of Features Observed in the Infrared Spectrum of Gaseous cis-$C_2D_2H_2S$	128
14	Frequencies and Assignment of Features Observed in the Infrared Spectrum of Gaseous trans-$C_2D_2H_2S$	129
15	Various Force Fields of Ethylene Sulphide	145
16	Observed Frequencies and Those Calculated from the Various Force Fields for C_2H_4S	146
17	Observed Frequencies and Those Calculated from the Various Force Fields for C_2D_4S	148
18	Observed Frequencies and Those Calculated from the Various Force Fields for cis-$C_2D_2H_2S$	151
19	Observed Frequencies and Those Calculated from the Various Force Fields for trans-$C_2D_2H_2S$	152
20	The Assignment of the Fundamental Frequencies of C_2H_4S	157
21	The Assignment of the Fundamental Frequencies of C_2D_4S	158
22	The Assignment of the Fundamental Frequencies of cis-$C_2D_2H_2S$	160
23	The Assignment of the Fundamental Frequencies of trans-$C_2D_2H_2S$	162

LIST OF FIGURES

Figure		Page
1	The Six Vibrational Modes of an A-H---B Molecule	7
2	The Induced and A-H Dipoles of an A-H---B Molecule and Their Directions of Change During the ν_s and ν_b Vibrations	16
3	The Stepanov Energy Level Scheme for an A-H---B Molecule	21
4	The Six Vibrational Modes of the O---HCl Part of $(CH_3)_2O$---HCl	29
5	Stainless Steel Manifold for High Gas Pressures	37
6	Cross-sectional View of the Infrared Gas Cell	39
7	Absorption Between 90 and 140 cm^{-1} by $(CH_3)_2O$---HCl and the Free Components	47
8	Absorption Between 90 and 140 cm^{-1} by $(CH_3)_2O$---DCl and the Free Components	50
9	Absorption Between 90 and 140 cm^{-1} by $(CD_3)_2O$---HCl and the Free Components	51
10	Absorption Between 200 and 600 cm^{-1} by the Four Isotopic Forms of $(CH_3)_2O$---HCl and the Free Ethers	54
11	Absorption Between 700 and 875 cm^{-1} by $(CH_3)_2O$---HCl, $(CH_3)_2O$---DCl and the Free Components	63

Figure Page

12 Absorption Between 500 and 650 cm^{-1} by $(CD_3)_2$O---DCl and the Free Components 65

13 Absorption Between 850 and 1525 cm^{-1} by the Ethereal Modes of $(CH_3)_2$O---HCl and the Free Ether 73

14 Two Possible Geometries for $(CH_3)_2$O---HCl 78

15 Predicted Bandshapes for Absorption by $(CH_3)_2$O---HCl 81

16 Absorption Between 2300 and 2800 cm^{-1} by $(CH_3)_2$O---HCl at +35°C and -30°C 85

17 Absorption Between 2300 and 2800 cm^{-1} by $(CD_3)_2$O---HCl at +35°C and -30°C 88

18 The Stepanov Energy Level Scheme for $(CH_3)_2$O---HCl 92

19 Absorption Between 1500 and 2000 cm^{-1} by $(CH_3)_2$O---DCl at +30°C and -30°C 94

20 Absorption Between 1500 and 2000 cm^{-1} by $(CD_3)_2$O---DCl at +30°C and -30°C 95

21 The Structure of Ethylene Sulphide 105

22 The Orientation of cis-$C_2D_2H_2S$ with Respect to the Cartesian Axes and the Principal Axes of Inertia 136

23 The Orientation of trans-$C_2D_2H_2S$ with Respect to the Cartesian Axes and the Principal Axes of Inertia 138

CHAPTER 1

INTRODUCTION

1.1 General Introduction

The first three chapters of this thesis deal with the infrared spectra of the gas-phase, hydrogen-bonded molecules formed between dimethyl ether-h_6 and hydrogen chloride [$(CH_3)_2O$---HCl], dimethyl ether-h_6 and deuterium chloride [$(CH_3)_2O$---DCl], dimethyl ether-d_6 and hydrogen chloride [$(CD_3)_2O$---HCl], and dimethyl ether-d_6 and deuterium chloride [$(CD_3)_2O$---DCl]. In Section 1.2 a general discussion of the phenomenon of hydrogen bonding is presented. The normal modes of vibration of hydrogen-bonded molecules are defined and described in Section 1.3 and the current theories of intensity enhancement and broadening of the infrared absorption bands of these molecules are reviewed in Sections 1.4 and 1.5, respectively. The previous studies of the infrared spectra of the dimethyl ether-hydrogen chloride system and related hydrogen-bonded systems in the gas phase are reviewed in Section 1.6. The aims of the present study are presented in Section 1.7.

1.2 Hydrogen Bonding

Since the concept of hydrogen bonding was first definitively introduced by Latimer and Rodebush (1) in 1920, thousands of articles have appeared in the literature to illustrate the broad occurrence of this phenomenon. In addition to its well known role in determining the properties and structures of many biologically important compounds, hydrogen bonding has been shown to be of great importance in most other fields of chemistry. Despite the vast number of studies of hydrogen-bonded systems, the theoretical understanding of hydrogen bonding is still only semi-quantitative in nature. Much of the knowledge of hydrogen-bonded systems has been reviewed in texts by Pimentel and McClellan (2), Vinogradov and Linnel (3) and Hamilton and Ibers (4). Also, the book by Hadži and Thompson (5) and the review of the spectroscopic manifestations of hydrogen bonding by Murthy and Rao (6) are particularly useful in relation to the work presented in this thesis.

A hydrogen bond is said to exist when a hydrogen atom is bound simultaneously to two or more atoms (2). In this thesis the term 'hydrogen bond' refers to the weaker of the two bonds in the triatomic system A-H----B, and is the H----B bond. The energy of a hydrogen bond usually lies between 3 and 10 kcal/mole, with the average energy about 7 kcal/mole. These energies are intermediate between the energy of a normal covalent bond and those of the less specific van der Waals' interactions. The A-H bond in the A-H----B system is considered to be a normal covalent bond, although somewhat weaker than it would be in the absence of hydrogen bonding. A-H is the proton donor functional group and B is the proton acceptor atom or site of a molecule. Usually A is an electronegative atom such as O, N, F, S, Cl etc. and B is generally an atom or ion with one or more lone pairs of electrons, such as F, N, O, Cl, Cl^- etc.

When a hydrogen bond is formed, it is found that, if A and B are atoms, the A---B and H---B distances are usually shorter than the sum of the van der Waals' radii (7) of the A and B atoms and the H and B atoms, respectively. In X-ray and neutron diffraction studies these observations are used as criteria for the presence of hydrogen bonding. The A---B distances found by these studies have been used in theoretical calculations of the energy of the hydrogen bond (8). However, a complete and rigorous quantum mechanical model which can predict this energy does not exist at present, since the approximations which must be used in the calculation limit the accuracy to the same order of magnitude as the energy itself. Qualitatively, it is believed (9) that the energy of the hydrogen bond arises principally from four distinct interactions. Firstly, electrostatic interactions, predominantly Coulombic in nature, arise from attraction between the positive charge on the H atom and the negative charge on B. Secondly, the approach of the A-H group towards B causes distortions in the negative charge distributions on A-H and B and leads to delocalization effects in which part of the charge of B resides at A or H. Thirdly, the motion of the electrons in A-H and B gives rise to a dispersion interaction between a fluctuating dipole in A-H and the fluctuating dipole that it induces in B. Finally, a repulsive interaction results from the overlap of the electron charge clouds of the A, H and B atoms.

When A-H and B are portions of the same molecule, the interaction A-H---B is termed intramolecular hydrogen bonding. An example of this type of interaction is that which can occur in ortho-halophenols (10). Since intramolecular hydrogen bonds affect mainly the electronic stuctures on the proton donor and acceptor groups, the physical behaviour of systems with these types of hydrogen bonds is close to that of normal, non-hydrogen-bonded substances. When A-H and B are located in two separate molecules, the interaction is termed intermolecular hydrogen bonding. This thesis deals with intermolecular hydrogen bonding and specifically with that which occurs between the hydrogen atom of a hydrogen chloride molecule and one of the lone pairs of electrons on the oxygen atom of a dimethyl ether molecule. Since these types of hydrogen bonds change the number, mass, shape and electronic structure of the interacting molecules, studies of the physical properties of an intermolecular hydrogen-bonded system often yield information about these interactions. Non-spectroscopic methods (11,12) include studies of melting and boiling points, dielectric constants and dipole moments, viscosity, vapour pressure and molar volumes. Unfortunately, changes in these physical properties can also occur as a result of less specific interactions and, therefore, non-spectroscopic studies cannot provide unambiguous proof of hydrogen bonding. Spectroscopic techniques, however, are capable of providing evidence relating the involvement of a specific hydrogen atom and specific acceptor group in the formation of a weak bond. The most widely used techniques are infrared and Raman spectroscopy (13,14), nuclear magnetic resonance (15) and X-ray and neutron diffraction (16). Perhaps the most spectacular spectroscopic manifestation of hydrogen bonding occurs in the vibrational spectra of hydrogen-bonded molecules and, as a result, infrared and Raman studies provide the most commonly used criteria for the presence of hydrogen bonding.

1.3 The Infrared Spectra of Hydrogen-Bonded Molecules

In general, two effects of hydrogen bonding are observed in the infrared spectrum of a hydrogen-bonded molecule: 1) the frequencies, shapes and intensities of absorption bands that are present in the spectrum of the hydrogen-bonded molecule and in the spectra of the nonbonded proton donor and acceptor molecules are different in the two cases; 2) new bands appear in the spectrum of the hydrogen-bonded molecule as a result of the loss of rotational and translational degrees of freedom of the component molecules. It is particularly useful to consider the six vibrations which occur in the A-H---B part of a hydrogen-bonded molecule (13). Figure 1 displays these vibrations where B is treated as a point mass and the proton donor is considered to be a bent, triatomic molecule, R-A-H. Each vibrational mode is denoted by the appropriately subscripted letter ν (13), and may be described as shown in Figure 1, where the plane is that formed by the two bonds to atom A.

Of these modes, the A-H stretching mode, ν_s, has received most attention since it usually absorbs between 2500 and 3500 cm^{-1}, a region which is easily accessible to study. As far back as 1932 Freymann (17) observed that in the spectra of alcohols there are two regions of absorption by the O-H stretching mode, one due to the monomer at about 3700 cm^{-1} and one due to associated molecules at about 3400 cm^{-1}. Since then it has been shown that the A-H stretching mode in a hydrogen-bonded molecule is always lower in frequency than the corresponding mode in the absence of hydrogen bonding. Murthy and Rao (6) give an extensive list of these frequency shifts for a large number of hydrogen-bonded molecules.

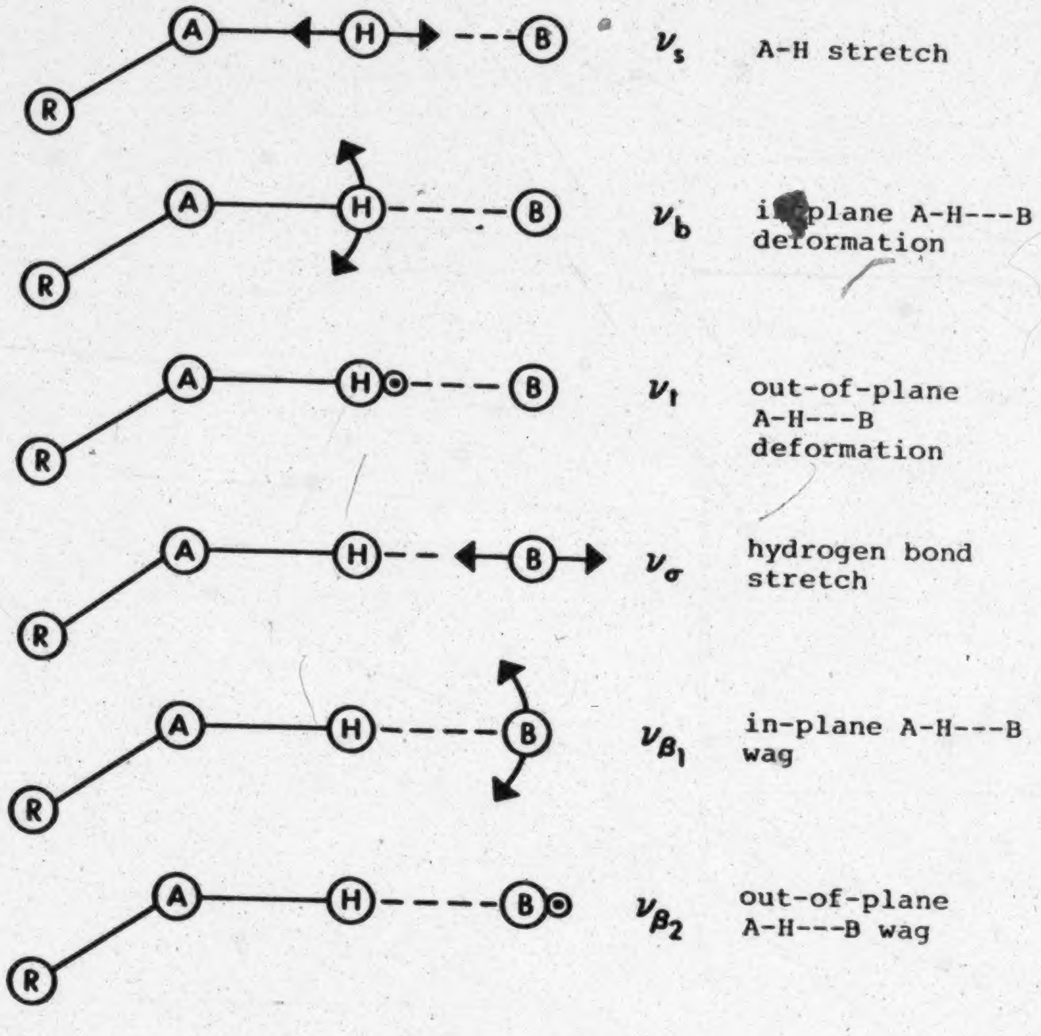
A
H
B
R
νs
A-H stretch
νb
in-plane A-H---B
deformation
νt
out-of-plane
A-H---B
deformation
νσ
hydrogen bond
stretch
νβ1
in-plane A-H---B
wag
νβ2
out-of-plane
A-H---B wag

FIGURE 1. The six vibrational modes involving the A, H and B atoms of the non-linear, hydrogen-bonded molecule, R-A-H---B.

There are cases in which a decrease in the A-H stretching frequency, $\Delta\nu_s$, indicates the presence of a hydrogen bond, although the A---B distance is greater than the sum of the van der Waals' radii of the A and B atoms. For example, Holzbecher, Knop and Falk (18) have shown that the ν_s absorption for the more weakly bound of the two hydroxyl groups in solid $Na_2[Fe(CN)_5NO].2H_2O$ is about 100 cm^{-1} below that expected for a non-hydrogen-bonded hydroxyl group, even though the nearest neighbour to the oxygen atom is a nitrogen atom 3.63 Å away. The sum of the van der Waals' radii for oxygen and nitrogen is 2.9 Å (7) and thus 3.63 Å is well outside the range predicted for the O---N distance when an O-H---N hydrogen bond is formed. Thus, the change in the A-H stretching frequency, $\Delta\nu_s$, clearly provides a very sensitive probe for detecting hydrogen bonding.

The decrease in frequency of the A-H stretching vibration when a hydrogen bond is formed must be brought about, at least in part, by a reduction of the A-H stretching force constant, caused by a redistribution of electron density of the A-H bond (19). Thus $\Delta\nu_s$ must reflect many of the properties of the hydrogen bond. The most important correlation is the relationship between $\Delta\nu_s$ and ΔH, the energy of the hydrogen bond. Such a relationship was first proposed by Badger and Bauer in 1937 (20) and an approximate, linear relationship between $\Delta\nu_s$ and ΔH has been established by Drago _et al_ (21,22) for molecules containing hydroxyl groups. The negative slope of the straight line corresponds to a decrease in the O-H stretching frequency by about 60 cm^{-1} for each kcal/mole. Unfortunately, a simple relationship has not been established to cover all A-H---B systems, because the slope of the $\Delta\nu_s$ vs ΔH line depends upon the nature of the interacting molecules (13). Also, correlations between $\Delta\nu_s$ and other properties of the hydrogen-bonded system, such as the A---B or H---B distance, or the base strength, depend largely upon the nature of the component molecules and only qualitative conclusions can usually be drawn from them (13).

In addition to decreasing the ν_s frequency, the formation of a hydrogen bond also causes an extreme increase in the breadth of the bands associated with this mode. The intensity of the ν_s fundamental absorption is also increased, usually by an order of magnitude (23), although the first overtone of ν_s is usually less intense than in the absence of hydrogen bonding (24). These phenomena are unique to hydrogen-bonded systems and are observed for gases, liquids, solutions and solids. However, the increases in the breadth and intensity of the ν_s absorption upon hydrogen bond formation are not well understood, and few correlations between these phenomena and properties of the hydrogen bond have been made. Because they are important in the interpretation of the spectrum of $(CH_3)_2O$---HCl, the theories of intensity enhancement and band-broadening in hydrogen-bonded systems are reviewed in Sections 1.4 and 1.5, respectively.

In A-D---B systems ν_s is found to absorb at a lower frequency than the corresponding mode in the non-associated deuterium donor molecule, and the ratio of the frequency ν_s in A-H---B to that in A-D---B usually lies between 1.3 and 1.4. Although the intensity enhancement of the ν_s fundamental absorption in A-D---B systems is usually as large as that in A-H---B systems, the increased breadth of the absorption is usually less pronounced for the deuterium bond (25).

The in-plane and out-of-plane A-H---B deformation modes, ν_b and ν_t respectively, are modes in which the hydrogen atom is displaced in directions perpendicular to the direction of the hydrogen bond. Unless the proton donating molecule is diatomic, ν_b is present in the absence of hydrogen bonding as the in-plane R-A-H deformation mode. If the donor molecule contains more than three atoms, ν_t is also present in the absence of hydrogen bonding as a torsional mode. When the proton donating molecule is diatomic, both ν_b and ν_t can be considered as new vibrational modes arising from the loss of two rotational degrees of freedom of the donor and acceptor molecules. This special case is discussed in Section 1.6 for the hydrogen halides hydrogen bonded to ethers and nitriles. In the most general case, when ν_b and ν_t are both present in the absence of hydrogen bonding, the hydrogen bond acts as a constraint to these vibrations and thus their force constants are increased, causing them to shift to higher frequencies. For example, it is known (26) that in unassociated alcohols ν_b and ν_t absorb between 1200 and 1300 cm^{-1} and at about 225 cm^{-1}, respectively, while in hydrogen-bonded alcohols they absorb between 1330 and 1410 cm^{-1} and at about 650 cm^{-1}, respectively. Usually, the infrared absorption bands due to ν_b and ν_t do not show any major intensity change when a hydrogen bond is formed but they do become somewhat broader (26,27).

Few successful correlations between the shifts in ν_b or ν_t with properties of the hydrogen bond have been made, although it has been shown that the absolute values of these shifts, as well as $\Delta\nu_s$, become larger as the strength of the hydrogen bond is increased (27,28). A major difficulty in correlating the shifts of ν_b and ν_t with properties of the hydrogen bond is that they often occur in the same spectral regions as many other transitions and cannot be definitively assigned, sometimes because they are coupled with some other vibrational mode. Since ν_b and ν_t are modes which involve the motion of the hydrogen atom to a large degree, they shift in frequency by a factor of about 0.7 when a deuterium atom is substituted for the hydrogen atom in A-H---B, and a study of the deuterium shift often leads to a definitive assignment. In cases where ν_b and ν_t mix with other modes, however, a vibrational analysis is needed to assign them (29).

The last three modes shown in Figure 1 arise from the loss of three translational degrees of freedom of the interacting molecules. The ν_σ mode involves motion of the interacting molecules against each other along the hydrogen bond and the ν_{β_1} and ν_{β_2} modes involve wagging motions of one molecule about the other, in directions perpendicular to the direction of the hydrogen bond. Because the hydrogen bond is very weak relative to normal covalent bonds, the force constants for ν_σ and the ν_β modes are very small and, thus, these modes absorb at low frequencies, usually below 200 cm^{-1}. This region also contains absorption by skeletal and torsional modes (30) which often complicate the assignment of ν_σ and ν_β. However, numerous studies have been made in which ν_σ has been unequivocally assigned, usually in the region between 100 and 200 cm^{-1} (31). The few studies in which ν_β modes have been successfully assigned indicate that these modes absorb weakly below 100 cm^{-1}. For example, Carlson, Witkowski and Fateley (32) assign a ν_β mode at 68 cm^{-1} in formic acid dimer and at 50 cm^{-1} in acetic acid dimer.

Due to the lack of experimental data on the ν_β modes no correlation has been made between their frequencies and properties of the hydrogen bond. However, it has been established that the frequency of the ν_σ mode depends upon the strength of the hydrogen bond in a similar manner to the magnitude of the shift of the A-H stretching frequency, $\Delta\nu_s$. For example, Brasch et al (33) have shown that in two different solid forms of phenol, the frequency of ν_σ was higher in the form which had the larger $\Delta\nu_s$ and, presumably, the stronger hydrogen bond.

No significant shift is observed in the frequency of ν_σ or ν_β when a deuterium atom is substituted for the hydrogen-bonded hydrogen atom (31). This arises from the fact that these modes involve the motion of whole molecules against each other and the substitution of one deuterium atom for a hydrogen atom causes little change in the vibrating masses.

In addition to the characteristic absorption by the six modes shown in Figure 1, the infrared spectra of hydrogen-bonded molecules show that the absorption by the other vibrational modes present in both the proton donor and acceptor molecules is influenced by the presence of the hydrogen bond. In particular, the frequencies of absorption of the modes involving the atoms participating directly in the hydrogen bond are shifted relative to their positions in the spectra of the non-associated molecules. This shift may be negative, as is found for the C=O stretching frequency of several carbonyl acceptor molecules (34), or positive, as is found for the skeletal vibrations of the pyridine-ethanol system (35). The vibrational modes which do not involve atoms participating directly in the hydrogen bond show smaller shifts. No large changes in the intensities and widths of the bands due to these modes are generally observed when a hydrogen bond is formed.

1.4 Theories of Intensity Enhancement

In general, the intensity of an infrared absorption band is proportional to the square of the dipole moment function, $\underline{\mu}$, which can be expanded as a power series in the normal coordinates, Q_i, of the molecule (36):

$$\underline{\mu} = \underline{\mu}_o + \sum_i \left(\frac{\partial \underline{\mu}}{\partial Q_i}\right)_o Q_i + \frac{1}{2} \sum_i \sum_j \left(\frac{\partial^2 \underline{\mu}}{\partial Q_i \partial Q_j}\right)_o Q_i Q_j + \ldots. \qquad [1]$$

where $\underline{\mu}_o$ is the permanent dipole moment of the molecule. Only the first two terms on the right hand side of equation [1] are considered in the approximation of electrical harmonicity while the second and higher order derivatives are referred to as the electrical anharmonicity.

It has been stated (23) that the large increase in intensity of the ν_s fundamental absorption and decrease in intensity of the first overtone arises from an increase in the absolute value of $\partial\underline{\mu}/\partial Q_s$ and a decrease in the absolute value of $\partial^2\underline{\mu}/\partial Q_s^{\,2}$, where Q_s is the normal coordinate of the ν_s vibration. However, the intensity of the overtone is also dependent upon the mechanical anharmonicity (37) and this explanation can only be acceptable if the mechanical anharmonicity is small. Sandorfy et al (38, 39) have shown that, in a number of hydrogen-bonded alcohols, the mechanical anharmonicity is large and, therefore, should also contribute to the intensity of the overtone. Calculations (40) have shown that, if mechanical anharmonicity is taken into account, a large increase in $\partial\underline{\mu}/\partial Q_s$ is, by itself, sufficient to increase the intensity of the fundamental and to lower that of the overtone.

Huggins and Pimentel (41) have suggested that polarization of the lone pairs of electrons on the acceptor atom, B, accounts for the intensity increase of the ν_s fundamental. Figure 2(a) shows that in an unperturbed A-H---B molecule, a dipole, $\underline{\mu}_i$, is induced in the lone pairs of electrons on B by the highly polar A-H bond and that this induced dipole has the same direction as the A-H dipole, $\underline{\mu}_{AH}$. During the ν_s vibration, as shown in Figure 2(b), $\underline{\mu}_i$ vibrates in phase with $\underline{\mu}_{AH}$ and contributes an additional component to the overall change of dipole moment, $\partial\underline{\mu}/\partial Q_s$. The lack of an intensity increase of the ν_b (or ν_t) absorption upon formation of a hydrogen bond can also be explained using this model, since during the ν_b vibration, as shown in Figure 2(c), the induced dipole vibrates exactly out-of-phase with the vibration of $\underline{\mu}_{AH}$. Thus $\partial\underline{\mu}_i/\partial Q_b$ is opposite in sign to $\partial\underline{\mu}_{AH}/\partial Q_b$, and $\partial\underline{\mu}/\partial Q_b$ is not in-

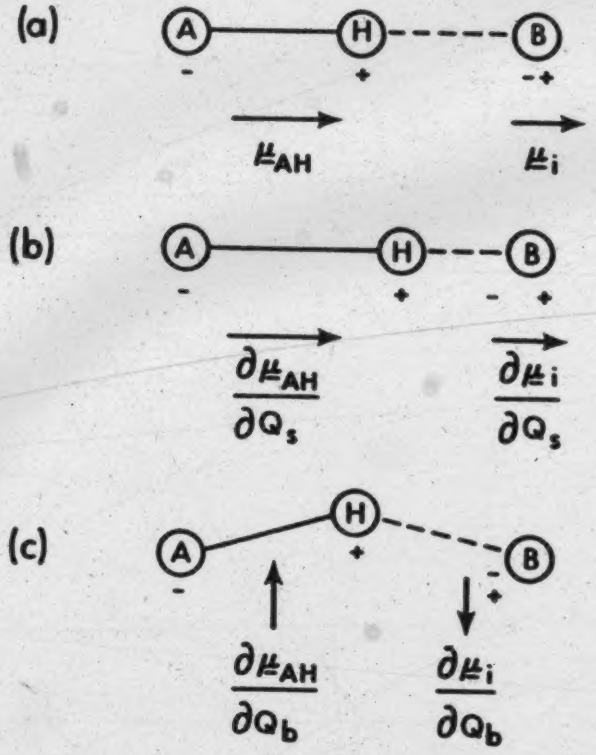
(a)
A
H
B
-
+
-+
μ_{AH}
μ_i
(b)
A
H
B
-
+
- +
$\frac{\partial \mu_{AH}}{\partial Q_s}$
$\frac{\partial \mu_i}{\partial Q_s}$
(c)
A
H
B
-
+
-
+
$\frac{\partial \mu_{AH}}{\partial Q_b}$
$\frac{\partial \mu_i}{\partial Q_b}$

FIGURE 2. (a) The induced dipole, $\underline{\mu}_i$, and the A-H dipole, $\underline{\mu}_{AH}$, of an unperturbed A-H---B molecule. (b) Directions of the changes in dipole moments during the ν_s vibration of an A-H---B molecule. (c) Directions of the changes in dipole moments during the ν_b vibration of an A-H---B molecule.

creased. This is obviously an oversimplified picture but it does provide a useful model to qualitatively explain the intensity behaviours of the ν_s and ν_b modes.

1.5 Theories of Band Broadening

It is generally believed that at least one of the following two mechanisms plays a major role in determining the breadth of the ν_s band of a hydrogen-bonded molecule:

[1] Interactions between ν_s and the low frequency vibrations which involve the hydrogen bond, ν_σ and ν_β, give rise to a series of combination bands and hot bands (42), which distribute the intensity of ν_s over a large frequency range.

[2] Overtone or summation bands of fundamentals other than ν_s which are close in frequency to ν_s are intensified through Fermi resonance (37) with ν_s.

Neither of these mechanisms is dependent upon the physical state of the system but, while broad ν_s absorptions are observed in the spectra of hydrogen-bonded molecules in all physical states, the bands are usually broader in the spectra of liquids and concentrated solutions (43). This additional broadening has been explained (43) by postulating the existence of a variety of hydrogen-bonded species, each with a unique ν_s frequency and corresponding absorption band which may be broadened through mechanisms 1 or 2.

Mechanisms 1 and 2 can only be operational if the potential energy surface for the hydrogen-bonded molecule is anharmonic in nature (44). The presence of anharmonicity is in itself a broadening mechanism, since it causes the frequency of a given vibrational mode, ν_i, to be dependent on the degree of excitation of other vibrational modes, ν_j, ν_k, etc. Consequently a band of frequencies results from each vibrational degree of freedom instead of the single, discrete frequency predicted for a harmonic oscillation (37). In addition, the presence of anharmonicity allows bands due to combinations of vibrations to appear in the spectrum. These bands are denoted by $2\nu_i$ if they are due to the overtone of the ν_i vibrational mode and by $\nu_i + n\nu_j$ or $\nu_i - n\nu_j$ if they are due to summation or difference transitions, respectively. A summation band, $\nu_i + n\nu_j$, arises from the simultaneous excitation of one quantum of the ν_i vibrational mode and n quanta of the ν_j vibrational mode. A difference band, $\nu_i - n\nu_j$, arises from the transition from a state in which n quanta of the ν_j vibration have been excited, to a state which is one quantum of ν_i above the ground state.

Mechanism 1 results from the anharmonic force field of a hydrogen-bonded molecule, which allows coupling between the A-H stretching mode, ν_s, and the hydrogen bond stretching mode, ν_σ (45). This coupling was described classically by the 'fluctuation' theory of Badger and Bauer (20), which is based on the observation that the A-H frequency decreases as the A---B distance, r_{AB}, decreases on hydrogen bond formation. The theory considers that the range of values of r_{AB}, which must exist due to the thermal vibrations of the relatively weak hydrogen bond, leads to a range of ν_s frequencies. This should give rise to a broad absorption band for ν_s, with the high frequency portion of the band arising from ν_s vibrations occurring at larger-than-average values of r_{AB} and the low frequency portion of the band arising from ν_s vibrations occurring at shorter-than-average r_{AB} values. For an isolated A-H---B system, however, the change in the r_{AB} distance occurs rhythmically with the frequency of the ν_σ vibration. In effect, the ν_s vibration is frequency modulated by the ν_σ vibration and this idea allowed Batuev (46,47) to extend the fluctuation theory to become the frequency modulation theory, still framed in classical mechanics. Batuev showed that the broad band which results should consist of a series of sub-bands with frequencies $\nu_s \pm n\nu_\sigma$, where n is integral. Since these bands must 'borrow' intensity from the fundamental ν_s band, the total intensity is then spread out over a wide frequency range.

The quantum mechanical treatment of the anharmonic coupling between ν_s and ν_σ also leads to the result that transitions of the type $\nu_s \pm n\nu_\sigma$, where n is integral should be observed. In the absence of special conditions, the intensities of the transitions are expected to decrease in the order ν_s, $\nu_s + \nu_\sigma$, $\nu_s + 2\nu_\sigma$, $\nu_s + 3\nu_\sigma$ ......, and $\nu_s + n\nu_\sigma$ is expected to be more intense than $\nu_s - n\nu_\sigma$ by the Boltzmann factor, $\exp(-nhc\nu_\sigma/kT)$.

A quantum mechanical treatment of the interaction between ν_s and ν_σ was first discussed by Stepanov (48) and later modified by Sheppard (45). It is necessary to outline its main features in some detail, because it leads to the possibility that the normal intensity distribution presented above may not apply. Stepanov argued that, because ν_σ is usually about ten times lower in frequency than ν_s, separate potential energy curves can be drawn for ν_σ in the $V_s = 0$ and $V_s = 1$ vibrational states. This separation is analogous to the separation of electronic and nuclear motion in the quantum mechanical treatment of molecules (49). The energy levels of ν_σ can then be drawn on these curves for each state of V_s, as shown in Figure 3 for an A-H---B molecule. At large A---B distances, no hydrogen bond is present and the curves are separated by the vibrational energy of the non-hydrogen-bonded A-H stretching mode, ν_{AH}(free). The separation of the curves close to their minima is approximately equal to the vibrational energy of ν_s in the hydrogen-bonded molecule. Thus the curve for the $V_s = 1$ state has a deeper minimum than that

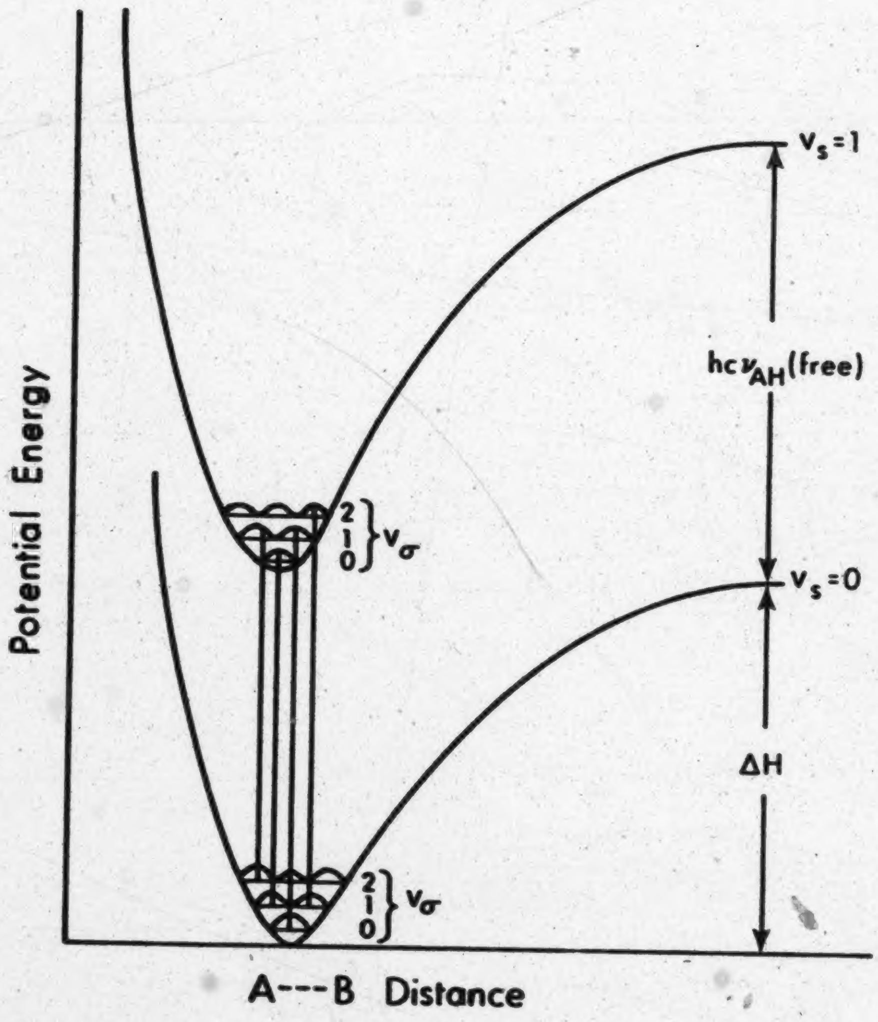
Potential Energy
A---B Distance
$v_s=1$
$hc\nu_{AH}$(free)
$v_s=0$
ΔH
2
1
0
v_σ
2
1
0
v_σ

FIGURE 3. The Stepanov energy level scheme for the interaction of ν_s and ν_σ vibrations in the hydrogen-bonded molecule, A-H---B. V_s and V_σ are the quantum numbers for the A-H and H---B stretching vibrations, respectively, and the curves drawn on the energy levels are the squares of the wavefunctions.

for the $V_s = 0$ state. Sheppard (45) has argued that since the hydrogen atom moves on the average closer to the center of the bond when $V_s = 1$, the hydrogen bond is stronger when $V_s = 1$ than when $V_s = 0$ and the potential energy minimum occurs at a shorter A---B distance when $V_s = 1$, as shown in Figure 3. Because the A---B motion during the ν_σ vibration is, classically, so much slower than the A-H motion during ν_s, Stepanov argued that the transitions from $V_s = 0$ to $V_s = 1$ occur at constant A---B distance and, therefore, the more probable transitions occur at A---B distances which are more probably occupied in the various ν_σ levels. The probability of occupancy of each ν_σ level, that is the square of the wave function (50), is sketched in Figure 3 and the most probable transitions are believed to originate and terminate at the maxima in these probability curves. This effect may be referred to as the vibrational Franck-Condon (51) effect, and it manifests itself in the case depicted in Figure 3 by allowing the summation band, $\nu_s + \nu_\sigma$ $[V_s = 0 \rightarrow 1,\ V_\sigma = 0 \rightarrow 1]$, to be more intense than the fundamental band, ν_s $[V_s = 0 \rightarrow 1, V_\sigma = 0 \rightarrow 0]$. These arguments, therefore, predict that combination bands of the type $\nu_s \pm n\nu_\sigma$ may appear in the spectrum with an unusual intensity distribution. They also predict that hot bands, from transitions of the type $\nu_s + n\nu_\sigma \leftarrow n\nu_\sigma$, $\nu_s + (n+1)\nu_\sigma - n\nu_\sigma$ or $\nu_s + n\nu_\sigma - (n+1)\nu_\sigma$ (42), may appear in the spectrum with unusually high intensities. Due to the mechanical anharmonicity, these hot transitions can absorb at frequencies significantly different from those of their corresponding ground state transitions and, thus, they can contribute to the general background of the ν_s band and, in some cases, lead to a diffuse band structure. However, hot transitions can contribute to a large degree only if the temperature is high enough to produce a large population in the excited V_σ states when $V_s = 0$, and at very low temperatures the band should be resolved into features separated by about the frequency of ν_σ.

Perhaps the best proof to date that combination bands involving ν_s and ν_σ and other low-lying vibrational modes, along with the hot bands associated with these transitions, can be responsible for the broad, diffuse band seen for some hydrogen-bonded systems is given by the studies by Evans and Lo (52,53) of the dibromide ion, $BrHBr^-$. This ion has two stretching modes, a symmetric mode which is analogous to ν_σ, and an asymmetric mode which is analogous to ν_s. An extremely broad, diffuse band between 500 and 1300 cm^{-1} in the spectra of $BrHBr^-$ at temperatures greater than 100°K has been assigned to the asymmetric stretch. In spectra of $BrHBr^-$ at about 20°K this band is resolved into well defined peaks which may be identified as bands of the type $\nu_s + n\nu_\sigma$, as well as sum bands involving ν_s and a lattice mode. The difference bands were not present in the spectra of $BrHBr^-$ at 20°K but were evident in spectra of $BrHBr^-$ at 100°K.

The importance of interactions between ν_s and the hydrogen-bond wagging modes, ν_β, has been pointed out by Thomas and coworkers (54,55), who have provided convincing evidence that hot bands of the hydrogen halide stretching vibration in CH_3CN---HCl and CH_3CN---HF from excited states of ν_β contribute significantly to the breadth of the observed band.

Mechanism 2 is the only other mechanism of band broadening which has received widespread attention. In a polyatomic molecule, if two vibrational levels belonging to two different vibrations or combinations of vibrations are nearly degenerate and are of the same symmetry, a perturbation of these levels can result from a resonance interaction (37). Thus, the two energy levels are split, causing the frequency of one vibration to be higher than expected and the frequency of the other to be lower than expected. In addition, the intensities of the bands due to transitions to these energy levels are mixed. Thus the intensity of an overtone or combination band, which is usually much weaker than that of a fundamental band, can appear to be much greater than expected. In other words, it is possible for the weaker band to borrow intensity from the stronger one. This has the effect of distributing the intensity of the stronger band over a larger frequency range than in the absence of an interaction. In the cases where the interaction occurs through anharmonic terms in the potential energy function, as must be the case if a combination level interacts with a fundamental level, this effect is known as Fermi resonance, and is well documented (37) in the spectra of non-hydrogen-bonded molecules. Bratoẑ, Hadẑi and Sheppard (56) pointed out that interactions between ν_s and overtone or combination transitions which absorb close to ν_s could account for the broad ν_s band in the spectra of hydrogen-bonded molecules. In particular, these authors were able to assign much of the complicated structure on the broad ν_s band observed in many carboxylic acid dimers (56) to summation transitions which involve vibrations of the COOH groups, and which are enhanced in intensity by Fermi resonance with the O-H stretching vibration. In addition, Haurie and Novak (57) have shown that many of the features on the ν_s band of acetic acid dimer can be assigned to summation transitions which involve vibrations in the aliphatic part of the acid and which are enhanced in intensity by Fermi resonance with ν_s. Clearly, thus, if the hydrogen-bonded molecule is large and many combination transitions have frequencies which are close to ν_s, this mechanism of band broadening can be very important. It is also clear that, since the enhancement of intensity of overtone or combination bands occurs to a greater degree as the frequency difference between these bands and ν_s

becomes smaller, these bands can be intensified over a larger range of frequencies if ν_s is not a single band but is instead a progression of bands of the type $\nu_s \pm n\nu_\sigma$. Thus mechanism 2 becomes a more powerful broadening mechanism when considered in conjunction with mechanism 1.

Witkowski (58) and Marechal et al (59-62) have had significant success in attempting to account for the complex spectra (56) of the carboxylic acid dimers without invoking Fermi resonance. While details of their theory are not completely clear, they consider the anharmonic coupling between ν_s and ν_σ and the interaction between the two hydrogen bonds in the molecule. Because of the interaction between the two hydrogen bonds in each dimer, the transitions that they calculate cannot be all clearly related to those in a simple sum and difference band series of the type $\nu_s \pm n\nu_\sigma$, although all of their transitions are of this type. The only system that they treat that does not contain the complications of two interacting hydrogen bonds is that of the N-H---N bond in solid imidazole (59). In this case their calculated transitions are simply those expected from the most elementary considerations of sum and difference bands of the type $\nu_s \pm n\nu_\sigma$, that is, an equi-spaced series of bands with relative intensities in the order $\nu_s > \nu_s + \nu_\sigma > \nu_s + 2\nu_\sigma > \nu_s + 3\nu_\sigma$, and $\nu_s + n\nu_\sigma$ being more intense than $\nu_s - n\nu_\sigma$ by the Boltzmann factor for the level $n\nu_\sigma$. Thus the details of their apparent success in explaining the spectra of the carboxylic acid dimers are obscure at present.

1.6 Infrared Spectra of Gaseous Hydrogen-Bonded Molecules

In order to develop the vibrational theory of hydrogen-bonded molecules, more vibrational data on isolated A-H---B systems are highly desirable. These data are best obtained through infrared studies of gaseous systems containing one hydrogen bond per molecule. Unfortunately, the number of systems which can be successfully studied in the gas phase is limited since a significant partial pressure of the hydrogen-bonded molecule is needed to obtain a good spectrum. The formation of a hydrogen-bonded molecule is controlled by the equilibrium

$$\text{A-H} + \text{B} \rightleftarrows \text{A-H---B}$$

and relatively few systems have sufficiently large equilibrium constants to produce enough of the hydrogen-bonded molecule. The carboxylic acids are perhaps the easiest to study in the gas phase since, even at room temperature, the majority of the molecules exist as hydrogen-bonded dimers (63). Unfortunately, each dimer has a cyclic structure containing two hydrogen bonds and infrared studies of these acids do not yield direct information about isolated hydrogen bonds. The most extensively studied gaseous molecules which contain one hydrogen bond are those formed between alcohols and amines (64-68), ethers and inorganic acids (25,68-79) and between cyanides and hydrogen halides (54,55,80,81). Of particular interest are studies of hydrogen-bonded molecules in which the proton donors are hydrogen halides (25,54,55,72-81). Since the proton donors are diatomic in these molecules, the forms of the vibrations involving the hydrogen bond, shown in Figure 4 for $(CH_3)_2O$---HCl, are slightly different from those presented earlier in Section 1.3. In particular, the ν_b and ν_t modes in $(CH_3)_2O$---HCl would correspond to pure rotations of the hydrogen chloride molecule in the absence of a hydrogen bond. Also, the ν_β modes in $(CH_3)_2O$---HCl are represented as wagging motion of the hydrogen chloride molecule in directions perpendicular to the direction of the hydrogen bond.

Arnold, Bertie and Millen (72) first reported that the infrared spectra of mixtures of gaseous hydrogen halides with aliphatic ethers contained the broad association band which is characteristic of hydrogen-bonded molecules. In particular, the spectra of mixtures of hydrogen chloride with various ethers (73) each revealed an intense band which was about 400 cm^{-1} wide and had its absorption maximum at about 2570 cm^{-1}. The absorption maximum was assigned to ν_s, the HCl stretching mode in R_2O---HCl, and two shoulders which were displaced by about 100 cm^{-1} to either

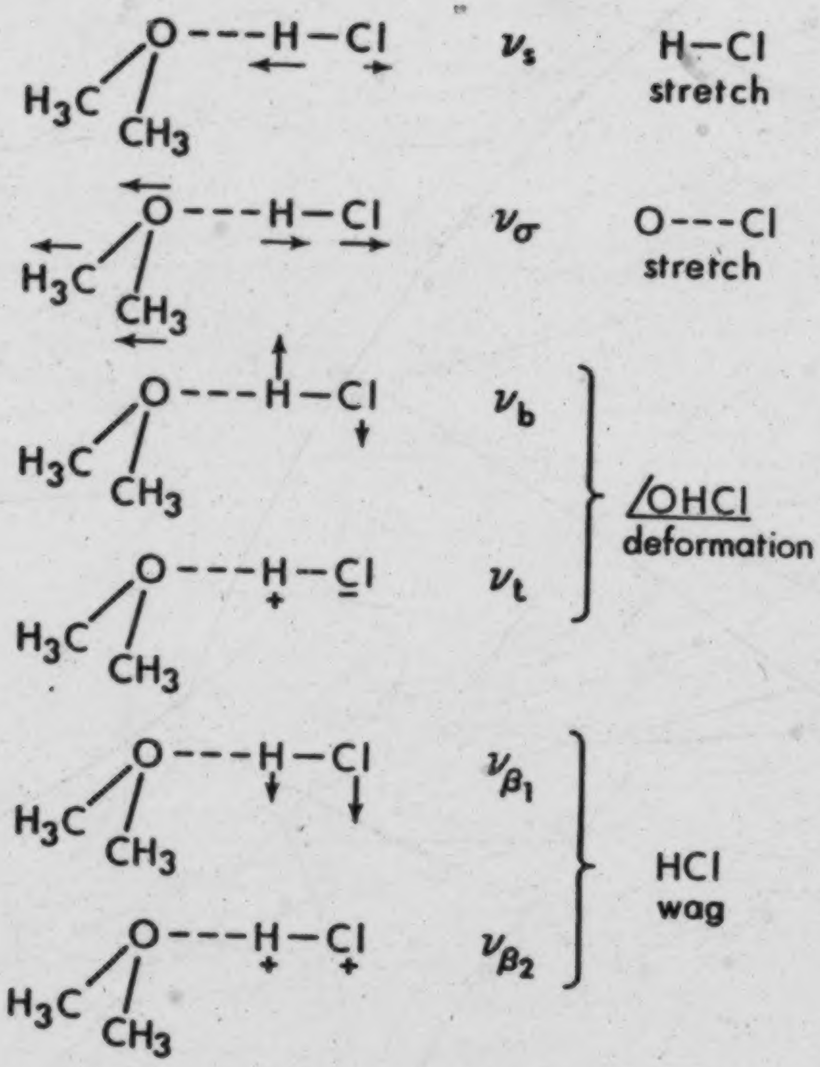
O---H–Cl
H3C
CH3
νs
H–Cl stretch
νσ
O---Cl stretch
νb
νt
∠OHCl deformation
νβ1
νβ2
HCl wag

FIGURE 4. The six vibrational modes involving the O---HCl part of the hydrogen-bonded molecule, $(CH_3)_2O$---HCl.

side of the maximum were assigned to the sum and difference bands $\nu_s \pm \nu_\sigma$. Broad bands observed in the spectra of $(CH_3)_2O$---DCl (25) and $(CH_3)_2O$---HF (77) were also interpreted in this manner. From these assignments the frequency of ν_σ was predicted to be about 100 cm^{-1} in $(CH_3)_2O$---HCl and $(CH_3)_2O$---DCl and about 170 cm^{-1} in $(CH_3)_2O$---HF. These frequencies are reasonably close to the observed values of 117 cm^{-1} (75) for ν_σ in $(CH_3)_2O$---HCl and 180 cm^{-1} (79) for ν_σ in $(CH_3)_2O$---HF. The ν_b and ν_t modes have been reported (78) to lie at 755 and 665 cm^{-1} in $(CH_3)_2O$---HF and at 550 and 490 cm^{-1} in $(CH_3)_2O$---DF, although it is not known which mode has the higher frequency. These modes have not been observed in the spectra of gaseous $(CH_3)_2O$---HCl and $(CH_3)_2O$---DCl.

At room temperature the equilibrium constant for formation of gaseous $(CH_3)_2O$---HCl is small (82-84) and therefore a large proportion of the component molecules is not hydrogen bonded. However, since the heat of formation of $(CH_3)_2O$---HCl from its component molecules is negative, having been reported to lie between -5.6 and -7.6 kcal/mole (75,82-84), a decrease in temperature of the system causes the equilibrium constant to become larger. Thus, by recording spectra of gaseous mixtures of dimethyl ether-h_6 with large excesses of hydrogen chloride at low temperatures, Le Calvé, Grange and Lascombe (76) were able to observe the bands due to the ethereal modes in $(CH_3)_2O$---HCl between 800 and 1300 cm^{-1}. Shchepkin and Belozerskaya (74) have suggested that a band shape analysis of the band due to the symmetric C-O stretching mode in $(CH_3)_2O$---HCl leads to the conclusion that this molecule has C_s symmetry (Section 3.4).

Studies of dimethyl ether and hydrogen chloride mixtures have also been made for the liquid (85) and solid (86,87) phases. It seems clear that a variety of hydrogen-bonded species in which the oxygen atom is protonated can exist in these phases in addition to the $(CH_3)_2O$---HCl molecule. There is, however, no evidence that any species other than $(CH_3)_2O$---HCl is formed in the gas phase.

The hydrogen-bonded molecules formed between the cyanides and hydrogen fluoride (55,80,81) or hydrogen chloride (54) give rise to ν_s bands which exhibit fine structures separated by about 2 or 3 cm^{-1} (54,55) which is in sharp contrast to the broad, diffuse bands usually observed for the ν_s vibration in other hydrogen-bonded molecules. Thomas et al (54,55) have interpreted this fine structure as due to hot transitions of the ν_s vibration arising from excited ν_β states. Similar fine structure was observed (55,81) on the band at 585 cm^{-1} due to the degenerate F-H---N deformation modes, $\nu_b = \nu_t$, in acetonitrile-hydrogen fluoride. Thomas (55) interpreted this fine structure as due to hot transitions of these modes arising from excited ν_β levels, but Huong and Couzi

(81) have assigned it to the normal fine structure of a perpendicular band of a symmetric top (88).

In his treatment of the anharmonic interaction between the A-H and hydrogen bond stretching modes, ν_s and ν_σ, Stepanov pointed out that the energy absorbed during the excitation of ν_s often exceeds the dissociation energy of the hydrogen-bonded molecule. If the excitation energy is transferred to the ν_σ mode, it could cause the molecule to predissociate (89) and this could cause the absorption bands due to the excitation of ν_s to be broad. The fine structure separated by 2 or 3 cm^{-1} on the ν_s bands in acetonitrile---hydrogen chloride and acetonitrile---hydrogen fluoride (54,55) proves that these molecules must have lifetimes greater than about 10^{-11} seconds and that broadening by predissociation cannot be of importance in these systems. The shift of ν_s on formation of the hydrogen bond in CH_3CN---HCl (54) is smaller than that when $(CH_3)_2O$---HCl (73) is formed, and this suggests (13) that the hydrogen bond in $(CH_3)_2O$---HCl is the stronger of the two. It is, therefore, very improbable that predissociation causes significant broadening of the band due to ν_s in $(CH_3)_2O$---HCl.

1.7 Aims of this Work

The initial aim of this work was to obtain the infrared spectra of the gaseous, hydrogen-bonded molecules

$(CH_3)_2O$---HCl, $(CD_3)_2O$---HCl, $(CH_3)_2O$---DCl and $(CD_3)_2O$---DCl in as much detail as possible, and, in particular, to locate the ν_b, ν_t and ν_β modes (Figure 4). A second aim was to study the temperature dependence of the shape of the ν_s bands in the spectra of these four molecules to test the proposed influence of difference bands (25,73). Further aims were to confirm the isotope shift of the 117 cm^{-1} band reported by Belozerskaya and Shchepkin (75) and to extend the work of LeCalvé et al (76) to determine the shapes of the remaining bands due to modes of the ethereal part of $(CH_3)_2O$---HCl.

CHAPTER 2

EXPERIMENTAL TECHNIQUES

2.1 Preparation and Purification of Chemicals

The dimethyl ether-h_6 was obtained from Matheson, the dimethyl ether-d_6 and deuterium chloride from Merck, Sharpe and Dohme and the argon from Linde. Each gas except argon was dried by repeated distillations from a methanol-dry ice bath until no water absorption could be detected in the infrared spectrum of about one-half an atmosphere of the gas. The argon was boiled from a cold trap at well below -100°C and no further purification was found necessary. The deuterium chloride always contained at least 10% hydrogen chloride in spite of repeatedly flushing the vacuum lines and the cell with the deuterated acid prior to use. Both the deuterium chloride and the commercially available hydrogen chloride contained traces of carbon dioxide which could not be readily removed. Its presence was unimportant in the deuterium chloride but its infrared spectrum interfered with a region of interest in the spectra of hydrogen chloride-ether mixtures. For this reason, hydrogen chloride free from carbon dioxide was prepared in vacuo by the hydrolysis of phosphorous pentachloride to phosphoric acid and gaseous hydrogen chloride (90). The reaction vessel was a one litre triple-neck flask fitted with a 250 ml. vented dropping funnel in one neck and connected to a conventional glass vacuum rack. The dropping funnel was modified by the inclusion of a stopcock on the venting tube. Distilled water was first introduced into the dropping funnel and degassed by direct pumping through the venting tube until freezing occurred. The ice was then allowed to melt, and the water was degassed again. The evacuated funnel was then isolated from the apparatus while the phosphorous pentachloride was put into the reaction vessel and degassed by direct pumping for several hours. The pump was then isolated from the apparatus and water was added drop-by-drop to the phosphorous pentachloride. The wet hydrogen chloride distilled in vacuum to a flask cooled with liquid nitrogen. The hydrogen chloride was then dried by repeated distillations from a methanol-dry ice bath.

2.2 Vacuum Lines and the Infrared Cell

When the total gas pressure required did not exceed one atmosphere, the infrared cell was connected to the manifold of a conventional glass vacuum rack. Gas pressures were measured to ± 1 Torr with the cell at room temperature using a mercury-filled U-tube manometer. When spectra of mixtures of gases were required, the cell was first filled to the desired pressure of one component and then isolated from the manifold. The manifold was evacuated to a pressure of at least 10^{-2} Torr and the second component was then introduced into the manifold at a pressure slightly above the desired total pressure. The cell valve was then quickly opened and closed repeatedly, allowing the two gases to mix within the cell but minimizing diffusion out of the cell, until the pressure in the manifold stopped decreasing. The final pressure minus the pressure of the first component was assumed to give the pressure of the second component.

When the total gas pressure did exceed one atmosphere, the gases were handled in the 7½ inch long, 1 inch i.d. and 1½ inch o.d. stainless steel manifold shown in Figure 5. Matheson type 32R stainless steel gas valves were screwed into 5/16 inch threaded sockets in the manifold and served to isolate the various parts of the system. To ensure a vacuum-tight system, the valve threads were taped with Teflon and each valve was screwed tightly against a lead washer between the manifold and the valve. The standard Teflon O-rings usually used in the valves were replaced by lightly greased 1/4" x 3/8" Buna N rubber O-rings. The manifold was connected to a glass vacuum rack by a rubber vacuum hose and to the infrared cell by a 1/4 inch Mason-Renshaw Industries 'compress-o-coupling' O-ring connector welded to a gas valve. Two stainless steel test tubes welded to the gas valves served as 'cold fingers'. Pressures of greater than one atmosphere in the manifold were measured by a Marsh Mastergauge type

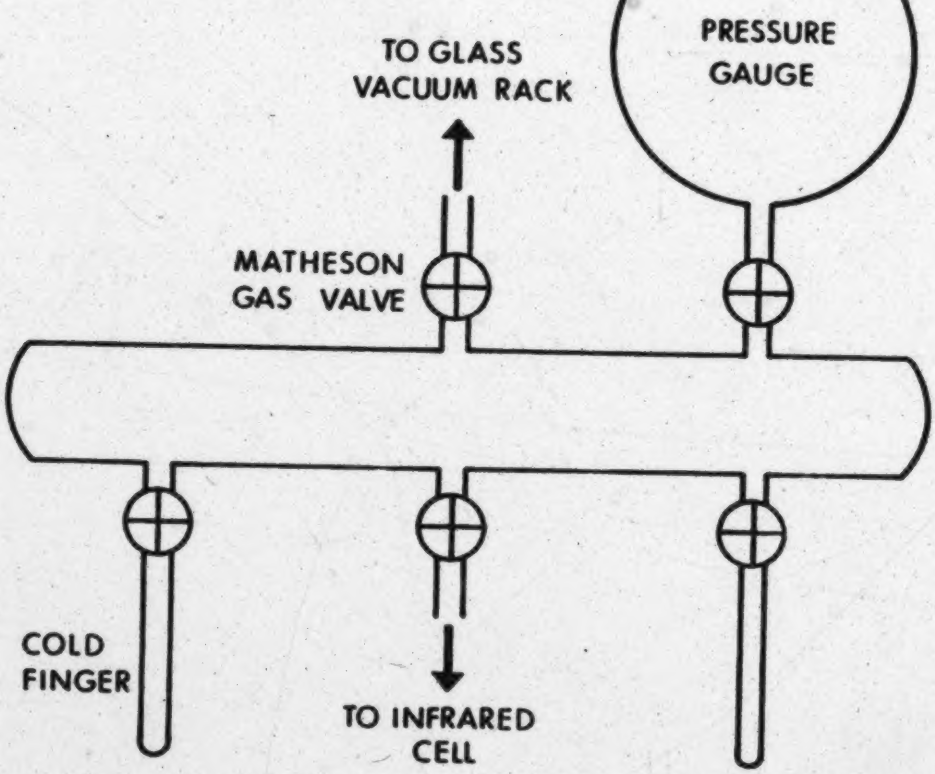
TO GLASS
VACUUM RACK
PRESSURE
GAUGE
MATHESON
GAS VALVE
COLD
FINGER
TO INFRARED
CELL

FIGURE 5. Stainless steel manifold used to handle gases at pressures exceeding one atmosphere (not drawn to scale).

100 M compound gauge, capable of measuring pressures up to 100 PSIG (5870 Torr) with an accuracy of ± 0.5 PSIG (26 Torr). Pressures of less than one atmosphere in the metal manifold and cell were measured by the U-tube manometer in the glass vacuum system. All pressures were measured with the cell at room temperature. To achieve pressures of greater than one atmosphere, the gas of interest was first condensed into one of the two cold fingers of the stainless steel manifold. The manifold was then isolated from the glass system and the condensate allowed to warm up until the vapour pressure reached the desired level. Mixtures of gases were prepared in a manner analogous to that used when the total pressure of gas did not exceed one atmosphere. The pressure of the component present in the least quantity was always known most accurately as it was measured by the U-tube manometer.

The cell used for the infrared measurements was cylindrical with a one inch internal diameter and ten centimeter path length and is shown in Figure 6. The windows were held in place against greased Buna N rubber O-rings by circular end caps which were screwed to the body of the cell. A coaxial, stainless steel jacket permitted the cell to be cooled with a stream of cold nitrogen gas. The cell was made of copper tube, with a 0.1 inch wall thickness, for optimum heat transfer. Without insulation of the outside of the coaxial jacket, tempera-

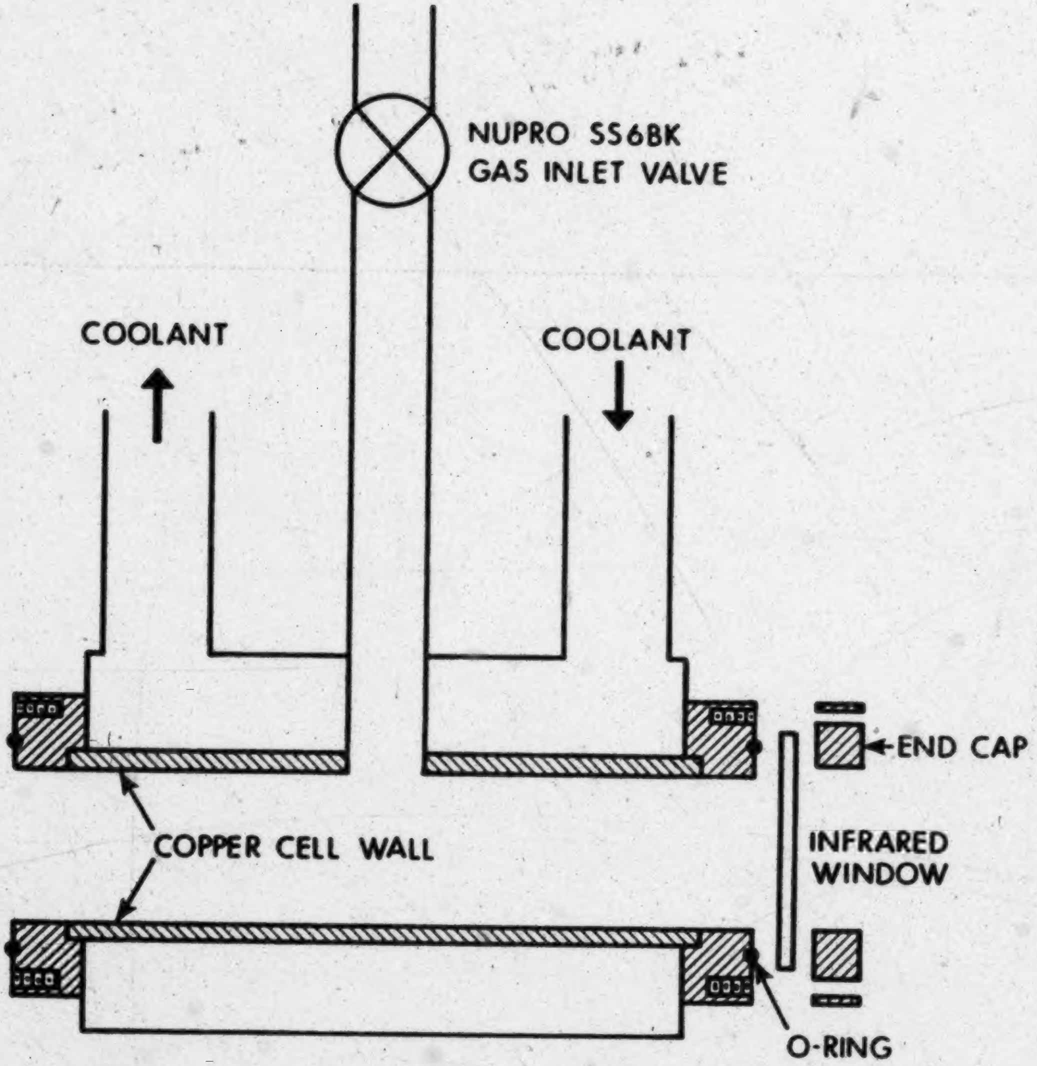
NUPRO SS6BK
GAS INLET VALVE
COOLANT
COOLANT
END CAP
COPPER CELL WALL
INFRARED
WINDOW
O-RING

FIGURE 6. Cross-sectional view of the infrared gas cell. All parts other than the copper cell wall are stainless steel.

tures down to -40°C could be maintained by regulating the flow rate of the nitrogen. The temperature of the cell wall was measured to ± 1°C by a calibrated thermometer or sometimes was measured by copper-constantan thermocouples in contact with the cell wall.

High density polyethylene, 1/16" thick, was used for windows in the range 20-400 cm^{-1} and 6 mm. thick potassium chloride windows were used for the 500 - 4000 cm^{-1} range. Six mm. thick cesium iodide windows were also used in the range 200-650 cm^{-1} but these had to be coated with a thin film of paraffin to prevent attack by hydrogen chloride. This film was applied by wetting the window on one side with a solution of paraffin wax in petroleum ether and allowing the ether to evaporate. These windows were less desirable than potassium chloride in the region above 650 cm^{-1} because the paraffin coating sometimes affected the infrared transmission. The infrared cell and high pressure manifold were tested for safety at high pressures by filling both with 100 PSIG (5870 Torr) of argon. No loss in pressure was noted over a period of at least ten hours with any of the above windows.

2.3 Infrared Spectrophotometers

The infrared spectra in the range 200-4000 cm^{-1} were recorded on a Beckman IR-12 spectrophotometer. A slit program was used such that the resolution was about 2 cm^{-1}

between 650 and 4000 cm^{-1} and about 4 cm^{-1} between 200 and 650 cm^{-1}. Scanning speeds of 20 cm^{-1}/min. between 200 and 2000 cm^{-1} and 40 cm^{-1}/min. between 2000 and 4000 cm^{-1} were used with a pen period of 2 seconds. The instrument was operated under double beam conditions with the reference beam either empty or containing enough ether in a gas cell at room temperature to cancel the absorption due to uncomplexed ether in the sample (Section 3.1). When water vapour was to be removed from the instrument it was purged with air which was dried using a Puregas model HR-211-112-9 dryer. If both water and carbon dioxide were to be removed, the instrument was purged with nitrogen gas, boiled from a liquid nitrogen storage dewar and warmed to room temperature. The infrared cell fitted into the spectrophotometer with the gas valve and the inlet and outlet tubes of the cooling jacket protruding from the sample compartment cover. This cover was made from two plexiglass plates and masking tape, and the cracks between the cover and the tubes passing through it were filled with plasticine. This allowed the instrument purge to be maintained so efficiently that no condensation on the cell was observed, even at -40°C. The frequencies between 200 and 1700 cm^{-1} were measured with respect to a fiducial marker, programmed to produce a mark on the spectrum at 25 cm^{-1} intervals and calibrated against the spectrum of water vapour and the standard gases (91). The frequencies between 1700 and 3000 cm^{-1} were measured with respect to the rotational fine structure of the fundamental vibrational band of either hydrogen chloride or deuterium chloride (91).

The far infrared spectra were recorded on a Beckman IR-11 spectrophotometer and also by using a Beckman R.I.I.C. FS 720 interferometer. Both instruments were calibrated using the hydrogen chloride pure rotation lines (92) and spectra were run at about 1 cm^{-1} resolution. The Beckman-IR 11 was used in the range 80-150 cm^{-1} with a scanning speed of 10 cm^{-1}/min. and a pen period of 8 seconds. The instrument was purged with dry nitrogen, and the cell was sealed into it in the same way as for the IR-12. The interferometer was fitted with a step-drive for the moving mirror and the standard Analogue-Digital converter plus paper tape output was replaced by a Hewlett-Packard model 2401C integrating Digital Voltmeter and an IBM model 026 card punch. The interferograms were recorded both sides of zero path and the spectra were calculated using the Cooley-Tukey, sine plus cosine, Fourier Transform subroutine, RHARM (93), called by a data manipulation program written in this laboratory. The spectra were plotted on an off-line Calcomp plotter. The gas cell used for the interferometer was identical to the one described above except that a metal plate was fixed to the cell, below the gas-inlet valve and the ends of the cooling tubes. An O-ring seal between the plate and cell compartment allowed the interferometer to be evacuated.

CHAPTER 3

RESULTS AND DISCUSSION

3.1 General

In this chapter the infrared absorption spectra of $(CH_3)_2O$---HCl and its isotopic modifications are presented and discussed. Section 3.2 deals with the far infrared region of the spectrum, where the hydrogen bond stretching vibration absorbs, and Section 3.3 deals with the region between 200 and 800 cm^{-1}, where absorptions are assigned to the O---HCl deformation vibrations. In Section 3.4 the absorption by the ethereal modes is presented and discussed in terms of the geometry of the hydrogen-bonded molecule. In Section 3.5 a study of the effect of temperature on the shapes of the bands due to the hydrogen chloride stretching vibrations in the various isotopic modifications of $(CH_3)_2O$---HCl is presented and the features on these bands are assigned. The relative intensities of the absorption bands in the spectrum of $(CH_3)_2O$---HCl are presented in Section 3.6.

In many of the spectral regions described in this chapter the absorption by the hydrogen-bonded molecule was complicated by overlapping absorption by the free components. Absorption by free hydrogen chloride was significant only in the 3000 cm^{-1} and far infrared regions but absorption by free ether occurred in most regions of interest. Attempts were made to minimize the amount of free ether present by cooling the cell and/or by preparing mixtures of high pressures of hydrogen chloride with low pressures of ether, thereby forcing a larger percentage of the ether present to become hydrogen bonded. Unfortunately, in many cases the onset of condensation occurred before the absorption by the free ether became insignificant and it was necessary to subtract this absorption from that by the mixture to obtain the absorption by the hydrogen-bonded molecule. This was done by placing an appropriate pressure of ether in a 10 cm. long gas cell at ambient temperature in the reference beam of the spectrophotometer, or by obtaining the absorbance spectrum of an appropriate pressure of ether in a 10 cm. path length and subtracting it from the absorbance spectrum of the mixture. The latter method proved to be the more advantageous in regions of strong free ether absorption. An uncertainty always existed in choosing the correct amount of ether absorption to subtract, but it was found that the resultant spectra were not critically dependent upon this amount, and in most cases the absorbance subtracted was that due to the same pressure of ether as was used in the mixtures. The absorption by the free ether was not found to be significantly affected by temperature or by pressure-broadening by an inert gas and thus the temperature of, and the total pressure within the reference ether cell was not important.

In addition to bands which could be assigned to either the hydrogen-bonded molecule or to the free components, the infrared spectra of mixtures of the components often contained bands which grew in intensity with time. To confirm that none of the bands assigned to the hydrogen-bonded molecule in fact arose from some reaction product, spectra of various mixtures of the components were recorded at various intervals over a period of twenty-four hours. Any band which grew in intensity could not then be assigned to some mode of the hydrogen-bonded molecule. The main reaction products were found to be methyl chloride, which formed fairly rapidly when the partial pressure of each component was large, and a thin yellow film, probably copper (II) chloride, which was slowly deposited throughout the cell and on the cell windows, causing a decrease in the infrared transparency of the cell.

3.2 Far Infrared Region

In the region below 200 cm^{-1} only one band which was not present in the spectra of the free components was observed. In Figure 7, curves A, B, and C show the spectra between 90 and 150 cm^{-1} of a mixture of 325 Torr of dimethyl ether-h_6 with 325 Torr of hydrogen chloride at 0°C, 10°C and 20°C respectively. A band which is not present in the spectrum of pressure-broadened hydrogen chloride (curve D) or pressure-broadened dimethyl ether-h_6 (curve E) is clearly visible close to the $J = 5 \rightarrow 6$ pure rotation line of the free hydrogen chloride. The absence of an absorption at this frequency in the spectra of the pressure-broadened unmixed components indicates that the absorption present in

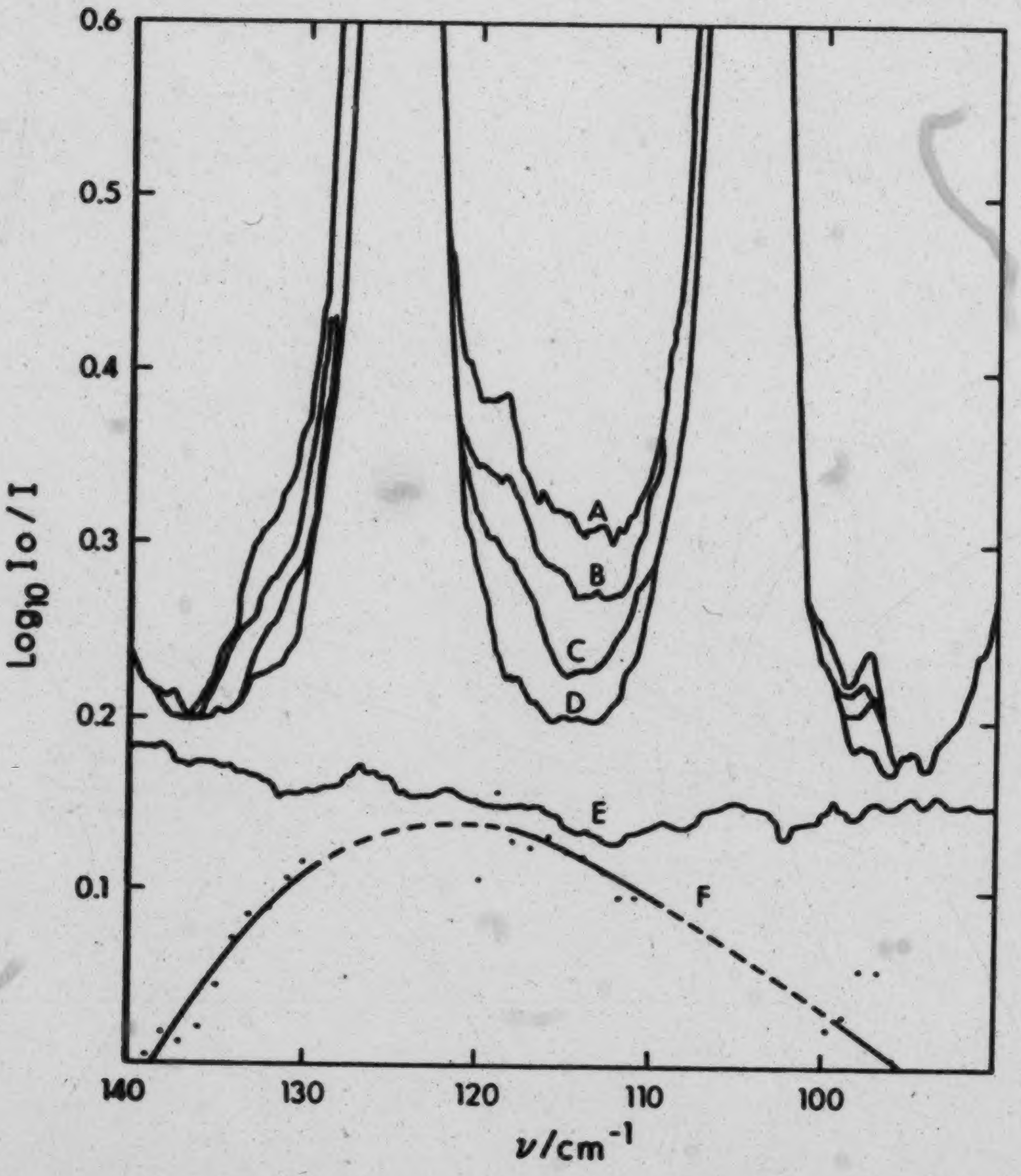

FIGURE 7. Curves A, B and C show absorption by 325 Torr of dimethyl ether-h_6 plus 325 Torr of hydrogen chloride at 0°C, 10°C and 20°C, respectively. Curves D and E show absorption at 0°C by 325 Torr of hydrogen chloride and 325 Torr of dimethyl ether-h_6, respectively, each pressure broadened with 325 Torr of air. Curve F was obtained by subtracting the absorption in curves D and E from that in curve A.

spectra of the mixtures arises from a specific interaction between the components rather than from a pressure-broadening effect such as is observed for the trimethylamine-methanol system (67,68). The intensity of the band increases reversibly as the sample temperature is lowered from 20°C to 0°C and is the kind of temperature dependence which is expected for an absorption by a hydrogen-bonded molecule in dynamic equilibrium with its component molecules. Curve F in Figure 7 shows the spectrum obtained by subtracting the absorption due to the unmixed gases from that of the mixture at 0°C. Due to the strong absorption by free hydrogen chloride, the resultant band in curve F is poorly defined but it has a half-width of about 25-30 cm^{-1} and its maximum is at 119 ± 4 cm^{-1}.

Spectra of 440 Torr of dimethyl ether-h_6 mixed with 220 Torr of hydrogen chloride and 220 Torr of dimethyl ether -h_6 mixed with 440 Torr of hydrogen chloride, both at 0°C, showed the same absorption as that shown in Figure 7. The intensity of the absorption by the 2:1 mixture was the same as that by the 1:2 mixture, but was slightly less intense than the absorption by the 1:1 mixture. This behavior can be predicted from a simple calculation of the equilibrium concentration of the hydrogen-bonded molecule if one assumes that the molecule is composed of dimethyl ether-h_6 and hydrogen chloride in equal proportions. Further, the 25-30 cm^{-1} half-width of the band is consistent with that calculated for the rotational envelope of a vibrational transition in the molecule $(CH_3)_2O$---HCl (Section 3.4), so the band can confidently be assigned to this molecule.

In Figure 8, curve A shows the spectrum of a mixture of 325 Torr of dimethyl ether-h_6 with 325 Torr of deuterium chloride at 0°C and curves B and C, respectively, show the spectra of free deuterium chloride and free dimethyl ether -h_6, both pressure-broadened with dry air at 0°C. In spite of the very strong absorption by the free deuterium chloride, a band close to 120 cm^{-1} is clearly visible in the spectrum of the mixture. The intensity of this band was found to decrease, reversibly, as the temperature was raised from 0°C. Curve D shows the spectrum obtained by subtracting the absorption by the unmixed gases from that by the mixture and, although curve D is poorly defined, it shows that the band is very similar in frequency and half-width to the band displayed in curve F of Figure 7. It follows, from the assignment of the latter band to $(CH_3)_2O$---HCl, that the band displayed in curve D of Figure 8 arises from $(CH_3)_2O$---DCl.

In Figure 9, curve A shows the spectrum of a mixture of 325 Torr of dimethyl ether-d_6 with 325 Torr of hydrogen chloride at 0°C and curves B and C show the spectra of the pressure-broadened unmixed gases at 0°C. The spectrum obtained by subtracting the absorption by the unmixed gases from that of the mixture is shown in curve D and reveals a band with a half-width which is comparable to the half-widths of the bands shown in Figures 7 and 8. The band shown in

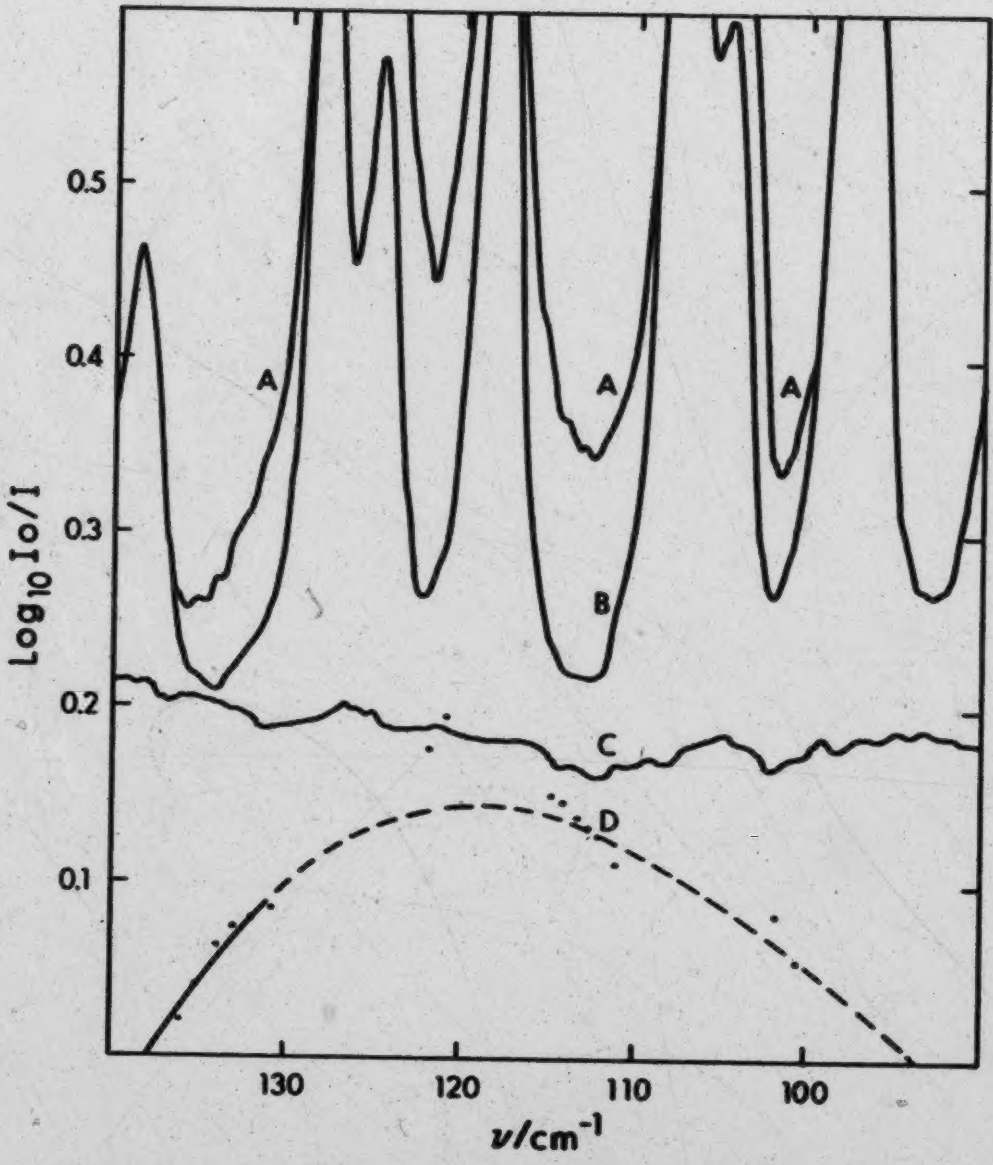

FIGURE 8. Infrared absorption by mixtures at 0°C of: 325 Torr of dimethyl ether-h_6 plus 325 Torr of deuterium chloride (curve A); 325 Torr of deuterium chloride plus 325 Torr of dry air (curve B); 325 Torr of dimethyl ether-h_6 plus 325 Torr of dry air (curve C). Curve D was obtained by subtracting the absorption in curves B and C from that in curve A.

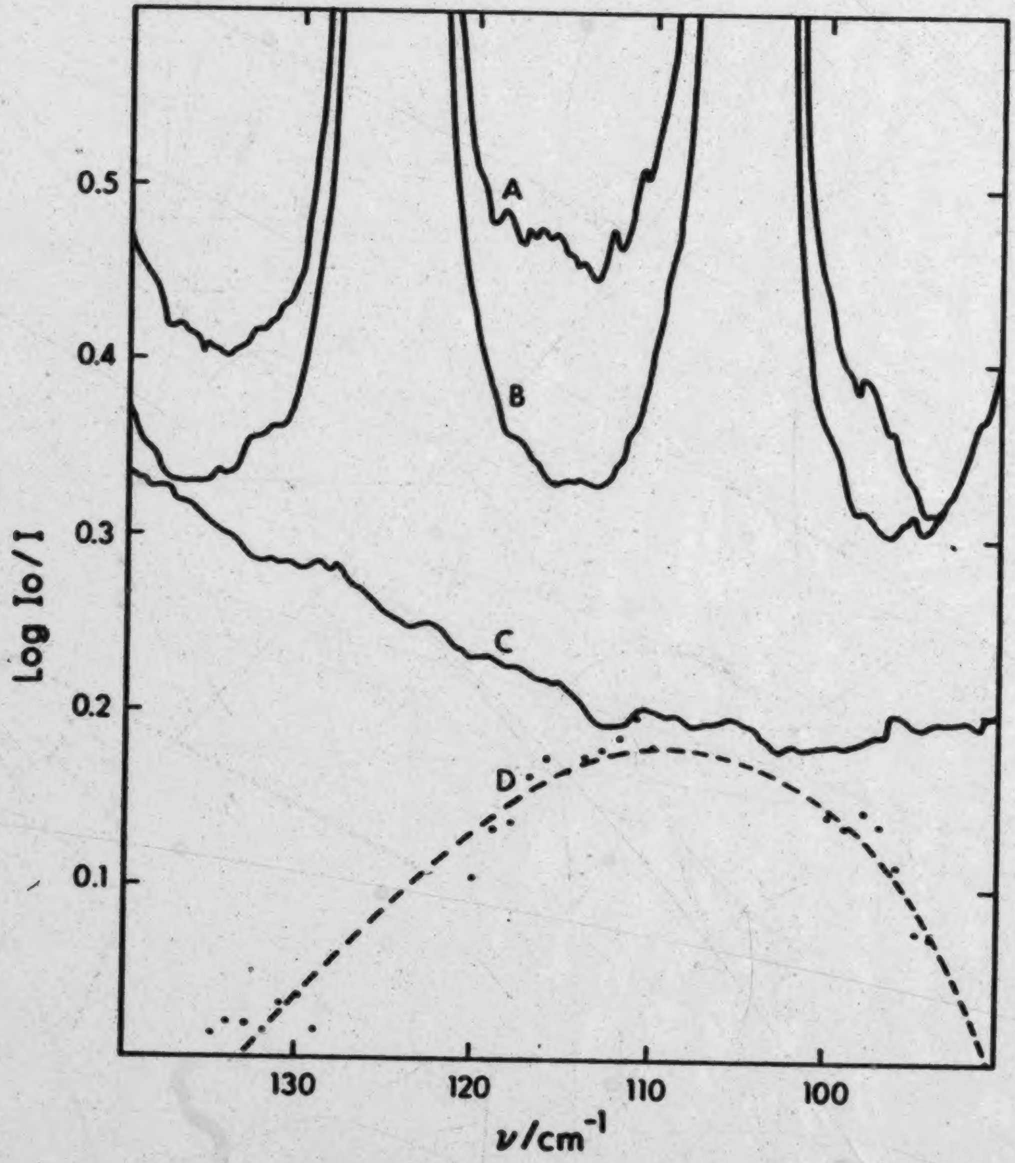

FIGURE 9. Infrared absorption by mixtures at 0°C of: 325 Torr of dimethyl ether-d_6 plus 325 Torr of hydrogen chloride (curve A); 325 Torr of hydrogen chloride plus 325 Torr of dry air (curve B); 325 Torr of dimethyl ether-d_6 plus 325 Torr of dry air (curve C). Curve D was obtained by subtracting the absorption in curves B and C from that in curve A.

curve D of Figure 9 lies about 5 - 10 cm^{-1} to low frequency of those shown in Figures 7 and 8 although this frequency shift may appear to be much larger than it really is due to errors in subtracting the absorption due to the unmixed gases. This band was found to decrease in intensity as the temperature was raised from 0°C and it is clear that the bands observed in all three mixtures arise from either the ν_σ or ν_β modes of the hydrogen-bonded molecule. In general, an angle bending or torsional mode is expected to absorb at a lower frequency than a stretching mode involving the same atoms (94), but no other band which could be assigned to one of these three modes was found above or below the band close to 119 cm^{-1}. The HCl wagging modes, however, are expected to absorb very weakly and below 100 cm^{-1} (13) and probably interact with the rotation of the molecule. Indirect evidence is also given in Section 3.3 that these modes absorb at about 50 cm^{-1}. Thus the band at 119 cm^{-1} is assigned to the hydrogen bond stretching mode, ν_σ, in agreement with Belozerskaya and Shchepkin (75). This frequency is close to the frequency predicted for ν_σ in $(CH_3)_2O$---HCl by Bertie and Millen (73).

A knowledge of the anharmonicity of the hydrogen bond stretching mode is important to the theoretical understanding of hydrogen-bonded systems. A study of the contribution of the hot bands of the fundamental (42) to the stfucture of the 119 cm^{-1} band could lead to a semi-quantitative evaluation of the anharmonicity of this mode in the ether-hydrogen chloride molecule, and attempts were made to obtain a clearer view of the band for this purpose. Calculations indicated that much of the interfering absorption due to free hydrogen chloride could be removed by simply increasing the partial pressure of the ether while decreasing the partial pressure of the hydrogen chloride. Spectra of mixtures of 50 to 100 Torr of hydrogen chloride with up to 1500 Torr of dimethyl ether-h_6 were recorded but the absorption by the ether in this region, which is not a problem at a pressure of 440 Torr, was sufficiently strong at the higher pressures to prevent better spectra from being obtained.

3.3 Infrared Spectra Between 200 and 800 cm^{-1}

In box I of Figure 10, curve A shows the spectrum between 300 and 600 cm^{-1} of a mixture at -30°C of 880 Torr of hydrogen chloride with 110 Torr of dimethyl ether-h_6 Curve B shows the spectrum of 110 Torr of dimethyl ether-h_6 at -30°C and curve C shows the spectrum obtained by subtracting the absorption due to the ether from the absorption due to the mixture. Hydrogen chloride does not absorb in this region and its spectrum is not shown. Curve C displays a broad absorption extending from about 325 to 590 cm^{-1} which has a half-width of about 150 cm^{-1} and is not present in the spectrum of the free ether. Superimposed on the band are several sub-bands, the most prominent of

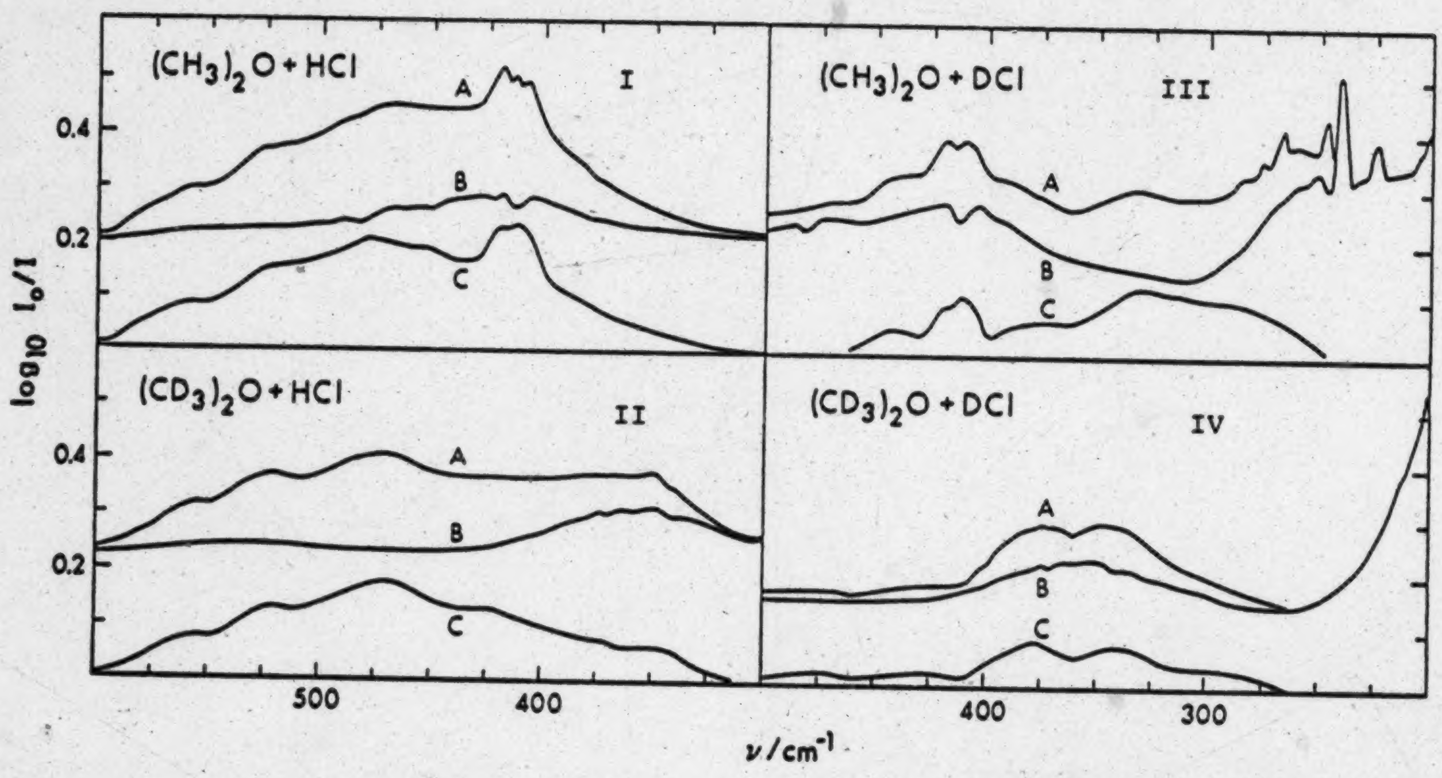

FIGURE 10 Curves A: infrared absorption by mixtures of 110 Torr of dimethyl ether-h_6 or dimethyl ether-d_6 plus 880 Torr of hydrogen chloride or deuterium chloride, as indicated, at -30°C. Curves B: infrared absorption by 110 Torr of dimethyl ether-h_6 (boxes I and III) or dimethyl ether-d_6 (boxes II and IV) at -30°C. In each box curve C was obtained by subtracting curve B from curve A.

which is a peak with a half-width of about 20 cm^{-1} centered at 415 cm^{-1}. In addition, three relatively strong features, at 480, 525 and 570 cm^{-1}, are evident as well as weak shoulders at about 440 and 380 cm^{-1}. Due to uncertainties in the appropriate amount of free ether absorption to subtract, these latter two features, as well as the doublet character of the peak at 415 cm^{-1} and the rather sharp top to the feature at 480 cm^{-1}, may not be real.

Spectra of samples at 30, -10 and -30°C showed that the intensity of the band increased with decreasing temperature in spite of some condensation occurring at -30°C. This temperature dependence of the intensity of the band and the absence of the absorption in spectra of the unmixed gases are consistent with the assignment of the band to a hydrogen-bonded product molecule. Further, spectra of 440 Torr of hydrogen chloride with 220 Torr of dimethyl ether-h_6 at -30°C showed the same absorption as shown in box I in Figure 10 and revealed that the relative intensities of the features at 570, 525, 480, 415 cm^{-1} did not depend upon whether the ratio of acid to ether was 2:1 or 8:1. This is consistent with the assignment of the whole band to the 1:1 hydrogen-bonded molecule, $(CH_3)_2O{-}{-}{-}HCl$.

In box II of Figure 10, curve A shows the spectrum between 300 and 600 cm^{-1} of a mixture at -30°C of 880 Torr of hydrogen chloride with 110 Torr of dimethyl ether-d_6 and curve B shows the spectrum of 110 Torr of dimethyl ether-d_6 at -30°C. The subtraction spectrum, shown in curve C, displays an absorption with a half-width of about 150 cm^{-1} between 325 and 590 cm^{-1} that is very similar to the absorption shown in curve C of box I. A study of the effect of temperature on the intensity of the band and of the effect of changing the acid to ether ratio showed that the absorption arises from the 1:1 hydrogen-bonded molecule, $(CD_3)_2O$---HCl.

The main differences between the bands displayed in curves C of boxes I and II occur below 450 cm^{-1}. Most striking is the absence, in box II, of a peak at 415 cm^{-1}. Since this peak is present only in spectra of mixtures containing dimethyl ether-h_6 it must arise from a vibrational mode in the ethereal part of the $(CH_3)_2O$---HCl molecule. The absorption by the free dimethyl ether-h_6 between 375 and 500 cm^{-1} has been assigned to the C-O-C deformation mode (95,96) and the 415 cm^{-1} absorption by $(CH_3)_2O$---HCl is clearly due to the analogous mode in the ethereal part of the molecule. Curve C of box II displays a weak feature at about 340 cm^{-1} which is not present in curve C of box I and which falls in the region of absorption by the C-O-C deformation mode of dimethyl ether-d_6 (95). By analogy with the argument used for the assignment of the 415 cm^{-1} peak in the spectrum of $(CH_3)_2O$---HCl, the feature at 340 cm^{-1} may be assigned to the C-O-C deformation mode in $(CD_3)_2O$---HCl. The very weak feature at about 370 cm^{-1} in the spectrum of $(CD_3)_2O$---HCl is probably spurious.

Above 450 cm^{-1} the absorption does not depend significantly upon which ether is present in the mixture. The shoulders at 570 and 525 cm^{-1} on the band displayed in box II coincide almost exactly with similar features in box I. The absorption maximum in $(CD_3)_2O{-}{-}{-}HCl$ is a smooth feature centered at 470 cm^{-1} and coincides closely with the feature at 480 cm^{-1} on the absorption by $(CH_3)_2O{-}{-}{-}HCl$ (this feature may be slightly higher in frequency than it should be due to poor cancellation of the free ether absorption). This series of sub-bands, at 570, 525 and 470 cm^{-1}, has a spacing of about 50 cm^{-1} and leads to the conclusion that the shoulder at 425 cm^{-1} in the spectrum of $(CD_3)_2O{-}{-}{-}HCl$ is also a member of the group, but due to overlapping absorption is not seen in the spectrum of $(CH_3)_2O{-}{-}{-}HCl$.

The features which are common to the spectra of $(CH_3)_2O{-}{-}{-}HCl$ and $(CD_3)_2O{-}{-}{-}HCl$ in this frequency region must have their origin in the O---H-Cl part of the molecules. Of the six vibrational modes confined to this part of the molecule (Figure 4), only ν_b or ν_t, the O---H-Cl deformation modes, can reasonably be expected to give rise to absorption in this region. Proof that this absorption is due to ν_b and/or ν_t was obtained by recording spectra analogous to those shown in boxes I and II of Figure 10, but with deuterium chloride in place of hydrogen chloride. In box III, curve A shows the spectrum of a mixture at -30°C of 880 Torr of deuterium chloride with 110 Torr of dimethyl ether-h_6 and curve B shows that of 110 Torr of dimethyl ether-h_6 at -30°C. The subtraction spectrum, shown in curve C, reveals that, except for the peak at 415 cm^{-1}, the absorption by $(CH_3)_2O{-}{-}{-}DCl$ is centered at a lower frequency than that by $(CH_3)_2O{-}{-}{-}HCl$ and thus can only arise from a vibrational mode involving the motion of the hydrogen-bonded hydrogen atom. Of the vibrational modes confined to the O---H-Cl part of the molecule, other than ν_b or ν_t, only ν_s, the H-Cl stretching mode, involves this motion. This mode, however, is known to absorb close to 2500 cm^{-1} (73) and therefore cannot give rise to absorption in the 450 cm^{-1} region.

The peak at 415 cm^{-1} in the spectrum of $(CH_3)_2O{-}{-}{-}HCl$ was assigned above to the C-O-C deformation mode and is not expected to shift in frequency by isotopic substitution of an atom outside the ethereal part of the molecule. Thus the peak at 415 cm^{-1} in the spectrum of $(CH_3)_2O{-}{-}{-}DCl$ clearly arises from this mode. The remainder of the absorption shown in curve C of box III is rather weak but features at 440, 375, 330 and 285 cm^{-1} are evident. These features are nearly coincident with features at about 430, 380, 340 and 290 cm^{-1} seen on curve C in box IV, which shows the analogous subtraction spectrum of $(CD_3)_2O{-}{-}{-}DCl$. Although vibrational modes in the ethereal parts of the $(CH_3)_2O{-}{-}{-}DCl$ and $(CD_3)_2O{-}{-}{-}DCl$ molecules clearly influence the relative intensities and, to a lesser extent, the frequencies of the features, the major portion of these absorptions must be assigned to modes in the O---D-Cl part of the molecules. The feature at 340 cm^{-1} in the spectrum of $(CD_3)_2O$---DCl must include absorption by the C-O-C deformation mode as this mode absorbs at 340 cm^{-1} in $(CD_3)_2O$---HCl and is not expected to shift in frequency in $(CD_3)_2O$---DCl.

Some of the differences between the spectra of $(CH_3)_2O$---DCl and $(CD_3)_2O$---DCl may arise from errors in the subtraction of the free ether absorption from that of the mixture since the absorption by the ether is of the same order of magnitude as that by the hydrogen-bonded molecule. However, spectra of other mixtures with the same partial pressures of components contained features at the same frequencies although their relative intensities varied somewhat in different spectra. Attempts were made to obtain more intense absorption by all four isotopic modifications of $(CH_3)_2O$---HCl by increasing the partial pressure of the acid in the mixtures and by cooling the gas cell below -30°C. Unfortunately, the onset of condensation and the rapid formation of reaction products under these conditions prevented better spectra than those presented from being obtained.

The bands assigned above to the O---H-Cl deformation modes, ν_b and/or ν_t, have many of the characteristics of those due to the H-Cl stretching mode, ν_s (Section 3.5). In each case the bands are extremely broad, with a half-width about five to ten times that expected for a band due to a single fundamental transition in $(CH_3)_2O$---HCl or $(CD_3)_2O$---HCl, and complex, with four equally-spaced features. The breadth and complexity of the band due to the ν_s mode has been attributed (73) to interactions between ν_s and ν_σ, the hydrogen bond stretching mode. By analogy, the breadth and complexity of the bands due to ν_b and/or ν_t probably arise from interaction of these modes with the HCl wagging modes, ν_{β_1}, and ν_{β_2}. Thus the observed features on these bands may be assigned to transitions of the type ν_b, or ν_t, $\pm\ n\nu_\beta$, where n is integral or zero. From the separation of the features the fundamental frequency of the ν_β modes must be about 50 cm^{-1}. The frequency of the ν_β modes is not expected to be significantly different in the DCl complexes and thus the observation that the features on the bands due to the O---D-Cl deformation modes are separated by about 50 cm^{-1} leads to the conclusion that these features also are due to transitions of the type ν_b, or ν_t, $\pm\ n\nu_\beta$.

If the hydrogen chloride molecule attaches itself to one of the lone pairs of electrons on the oxygen atom of the ether molecule, the hydrogen-bonded molecule belongs to the point group C_s (Section 3.4). The only element of symmetry is a mirror plane which contains the hydrogen chloride molecule and the oxygen atom of the ether and which bisects the C-O-C bond angle. ν_b is defined as the in-plane O---H-Cl deformation mode in which motion of the hydrogen-bonded hydrogen atom is parallel to this plane and ν_t is the out-of-plane mode and involves motion of the hydrogen atom perpendicular to this plane. Thus ν_b and ν_t have different symmetries and cannot interact with each other. Symmetry arguments, however, permit any sum or difference band of ν_b or ν_t with either ν_{β_1} the in-plane HCl wagging mode, or ν_{β_2} the out-of-plane HCl wagging mode. Thus, the bands of the type $\nu_b \pm n\nu_{\beta_2}$ and $\nu_t \pm n\nu_{\beta_1}$ are as probable as those of the type $\nu_b \pm n\nu_{\beta_1}$ and $\nu_t \pm n\nu_{\beta_2}$, although the modes in the former combinations do not take place in the same plane while those in the latter combinations do. Thus no distinction between the ν_β modes in the combinations with ν_b and ν_t can be made on symmetry grounds, although intuitively one would expect combinations of modes in which atomic displacements take place in the same plane to be more likely to occur than those in which the atomic displacements are perpendicular to each other.

Since a difference transition originates in an excited vibrational energy level, a difference band must decrease in intensity as the temperature is lowered due to depopulation of molecules of that level. However, calculations showed that the Boltzmann distribution of molecules between the ground state and levels up to 100 cm^{-1} above it was not significantly dependent upon the temperature between +30°C and -30°C, and a change in intensity of a difference band such as $\nu_b - \nu_\beta$ would not be detected in this temperature range. Thus the observed constancy of the bandshape with temperature does not rule out the contribution of such difference bands to the structure of the O---H-Cl and O---D-Cl deformation bands.

Before the assignment of the features of these bands is discussed in more detail, the spectra shown in Figure 11 must be presented. Curves A and B, respectively, show the absorption between 700 and 875 cm^{-1} by a mixture of one atmosphere of dimethyl ether-h_6 with two atmospheres of hydrogen chloride, and by a mixture of two atmospheres of dimethyl ether-h_6 with one atmosphere of hydrogen chloride, both at +35°C. A broad band, centered at about 790 cm^{-1}, is clearly evident in both curves, but is not present in the spectra of the free ether (curve D) or the free hydrogen chloride (curve E). The absorption is overlapped above 825 cm^{-1} by a strong band due to the symmetric C-O stretching mode of dimethyl ether-h_6 (95,96) and thus no reliable measurement of its half-width can be made. Its intensity, which is about one-sixth of that of the band centered at 470 cm^{-1} in $(CH_3)_2O$---HCl, is the same for dimethyl ether -h_6 : hydrogen chloride ratios of 1:2 and 2:1. In the spectra of mixtures with a total pressure of one atmosphere the intensity at 790 cm^{-1} was found to increase reversibly as the temperature was lowered to the onset of condensation. Thus the band is assigned to the $(CH_3)_2O$---HCl molecule. Curve C shows the spectrum of a mixture of two atmospheres of dimethyl ether-h_6 with one atmosphere of deuterium chloride at +35°C. Comparison of curves B and C shows that

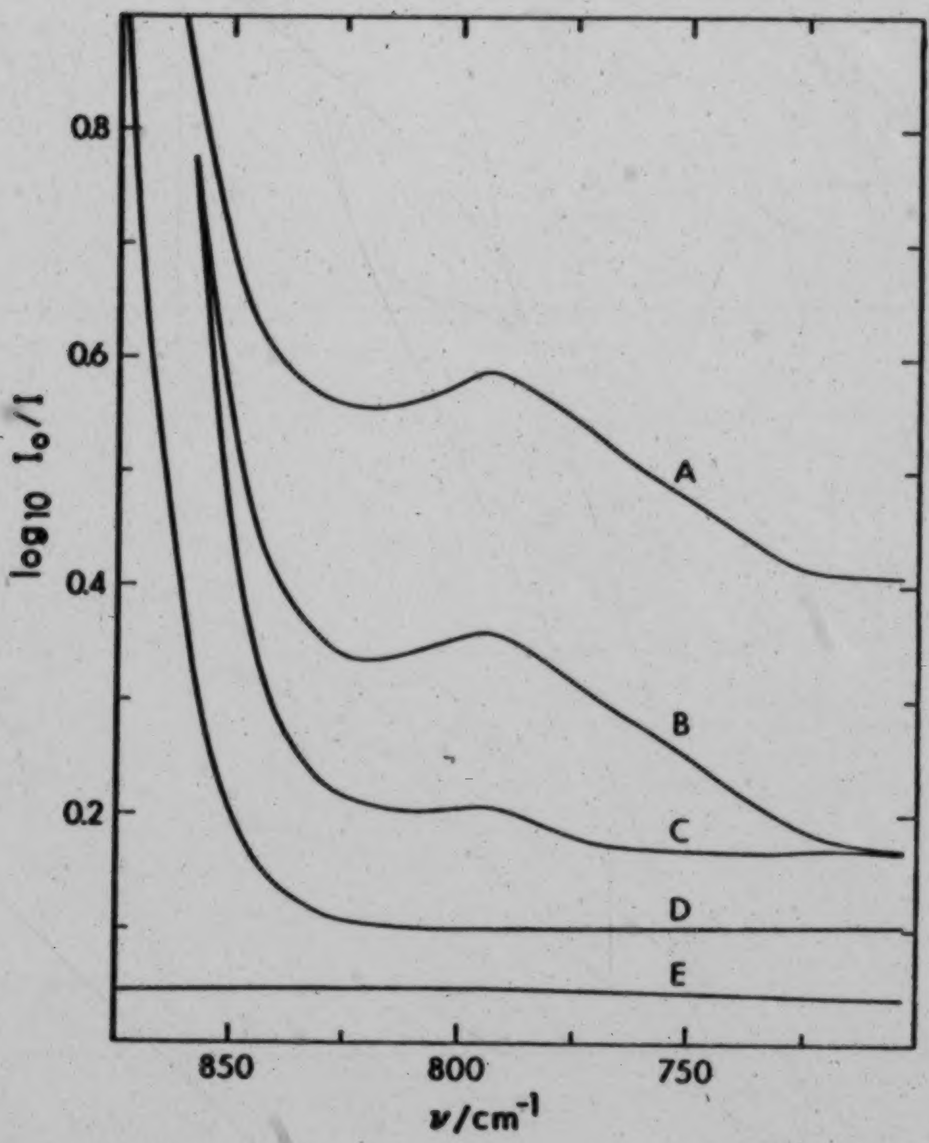

__FIGURE 11__. Infrared absorption at +35°C by: 1 atm of dimethyl ether-h_6 mixed with 2 atm of hydrogen chloride (curve A); 2 atm of dimethyl ether-h_6 mixed with 1 atm of hydrogen chloride (curve B); 2 atm of dimethyl ether-h_6 mixed with 1 atm of deuterium chloride (curve C); 1 atm of dimethyl ether-h_6 (curve D); 1 atm of hydrogen chloride (curve E).

the broad absorption at 790 cm^{-1} has almost completely disappeared in the latter case, leaving only a weak feature about one-twentieth as intense as that in curve B. The deuterium chloride contained at least 5% hydrogen chloride as an impurity and the residual band may be assigned to $(CH_3)_2O$---HCl rather than $(CH_3)_2O$---DCl.

Since the band is not present at 790 cm^{-1} in the spectrum of $(CH_3)_2O$---DCl, it must arise from a mode in which the motion of the hydrogen-bonded hydrogen atom is important. Only two assignments appear to be possible for this feature. Either it is due to one of the O---H-Cl deformation modes or to the first overtone of one of these modes. In either case a band should be present at 790 cm^{-1} in the spectrum of $(CD_3)_2O$---HCl and one at a lower frequency in the spectrum of $(CD_3)_2O$---DCl or $(CH_3)_2O$---DCl. The spectrum of $(CD_3)_2O$---HCl in the 790 cm^{-1} region could not be obtained because of a strong overlapping absorption due to the symmetric C-O stretching mode of the dimethyl ether-d_6 (95) but the spectrum between 500 and 650 cm^{-1} of $(CD_3)_2O$---DCl is presented in Figure 12. Curve A shows the absorption by a mixture of two atmospheres of dimethyl ether-d_6 with one atmosphere of deuterium chloride at +35°C. A very weak, broad absorption extending from about 550 to 620 cm^{-1} is just visible in the spectrum of the mixture but is not present in the spectrum of the free ether (curve B) or free deuterium chloride (curve C). The weak absorption

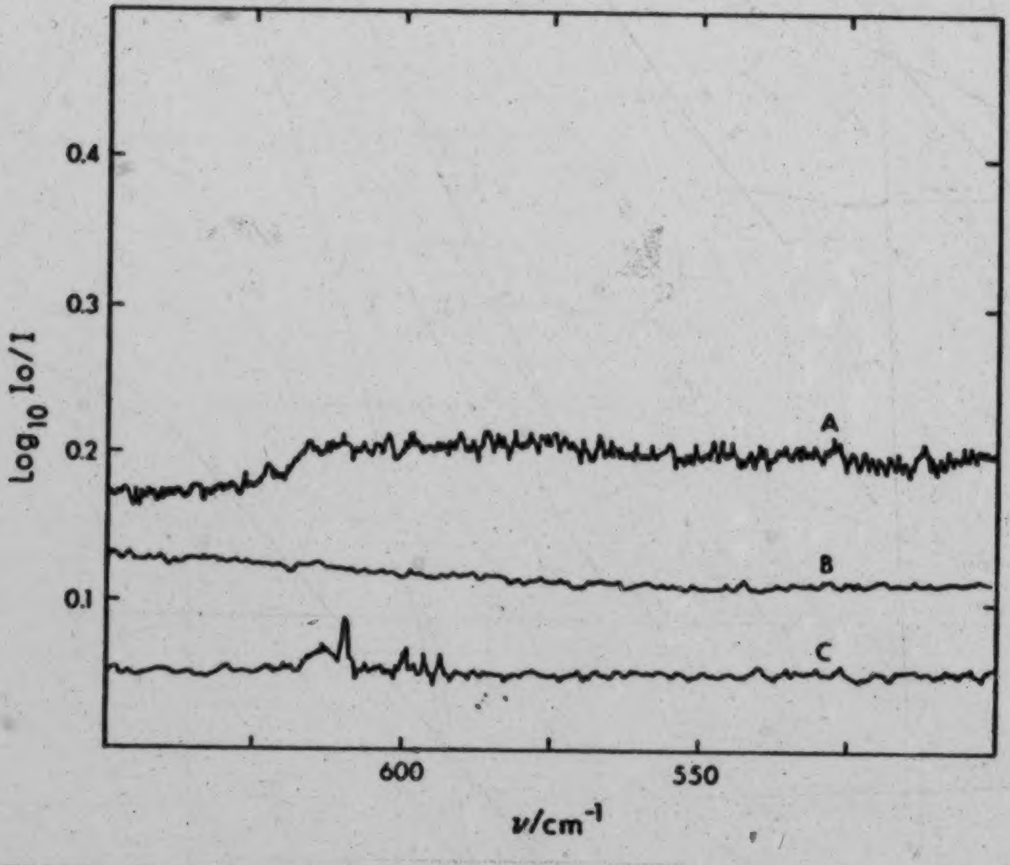

FIGURE 12. Infrared absorption at +35°C by: 2 atm of dimethyl ether-d_6 mixed with 1 atm of deuterium chloride (curve A); 2 atm of dimethyl ether-d_6 (curve B); 1 atm of deuterium chloride (curve C).

close to 600 cm^{-1} shown in curve C arises from a thin yellow film which was present as an impurity on the cell windows (Section 3.1). To show that the weak feature shown in curve A actually arose from $(CD_3)_2O{-}{-}{-}DCl$ rather than from this film, the infrared cell was evacuated immediately after recording the spectrum of the mixture and the spectrum of the cell was recorded. The feature was not observed in this spectrum and therefore cannot arise from absorption by the cell. Attempts to observe this band with greater intensity, by cooling the cell and increasing the pressures of the components, resulted in either condensation of the complex or rapid formation of methyl chloride and were not successful.

The assignment of the 790 cm^{-1} absorption by $(CH_3)_2O{-}{-}{-}HCl$ and the 600 cm^{-1} absorption by $(CD_3)_2O{-}{-}{-}DCl$ to analogous modes necessitates a discussion of the relative intensities of the bands. It has been shown (97) that the intensity of ν_s in free deuterium chloride is about one half of that in free hydrogen chloride. Since ν_b and ν_t involve primarily the motion of the hydrogen-bonded hydrogen atom, one would expect the intensity of ν_b or ν_t in the deuterium chloride complexes to be about one-half of that in the hydrogen chloride ones. Clearly the intensity of the absorption by $(CD_3)_2O{-}{-}{-}DCl$ is much less than one-half of that by $(CH_3)_2O{-}{-}{-}HCl$. However, the absorption at 790 cm^{-1} is not far removed from an extremely strong absorption due to the C-O symmetric stretching mode of the ether.

If the 790 cm^{-1} absorption is due to a mode which has the same symmetry as the ethereal mode, it is possible for the weaker absorption to gain intensity through Fermi resonance (Section 1.6). The symmetric C-O stretching mode belongs to the A' symmetry species under the point group C_s, allowing such an interaction to take place if the 790 cm^{-1} band were due to either ν_b or to the first overtone of either ν_b or ν_t. In $(CD_3)_2O$---DCl there is no strong absorption close to 600 cm^{-1} and thus no intensity enhancement through Fermi resonance is possible.

The ν_b and ν_t modes have been assigned to features of approximately the same intensity at 755 and 655 cm^{-1} in the spectrum of $(CH_3)_2O$---HF (78) and at 550 and 490 cm^{-1} in the spectrum of $(CH_3)_2O$---DF (78). As is the case for $(CH_3)_2O$---HCl and $(CH_3)_2O$---DCl, it is impossible to determine which mode has the higher frequency as both ν_b and ν_t show similar isotopic shifts and neither exists in the absence of the hydrogen bond. The separation of 90 cm^{-1} between the modes in $(CH_3)_2O$---HF makes it very difficult to justify the assignment of one of these modes in $(CH_3)_2O$---HCl at 790 cm^{-1} and the other near to 470 cm^{-1}. It is probable, therefore, that ν_b and ν_t are both contained in the 470 cm^{-1} band and that the 790 cm^{-1} band is the absorption by $2\nu_b$ or $2\nu_t$. The 600 cm^{-1} absorption by $(CD_3)_2O$---DCl must then be assigned to $2\nu_b$ or $2\nu_t$, with the fundamentals absorbing below 400 cm^{-1}.

Unfortunately, the ν_b and ν_t modes cannot be uniquely assigned. If the ratio of the frequencies of ν_b and ν_t is the same for the HCl and DCl complexes as for the HF and DF ones, respectively, then ν_b and ν_t must be separated by about 60 cm^{-1} close to 500 cm^{-1} and by about 40 cm^{-1} close to 350 cm^{-1}. Since features were observed at 340 and 380 cm^{-1} in the spectrum of $(CD_3)_2O$---DCl, they may be assigned to ν_b and ν_t. Their assignment at 470 and 525 cm^{-1} for the HCl complexes yields an isotopic ratio of 1.38 for both bands, compared to 1.40 under the harmonic approximation, if it is assumed that ν_b is higher (or lower) than ν_t in both the HCl and DCl complexes. This assignment, however, suggests that 790 cm^{-1} is a very low frequency for the first overtone of ν_b or ν_t. It is possible that this feature is at the low frequency end of a broad absorption, most of which is hidden by the much stronger band above 850 cm^{-1}. It is also possible that, because of the vibrational Franck-Condon effect (Section 1.6), the most intense transition in the overtone band is not the overtone of the most intense transition in the fundamental band. An alternative assignment which uses this feature is to assign ν_b and ν_t at 470 and 420 cm^{-1} in the HCl complexes and at 340 and 290 cm^{-1} in the DCl complexes but the isotopic ratio, 420/290 = 1.45, is somewhat large.

It is useful to use these frequencies to calculate ω_e and $\omega_e x_e$ where

$$G(v) = \omega_e(v + 1/2) - \omega_e x_e(v + 1/2)^2 \qquad (1)$$

as defined by Herzberg (98). G(v) is the energy term of the v^{th} vibrational energy level, ω_e is the harmonic contribution to G(v), and $\omega_e x_e$ is the anharmonic constant. From this equation the following expressions are obtained for the fundamental and first overtone frequencies of the ν_b (or ν_t) mode:

$$\nu_b = \omega_e - 2\omega_e x_e \qquad (2a)$$

$$2\nu_b = 2\omega_e - 6\omega_e x_e \qquad (2b)$$

Once ω_e and $\omega_e x_e$ for the HCl complexes have been calculated from these expressions, those for the DCl complexes, denoted by ω_e^D and $\omega_e x_e^D$, may be computed (99) from the following formulae:

$$\omega_e^D = \rho\omega_e \qquad (3a)$$

$$\omega_e x_e^D = \rho^2\omega_e x_e \qquad (3b)$$

where $\rho^2 = G_D/G_H$, where G_D and G_H are the G matrix elements (100) for the O---D-Cl and O---H-Cl deformation coordinates, respectively. These elements correspond to the element $G^3_{\phi\phi'}$, defined in appendix VI of reference 36. If the oxygen, hydrogen and chlorine atoms are taken to be colinear, with $r_{O--H} = r_{O--D} = 1.7$ Å and $r_{HCl} = r_{DCl} = 1.4$ Å, G_H and G_D

are 1.7193 and 0.8786 amu^{-1} Å^{-2}, respectively. The masses of the atoms used in the calculation were taken from reference 101. The values of G_D and G_H yield $\rho^2 = 0.5111$ and $\rho = 0.7149$.

For the sake of simplicity in the following discussion the 790 cm^{-1} band is assumed to arise from $2\nu_b$, the first overtone of the ν_b mode, although it is impossible to determine whether it arises from $2\nu_b$ or $2\nu_t$. The most reasonable agreement with this overtone frequency is obtained if ν_b is assigned at 420 or 470 cm^{-1}. To assign ν_b at 570 or 525 cm^{-1} leads to unreasonably large positive anharmonic terms, but one of these features may well be due to the other deformation mode, ν_t. If ν_b is assigned at 470 cm^{-1} then $\omega_e = 620$ cm^{-1}, $\omega_e x_e = 75$ cm^{-1}, $\omega_e^D = 443$ cm^{-1} and $\omega_e x_e^D = 38.3$ cm^{-1}. Substitution of these values into equations 2a and 2b predicts $\nu_b = 367$ cm^{-1} and $2\nu_b = 657$ cm^{-1} in the DCl complexes. The weak feature observed in the spectrum of $(CD_3)_2O$---DCl (Figure 12) was definitely at a lower frequency than 657 cm^{-1}, but 367 cm^{-1} is close to an observed feature at 380 cm^{-1}. The pairing of 470 and 380 cm^{-1} indicates that 525 and 340 cm^{-1} must correspond to the same vibration. Thus, this assignment requires that the anharmonicities be very large indeed, and does not agree well with the overtone frequency for $(CD_3)_2O$---DCl. The second assignment, in which 790 cm^{-1} is taken to be the first overtone of 420 cm^{-1}, yields

$\omega_e = 470\ \text{cm}^{-1}$, $\omega_e x_e = 25\ \text{cm}^{-1}$, $\omega_e^D = 336\ \text{cm}^{-1}$, and $\omega_e x_e^D = 12.8\ \text{cm}^{-1}$, and predicts the corresponding frequencies for the DCl complex to be 595 and 310 cm^{-1}. The former agrees well with the observed overtone absorption in the DCl complex but 310 cm^{-1} does not correspond to any obvious feature in the observed spectrum. Thus, with the present data no unique assignment can be made, although of the two discussed, the second one is to be preferred on the basis of the smaller anharmonicity that it implies for this mode.

3.4 Infrared Spectra Between 800 and 1500 cm^{-1}

Because absorption by the free ether is very strong in this region, it was necessary to record spectra of mixtures containing very high partial pressures of hydrogen chloride and low partial pressures of ether. The large excesses of hydrogen chloride in the mixtures caused most of the ether to become hydrogen bonded, even at ambient temperature. To further increase the percentage of ether present in the hydrogen-bonded form, the infrared cell was cooled. At -10°C the equilibrium constant for the formation of $(CH_3)_2O{-}{-}{-}HCl$ is computed from the mean enthalpy and entropy reported by Govil, Clague and Bernstein (84) to be 1.86, standard state one atmosphere. Substitution of this value into the equilibrium expression for formation of $(CH_3)_2O{-}{-}{-}HCl$ reveals that at -10°C only six percent of the ether present in a mixture of 5860 Torr of hydrogen chloride with 10 Torr of dimethyl ether-h_6 remains uncomplexed. Under these conditions some condensation of the hydrogen-bonded complex undoubtedly occurs, but this has no effect upon the shapes and frequencies of the bands reported in this section. Due to the very large hydrogen chloride to ether ratios there exists a possibility that hydrogen-bonded species other than a 1:1 complex are present in these mixtures. However, the hydrogen chloride stretching mode, ν_s, in the 1:1 complex is known to give rise to a band close to 2500 cm^{-1} (73) and a comparison of this band with the absorption by the high pressure mixtures in this region did not reveal any differences which could be attributed to other complexes.

In Figure 13, boxes II and III show spectra of 10 Torr of dimethyl ether-h_6 mixed with 5860 Torr of argon at +35°C (curves A), and of 10 Torr of dimethyl ether-h_6 mixed with 5860 Torr of hydrogen chloride at +35°C, +10°C, 0°C and -10°C (curves B, C, D and E, respectively). The intensities of the spectra shown in the latter four curves become progressively weaker as the temperature is lowered as a result of condensation of $(CH_3)_2O{-}{-}{-}HCl$. In box II, curve A shows two bands with PQR structures, one at 1102 cm^{-1} with a half-width of about 45 cm^{-1} and PR separation of 26.1 cm^{-1}, and one at 1179 cm^{-1} with a half-width of about 40 cm^{-1} and a PR separation of 22.0 cm^{-1}.

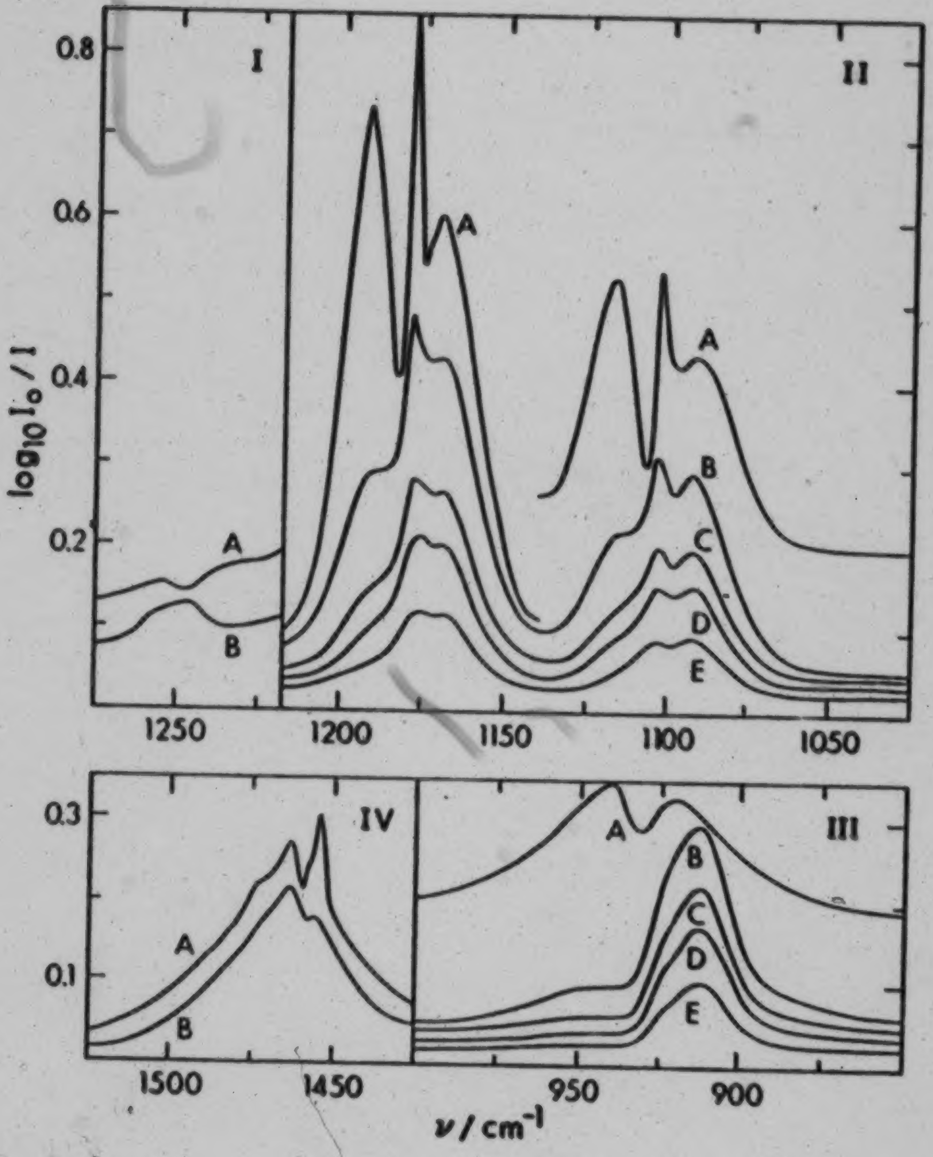

FIGURE 13. Infrared absorption spectra of: boxes I and IV, 20 Torr of dimethyl ether-h_6 mixed with 5850 Torr of Argon (curves A) or with 5850 Torr of hydrogen chloride (curves B), at 0°C; boxes II and III, 10 Torr of dimethyl ether-h_6 mixed with 5860 Torr of Argon at +35°C (curves A), or with 5860 Torr of hydrogen chloride at +35°C (curves B), +10°C (curves C), 0°C (curves D), or -10°C (curves E).

Curves B through E show that, as the temperature is lowered and the absorption by free ether is decreased, the spectrum approaches a limit of two bands with half-widths of 25-30 cm^{-1} and PR type structures. One band is centered at 1097 cm^{-1} and has a PR separation of 11 cm^{-1} and the other is centered at 1171 cm^{-1} and has a PR separation of 9 cm^{-1}. The bands at 1102 and 1179 cm^{-1} in the spectrum of dimethyl ether-h_6 have been assigned (95,96) to mixtures of the asymmetric C-O stretching and CH_3 rocking modes and thus the bands at 1097 and 1171 cm^{-1} in the spectrum of $(CH_3)_2O$---HCl must arise from analogous modes. In box III, curve A displays a band centered at 934 cm^{-1} with P and R branches separated by about 24 cm^{-1}. Curves B through E show that the corresponding band in the spectrum of $(CH_3)_2O$---HCl has a halfwidth of about 20 cm^{-1}, its absorption maximum at 912 cm^{-1}, and a weak shoulder at about 925 cm^{-1}. The band at 934 cm^{-1} in the free ether has been assigned (95,96) to the symmetric C-O stretching mode, which must therefore be assigned at 912 cm^{-1} in $(CH_3)_2O$---HCl.

Boxes I and IV of Figure 13 show spectra of 20 Torr of dimethyl ether-h_6 mixed with 5850 Torr of argon at 0°C (curves A) and of 20 Torr of dimethyl ether-h_6 mixed with 5850 Torr of hydrogen chloride at 0°C (curves B). The shapes of the bands shown in curves B did not change as the temperature of the mixtures was lowered below 0°C and therefore these bands must arise almost completely from $(CH_3)_2O$---HCl. In box I, curve A displays a weak band, centered at 1245 cm^{-1}, with P and R branches separated by about 20 cm^{-1}. This band has been assigned (95, 96) to the totally symmetric CH_3 rocking mode of dimethyl ether-h_6. The weak, slightly asymmetric band shown in curve B is centered at 1248 cm^{-1} and undoubtedly arises from the analogous mode in the ethereal part of $(CH_3)_2O$---HCl. In box IV, curve A displays a band with a half-width of about 35 cm^{-1} and with sharp features at 1454 and 1462 cm^{-1} and a shoulder at about 1475 cm^{-1}. This band has been assigned (95,96) to the five infrared active CH_3 deformation modes in dimethyl ether-h_6. Curve B shows that the band due to these modes in $(CH_3)_2O$---HCl has a half-width of about 25 cm^{-1} and is centered at 1465 cm^{-1}, although the absorption maximum is at 1462 cm^{-1}.

The region between 900 and 1200 cm^{-1} has been studied by Le Calvé, Grange, and Lascombe (76). The temperatures and the acid to ether ratios were higher in the present work, but the limiting band shapes reached as the temperature was lowered are essentially the same in both studies, except that the shoulder at 925 cm^{-1} is less pronounced in this work than in reference 76. The bands at 1248 and 1465 cm^{-1} in the spectrum of $(CH_3)_2O$---HCl are reported here for the first time. All of the bands between 900 and 1500 cm^{-1} appeared unshifted in frequency in the spectrum of $(CH_3)_2O$---DCl, so there cannot be any significant coupling between the ethereal modes and the modes involving primarily motion of the hydrogen-bonded hydrogen atom. The spectrum between 800 and 1500 cm^{-1} of $(CD_3)_2O$---HCl was not studied in as much detail as that of $(CH_3)_2O$---HCl but four bands, centered at 816, 925, 1057, and 1160 cm^{-1}, with approximate half-widths of 20, 40, 25, and 30 cm^{-1}, respectively, were clearly evident and were close in frequency to four corresponding bands in the spectrum of dimethyl ether-d_6. The frequencies of the bands in the spectra of $(CH_3)_2O$---HCl, $(CD_3)_2O$---HCl and the ethers are presented in Table 1, along with their assignment (95,96).

Figure 14 shows two possible geometries for $(CH_3)_2O$---HCl. In structure I the hydrogen chloride molecule bonds to one of the lone pairs of electrons on the oxygen atom. The only element of symmetry in structure I is a mirror in the plane of the a- and c-principal axes of inertia and thus structure I has C_s symmetry. In structure II the hydrogen chloride molecule bonds simultaneously to both lone pairs of electrons on the oxygen atom and lies in the C-O-C plane of the ether molecule, forming a hydrogen-bonded molecule of C_{2v} symmetry. It has been suggested (74) that an analysis of the shape of the band due to the symmetric C-O streching mode at 912 cm^{-1} proves that the complex has C_s symmetry. To test the conclusion of reference 74, calculations were

TABLE 1

Frequencies [a] and Assignments [b] of Absorptions Between 800 and 1500 cm^{-1} in $(CH_3)_2O$---HCl, $(CD_3)_2O$---HCl and the Free Ethers

$(CH_3)_2O$	$(CH_3)_2O$---HCl	Assignment
934	912	Symmetric C-O Stretch
1102	1097	CH_3 Rock + Asymmetric Stretch
1179	1171	
1245	1248	CH_3 Rock
1462	1465	CH_3 Deformations

$(CD_3)_2O$	$(CD_3)_2O$---HCl	Assignment
829	816	Symmetric C-O Stretch
931	925	CD_3 Rock
$\sim$1060	1057	CD_3 Deformations
1163	1160	Asymmetric C-O Stretch

a) Frequencies are reported in cm^{-1}.

b) References 95 and 96.

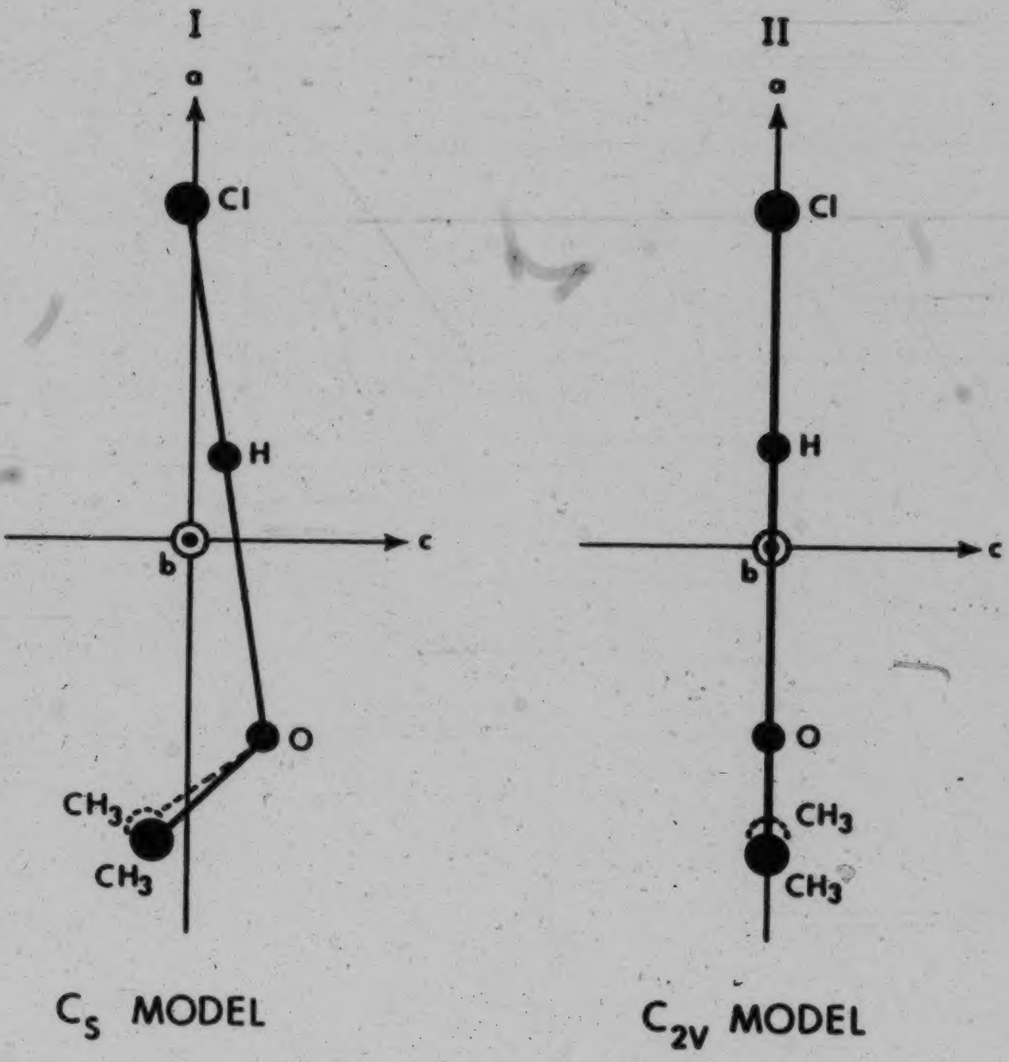
I
a
Cl
H
b
c
O
CH3
CH3
Cs MODEL
II
a
Cl
H
b
c
O
CH3
CH3
C2V MODEL

FIGURE 14. The two possible geometries for the $(CH_3)_2O$---HCl molecule. The axes marked a, b and c are the principal axes of inertia.

made to determine the band shapes of the C-O symmetric stretching mode using both the C_s and C_{2v} models. For each model the geometry of the ether part of $(CH_3)_2O$---HCl was assumed to be that reported by Buikis et al (102) for free dimethyl ether-h_6, and the O---H and O---Cl distances were assumed to be 1.7 Å and 3.1 Å, respectively. The Schachtschneider program, CART (103), and values of the atomic masses tabled in reference 101 were used to calculate the rotational constants (104) for each model. These constants, A, B, and C, respectively, are proportional to the inverse of the moments of inertia about the a-, b-, and c- principal axes of rotation which are defined in Figure 14 for each model. For the C_s model the values of the constants are A = 0.316, B = 0.068, C = 0.058 cm^{-1} and for the C_{2v} model the constants are A = 0.337, B = 0.061, C = 0.053 cm^{-1}. Thus both models are asymmetric rotors but closely approximate prolate symmetric top molecules.

For the C_{2v} model, the C-O symmetric stretching vibration would cause a dipole moment change along the a- principal axis of rotation and hence an A-type infrared absorption band (104) is predicted. The analogous mode for the C_s model would cause a dipole moment change in the ac plane, with almost equal components along the a- and c- axes, and hence an AC hybrid band (104,105) is predicted. Ueda and Shimanouchi (105) have calculated the shapes of A-, B-, and C-type infrared absorption bands for forty different asymmetric rotors which are characterized according to their molecular shape by two parameters, X and Y, where

$$X = 2C/B \qquad (1)$$

and $$Y = 1 - (C/A) - (C/B). \qquad (2)$$

Substitution of the appropriate rotational constants into these equations yields $X = 1.74$ and $Y = -0.026$ for the C_{2v} model and $X = 1.72$ and $Y = -0.036$ for the C_s model. The values of these parameters in each case most closely approximate those of rotor number 8 of reference 105. The A-, B-, and C-type infrared absorption bands predicted for this rotor are shown in box I of Figure 15, as reproduced from reference 105. The A-type band, predicted for the C_{2v} model, has a PQR structure with a prominent Q branch. An AC hybrid band, such as that predicted for the C_s model, can be constructed by the superposition of A- and C-type bands. Since both the A- and C-type bands have PQR structures, the AC hybrid band will also have P, Q and R branches, and no distinction between the C_s and C_{2v} models can be made on the basis of band shape.

A more detailed look at the shapes of the bands predicted for the two models of $(CH_3)_2O$---HCl is warranted because the bands shown in box I of Figure 15 were calculated with the assumption that the sum of the rotational

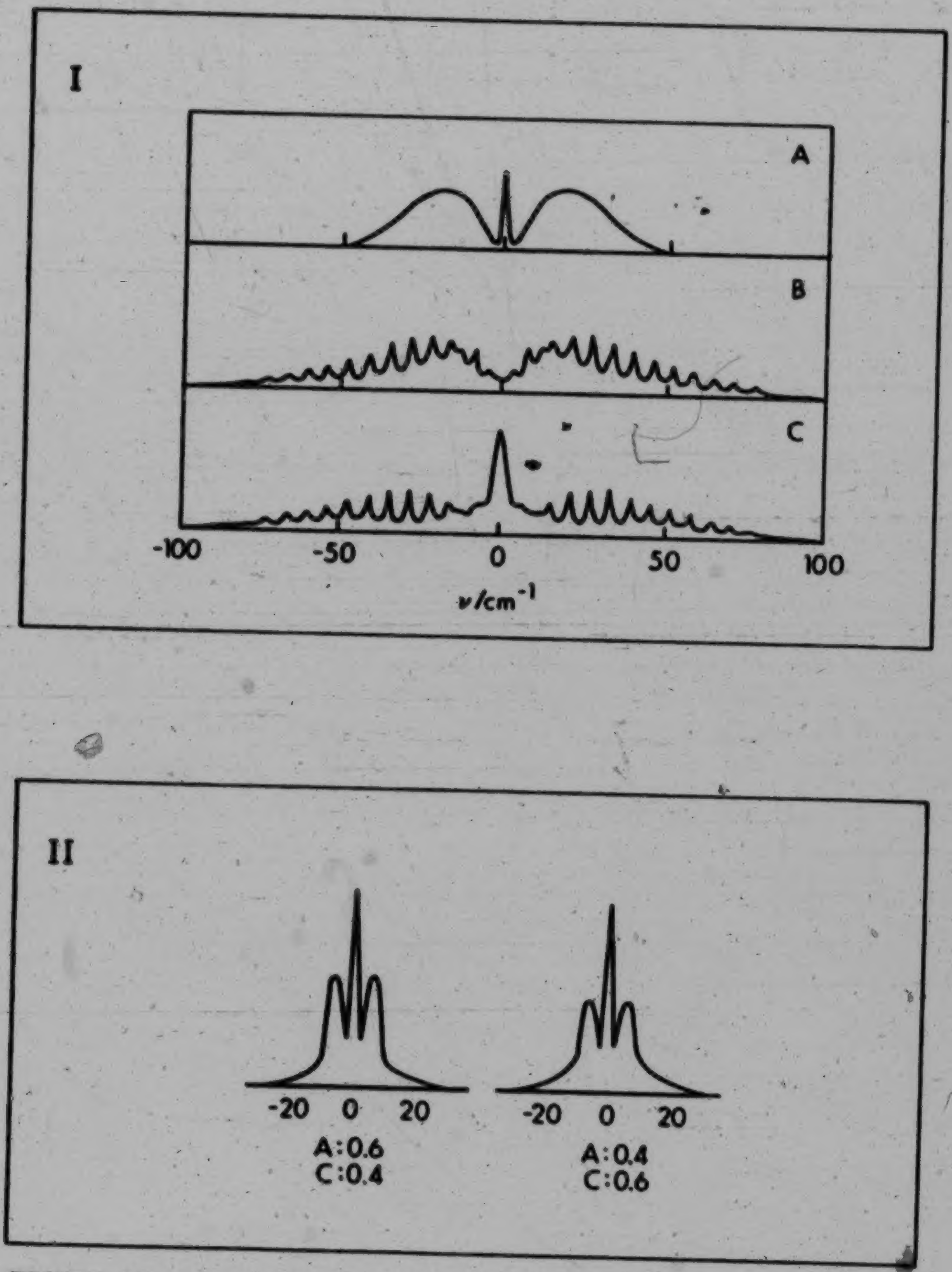

FIGURE 15. Box I, A-, B- and C- type bandshapes predicted for $(CH_3)_2O$---HCl; box II, typical AC hybrid bands of *gauche*-1,2-dichloroethane. These bands have been reproduced from reference 105.

constants, A + B + C, was 5 cm^{-1}, which is of the order of ten times the sum calculated for either model of $(CH_3)_2O$---HCl. As a result, the bands shown in box I of Figure 15 have much larger PR separations and therefore larger half-widths than would be expected for bands in the spectrum of $(CH_3)_2O$---HCl. The PR separations and half-widths of bands due to $(CH_3)_2O$---HCl can be calculated since, at a given temperature, T, they are approximately proportional to $\sqrt{(A + B + C)/T}$. Therefore, the PR separation of an A-type band in the spectrum of the C_{2v} model, for which A + B + C = 0.451 cm^{-1}, would be that measured from the A-type band in box I of Figure 15, which is about 40 cm^{-1}, multiplied by $\sqrt{0.451/5}$. This yields a value of about 12 cm^{-1} and thus the separation of the Q branch from either the P or R branch should ideally be one half of this value, or about 6 cm^{-1}. The half-width of the A-type band shown in box I of Figure 15 is about 70 cm^{-1} and therefore the half-width of an A-type band in the spectrum of the C_{2v} model of $(CH_3)_2O$---HCl would be about 20 cm^{-1}. The AC hybrid band predicted for the C-O symmetric stretching mode of the C_s model should correspond closely to the AC hybrid band calculated in reference 105 for gauche-1,2-dichloroethane. This molecule has the rotational constants A = 0.3169 cm^{-1}, B = 0.0784 cm^{-1} and C = 0.0675 cm^{-1}, which yield X = 1.72 and Y = -0.074. These values are very close to those calculated for the C_s model of $(CH_3)_2O$---HCl and the sum of the rotational constants of gauche-1,2-dichloroethane is very close to the sum of the rotational constants of the C_s model, being 0.4628 and 0.442 cm^{-1}, respectively. Box II of Figure 15 displays two AC hybrid bands of gauche 1,2-dichloroethane with A:C ratios of 6:4 and 4:6. The AC hybrid band due to the symmetric C-O stretching mode in the C_s model is predicted to have an A:C ratio of approximately unity and should, therefore, correspond closely to the bands shown in box II of Figure 15. Each of these bands has a prominent Q branch, a PR separation of about 10 cm^{-1} and a half-width of about 25 cm^{-1}.

The half-widths of the bands predicted for both the C_s and C_{2v} models are close to the observed value of 20 cm^{-1}, but neither model predicts band shapes which correspond at all to the shape of the band at 912 cm^{-1}, for which no P, Q or R branches are resolved. The failure to predict the observed band shape must be influenced by the rather high population of the excited states of the ν_σ and ν_β modes which must exist in the temperature range studied. Thus, excitation of the symmetric C-O stretching vibration must take place simultaneously from a large number of vibrational states which differ only in the number of quanta of the ν_σ or ν_β modes which have been excited. Since the ν_σ and ν_β modes involve motion of the hydrogen chloride molecule, large deviations from the equilibrium molecular geometry probably exist in these states. Transitions from these excited states should, then, give rise to significantly different band shapes from those predicted from the equilibrium geometry, and since the observed band is a superposition of the bands due to these transitions, any PQR structure may well be lost.

3.5 Infrared Spectra above 1500 cm^{-1}

In Figure 16, curve A shows the spectrum between 2200 and 2800 cm^{-1} of a mixture of 250 Torr of dimethyl ether-h$_6$ with 250 Torr of hydrogen chloride at +35°C and curve B shows the spectrum of a mixture of 100 Torr of dimethyl ether-h$_6$ with 100 Torr of hydrogen chloride at -30°C. Each spectrum was recorded with enough ether at +35°C in the reference beam of the spectrophotometer to cancel the free ether absorption, which is shown in curve C. The sharp lines visible on the high frequency sides of the bands in curves A and B arise from free hydrogen chloride. The pressures of the components in the mixture at -30°C were smaller than in the mixture at +35°C but, as a result of the larger equilibrium constant for formation of $(CH_3)_2O{-}{-}{-}HCl$ at the lower temperature, the concentration of $(CH_3)_2O{-}{-}{-}HCl$ was approximately the same in both mixtures. Curve A displays a broad band with a half-width of about 250 cm^{-1} and its absorption

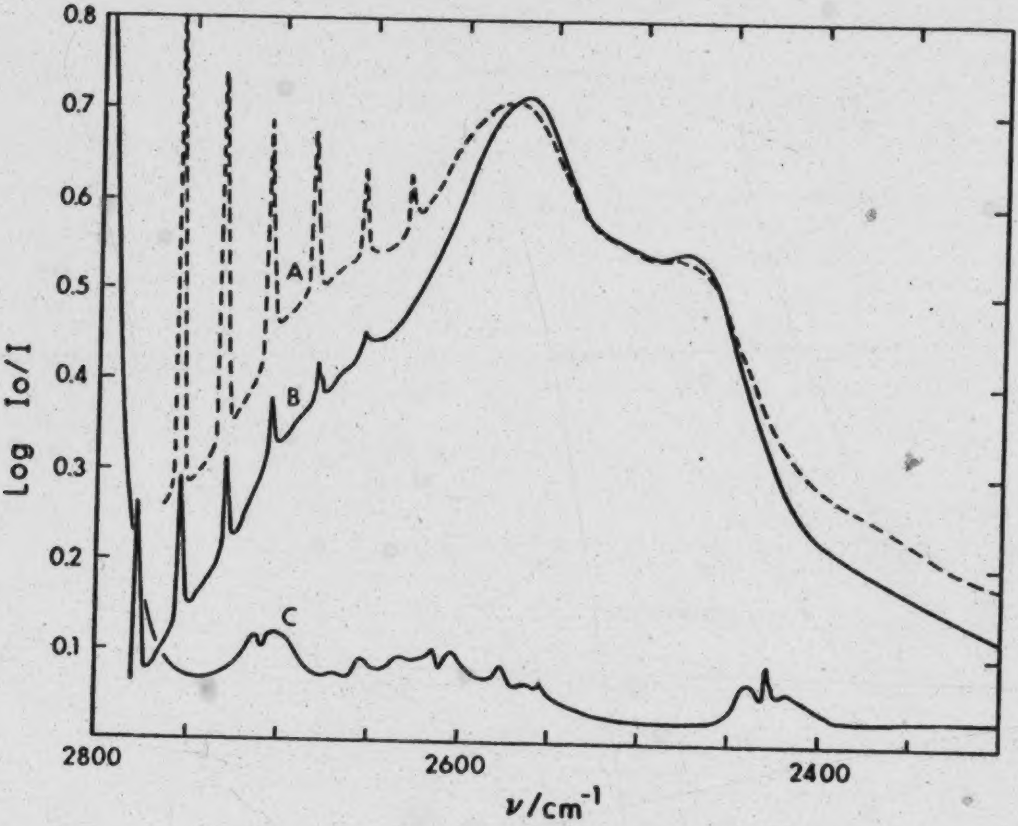

FIGURE 16. Infrared absorption by: 250 Torr of dimethyl ether-h_6 plus 250 Torr of hydrogen chloride at +35°C (curve A); 100 Torr of dimethyl ether-h_6 plus 100 Torr of hydrogen chloride at -30°C (curve B); 100 Torr of dimethyl ether-h_6 at +35°C (curve C). Curves A and B were recorded with 250 and 100 Torr, respectively, of dimethyl ether-h_6 at +35°C in a 10 cm. long cell in the reference beam.

maximum at 2574 cm^{-1}. Also evident are shoulders of approximately equal intensity at about 2680 and 2480 cm^{-1}, as well as a third, weak shoulder at about 2360 cm^{-1}. The shape of the band is identical to that reported by Bertie and Millen (73), who assigned the absorption maximum to the HCl stretching mode, ν_s, and the three shoulders to various combination transitions of ν_s with the hydrogen bond stretching mode, ν_σ. Thus the shoulder at 2680 cm^{-1} was assigned to the sum band, $\nu_s + \nu_\sigma$, which represents the vibrational transition, $[V_s = 0 \rightarrow 1, V_\sigma = 0 \rightarrow 1]$. The shoulders at 2480 and 2360 cm^{-1} were assigned to the difference bands $\nu_s - \nu_\sigma$, i.e. the transition $[V_s = 0 \rightarrow 1, V_\sigma = 1 \rightarrow 0]$, and $\nu_s - 2\nu_\sigma$, the transition $[V_s = 0 \rightarrow 1, V_\sigma = 2 \rightarrow 0]$, respectively. On the basis of this assignment one expects the intensities of the features at 2480 and 2360 cm^{-1} to decrease relative to the absorption maximum as the sample temperature is lowered, since difference transitions originate in excited vibrational energy levels (42). The relative intensities of the features at 2574 and 2680 cm^{-1} should show little temperature dependence if the above assignment is correct, since both features are assigned to transitions originating in the vibrational ground state. Comparison of curves A and B shows that the weak feature at 2360 cm^{-1} is less intense relative to the absorption maximum at -30°C than at +35°C, which is consistent with its assignment to a difference band. However, the intensity of the shoulder at 2480 cm^{-1} does not appear to be dependent upon the temperature although the entire portion of the band to high frequency of the absorption maximum has lower intensity relative to that of the maximum at -30°C than at +35°C. These observations contradict the assignment of the 2680 cm^{-1} feature to a simple sum band and the 2480 cm^{-1} feature to a difference band.

In Figure 17, curve A shows the spectrum between 2200 and 2800 cm^{-1} of a mixture of 250 Torr of dimethyl ether-d_6 with 250 Torr of hydrogen chloride at +35°C and curve B shows the spectrum of a mixture of 100 Torr of dimethyl ether-d_6 with 100 Torr of hydrogen chloride at -30°C. The absorption shown in curve A is identical to that reported by Bertie and Millen (73) for $(CD_3)_2O$---HCl. Comparison of curves A and B shows that the effect of sample temperature on the absorption by $(CD_3)_2O$---HCl is the same as that observed for $(CH_3)_2O$---HCl. The only differences between these spectra and those shown in Figure 16 are that for $(CD_3)_2O$---HCl the 2480 cm^{-1} feature is slightly better resolved as a peak at the lower temperature, the absorption maximum is slightly narrower than for $(CH_3)_2O$---HCl and an absorption corresponding to the weak feature at 2360 cm^{-1} in $(CH_3)_2O$---HCl is not visible. The latter difference is due to overlapping absorption by the C-D stretching modes (95,96) in both the free dimethyl ether-d_6 (curve C) and $(CD_3)_2O$---HCl. The

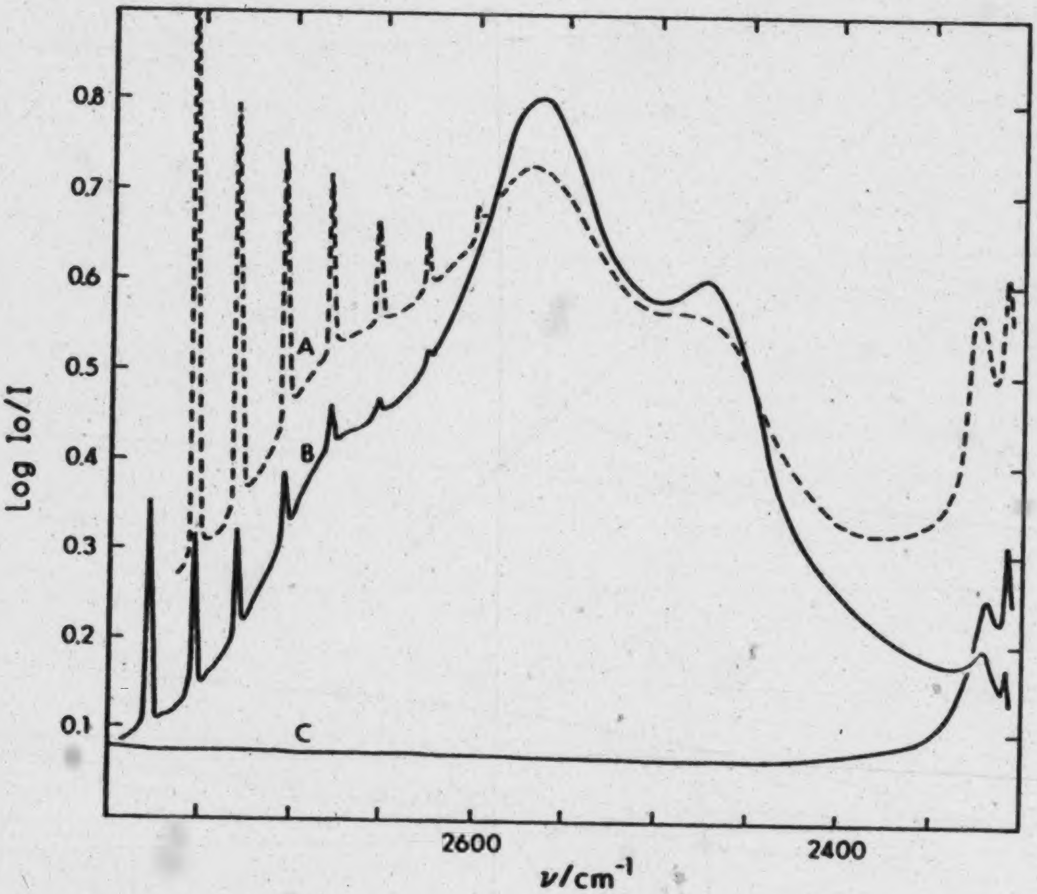

FIGURE 17. Infrared absorption by: 250 Torr of dimethyl ether-d_6 plus 250 Torr of hydrogen chloride at +35°C (curve A); 100 Torr of dimethyl ether-d_6 plus 100 Torr of hydrogen chloride at -30°C (curve B); 50 Torr of dimethyl ether-d_6 at +35°C (curve C). Curves A and B were recorded with 250 and 100 Torr, respectively of dimethyl ether-d_6 at +35°C in a 10 cm. long cell in the reference beam.

smaller width of the absorption maximum of $(CD_3)_2O$---HCl may well be due to the moments of inertia of this molecule being larger than those of $(CH_3)_2O$---HCl, and causing a narrower rotational envelope for each vibrational transition.

Since the shape of the band at the two temperatures is independent of the ether used, the general interpretation of the structure of the band given by Bertie and Millen (73), that it is due to sum and difference bands of the type $\nu_s \pm n\nu_\sigma$ with no influence from Fermi resonance, must be correct. However, on the basis of the experimental evidence presented above, it is more reasonable to assign the 2480 cm^{-1} feature to ν_s and the absorption maximum at 2574 cm^{-1} to $\nu_s + \nu_\sigma$. Thus the sum band, $\nu_s + 2\nu_\sigma$, must contribute to the intensity at 2680 cm^{-1} and the difference band, $\nu_s - \nu_\sigma$, must contribute to the 2360 cm^{-1} absorption. The observed decrease in intensity at 2680 cm^{-1} with decrease in temperature can be explained by postulating that hot transitions of $\nu_s + 2\nu_\sigma$ of the type $[V_s = 0 \rightarrow 1,\ V_\sigma = n \rightarrow n + 2]$, where n is a non-zero integer, make an unusually large contribution to the intensity. In a study concurrent with but independent of this work, Lassegues, Huong and Lascombe (106,107) have quantitatively studied the ν_s band in $(CH_3)_2O$---HCl between -50°C and +90°C, and have shown that the temperature dependence requires an assignment of this sort. These authors observed that the intensities of the features at 2360 and 2680 cm^{-1} show temperature dependencies which are compatible with transitions starting in levels which are higher in energy by approximately 1.8 quanta of ν_σ than the starting levels for the transitions associated with the 2480 and 2574 cm^{-1} features. This implies that, if the transitions $[V_s = 0 \rightarrow 1, V_\sigma = 0 \rightarrow 0]$ and $[V_s = 0 \rightarrow 1, V_\sigma = 0 \rightarrow 1]$ make the major contribution to the intensity at 2480 and 2574 cm^{-1}, respectively, the hot transitions $[V_s = 0 \rightarrow 1, V_\sigma = 2 \rightarrow 4]$ and $[V_s = 0 \rightarrow 1, V_\sigma = 2 \rightarrow 1]$, must make the major contribution to the intensity at 2680 and 2360 cm^{-1}, respectively.

It seems clear, however, that these four transitions, each of which should have a rotational envelope of about 25-30 cm^{-1} (Section 3.4), cannot account for the diffuseness of the entire band unless some special mechanism, such as an abnormally large effect of centrifugal distortion (106), broadens the rotational envelope of each transition. Any such effect can only be operative in the $V_s = 1$ (and possibly $V_b = 1$ and $V_t = 1$) states, because the half-widths of the bands due to the ethereal modes and ν_σ, for which $V_s = 0$ (and $V_b = V_t = 0$), can be explained without invoking it. It seems more likely that, in addition to the four transitions proposed above, transitions starting in different V_σ levels also contribute significantly to the intensity of each sub-band and, due to mechanical anharmonicity, the intensity can be spread out over a large frequency range. It is also possible that hot transitions of the ν_s vibration from excited ν_β states, which have been shown to be important in the interpretation of the spectra of CH_3CN---HCl (54) and CH_3CN---HF (55), contribute to the diffuseness of the ν_s band in $(CH_3)_2O$---HCl. It is probable that these hot transitions are responsible for the slight shift of the ν_s band and sharpening of the 2480 cm^{-1} feature at the lower temperature.

The assignment of the absorption maximum to $\nu_s + \nu_\sigma$ rather than to ν_s and the implication that hot transitions contribute significantly to the intensity of the whole band can be rationalized in terms of the vibrational Franck-Condon effect (Section 1.6). From a consideration of the observed band and its assignment, reasonable potential energy curves, such as those shown in Figure 18, can be drawn to illustrate this effect in $(CH_3)_2O$---HCl. The energy separation of the curves, given in cm^{-1} for easy comparison with vibrational frequencies, is about 2500 cm^{-1} close to the minima and 2886 cm^{-1}, equal to the vibrational frequency of free hydrogen chloride (91), at large O---Cl distances. The dissociation energy of 2485 cm^{-1} is the equivalent of the mean value of 7.1 kcal/mole reported by Govil, Clague and Bernstein (84). The assignment of ν_s at 2480 cm^{-1} and of $\nu_s - \nu_\sigma$ at 2360 cm^{-1} yields a value of 120 cm^{-1} for the separation of the $V_\sigma = 0$ and

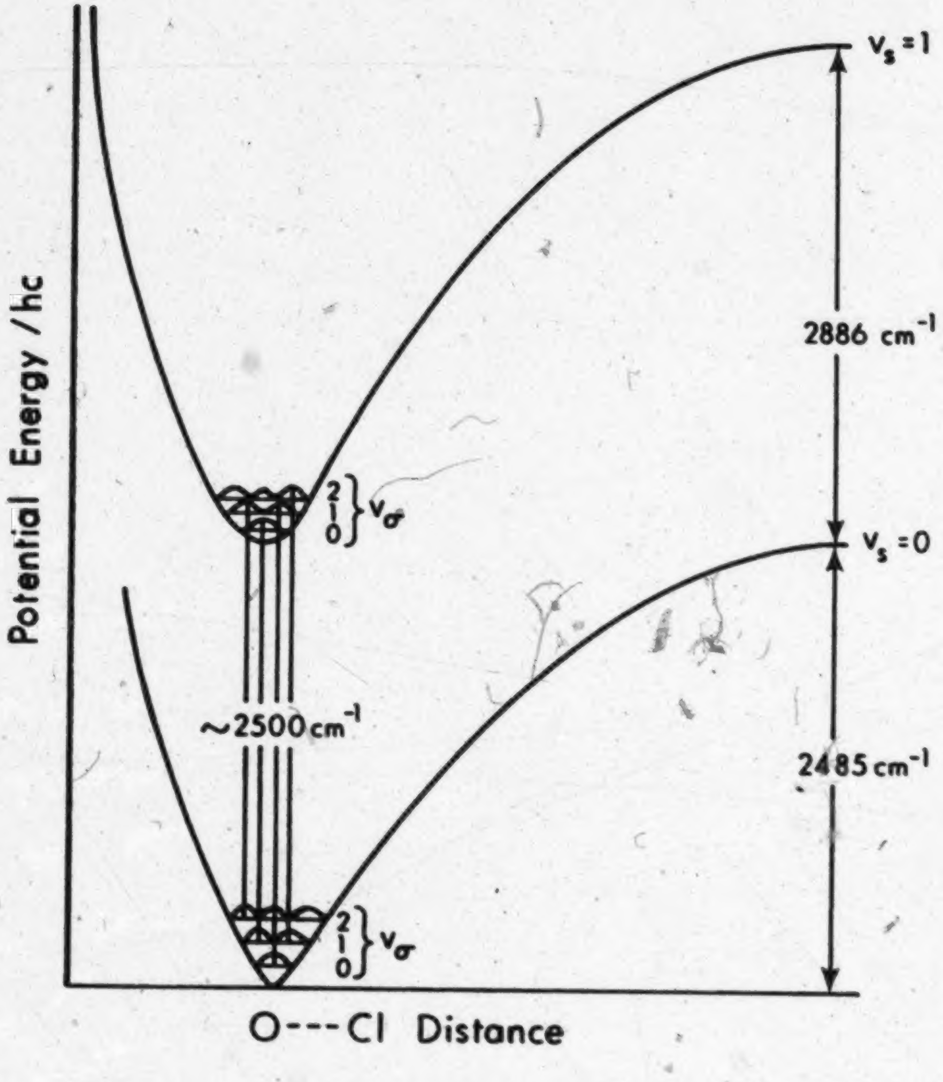
Potential Energy /hc
$V_s=1$
$V_s=0$
2886 cm^{-1}
2485 cm^{-1}
~2500 cm^{-1}
2
1
0
V_σ
2
1
0
V_σ
O---Cl Distance

FIGURE 18. The Stepanov energy level scheme for the interaction of the ν_s and ν_σ modes in $(CH_3)_2O$---HCl. V_s and V_σ are the quantum numbers for the HCl and hydrogen bond stretching vibrations, respectively, and the curves drawn on the energy levels are the squares of the wave functions.

$V_\sigma = 1$ levels when $V_s = 0$, which agrees very well with the observed frequency at 119 cm^{-1}. When $V_s = 1$, the separation is 94 cm^{-1} if the assignment of the 2574 cm^{-1} feature is correct. Thus the force constant for the ν_σ mode must be smaller when $V_s = 1$ than when $V_s = 0$, which implies that, although the potential curve for the $V_s = 1$ state has a deeper minimum than that for the $V_s = 0$ state, the minimum for the $V_s = 1$ state is broader, so that the curvature is less. Since the intensity of $\nu_s + \nu_\sigma$ is greater than that of ν_s, the upper minimum must occur at a different O---Cl distance than the lower minimum, causing the transition $[V_s = 0 \rightarrow 1, V_\sigma = 0 \rightarrow 1]$ to be more probable than the transition $[V_s = 0 \rightarrow 1, V_\sigma = 0 \rightarrow 0]$. The different equilibrium distances for the two V_s states can also cause transitions starting in excited V_σ levels to be more probable than the corresponding transition from the ground state.

Figures 19 and 20 show spectra between 1500 and 2000 cm^{-1} of 1:1 mixtures of deuterium chloride with dimethyl ether-h_6 and with dimethyl ether-d_6, respectively, at -30°C (curves A) and at +30°C (curves B). The spectra were recorded with enough of the appropriate free ether in the reference beam of the spectrophotometer to cancel the absorption by the free ether, which is shown in curves C. Absorption by free deuterium chloride was not subtracted from these spectra and appears as the rather sharp lines on the portion of the bands above 1850 cm^{-1}. The broad

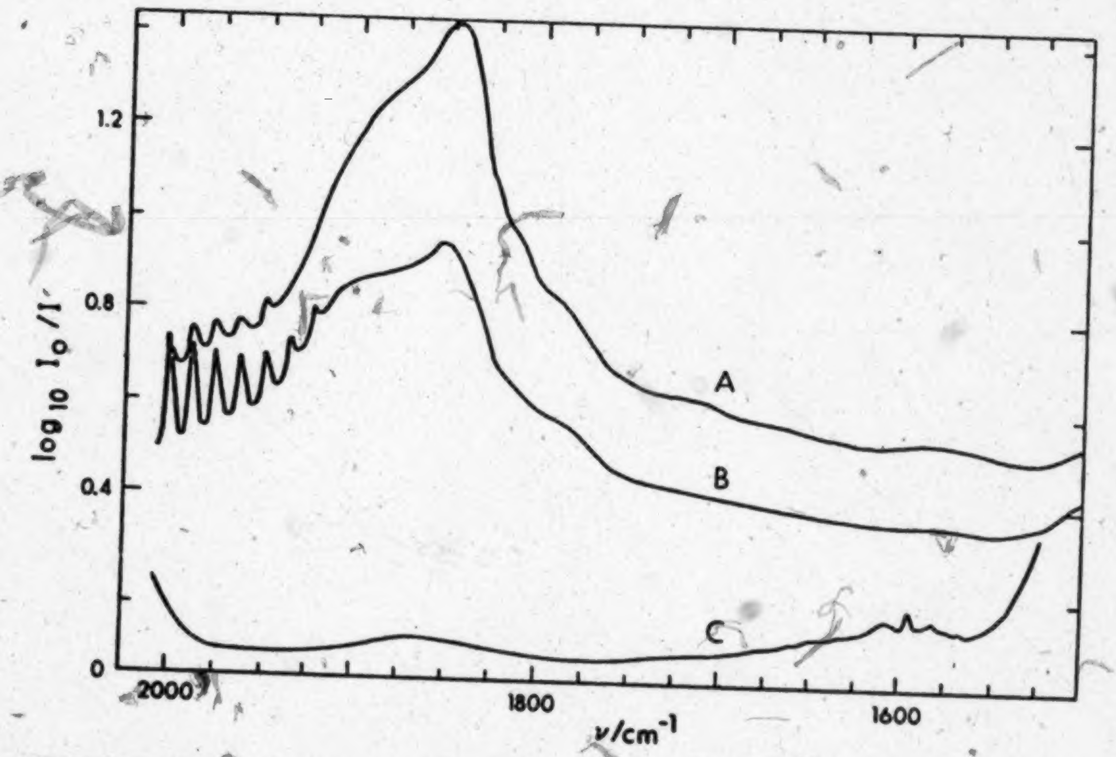

FIGURE 19. Infrared absorption by: 100 Torr of dimethyl ether-h_6 plus 100 Torr of deuterium chloride at -30°C (curve A); 250 Torr of dimethyl ether-h_6 plus 250 Torr of deuterium chloride at +30°C (curve B); 250 Torr of dimethyl ether-h_6 at +30°C (curve C). Curves A and B were recorded with 100 and 250 Torr, respectively, of diemthyl ether-h_6 at +30°C in a 10 cm. long cell in the reference beam.

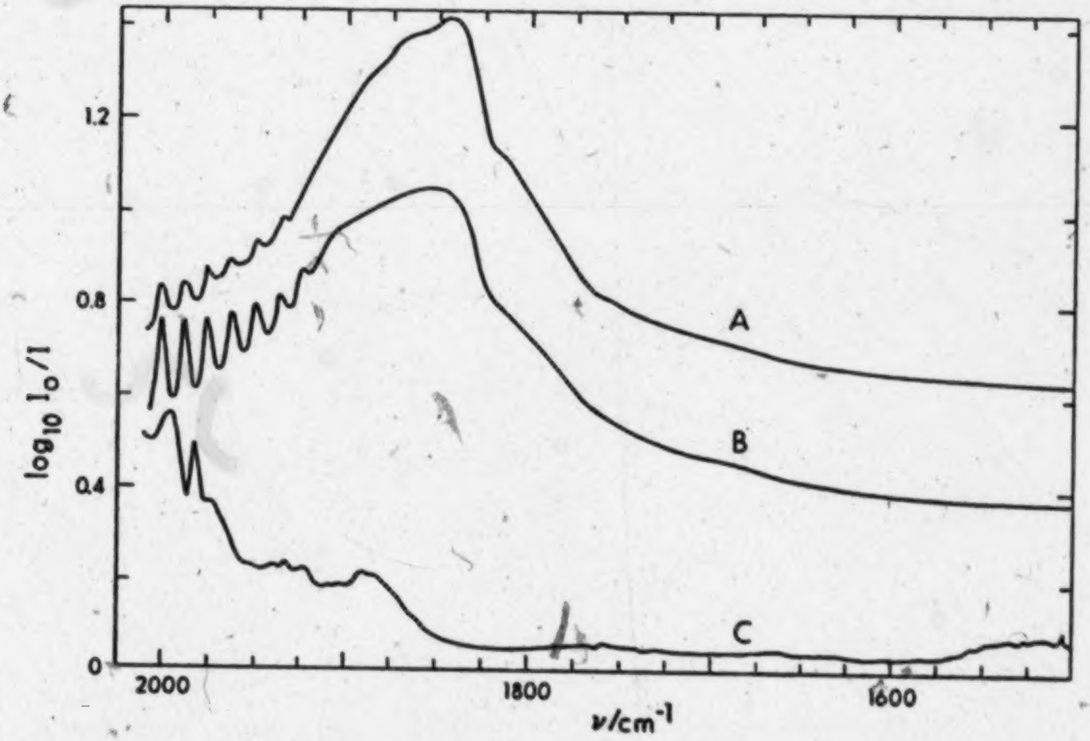

FIGURE 20. Infrared absorption by: 100 Torr of dimethyl ether-d_6 plus 100 Torr of deuterium chloride at -30°C (curve A); 250 Torr of dimethyl ether-d_6 plus 250 Torr of deuterium chloride at +30°C (curve B); 250 Torr of dimethyl ether-d_6 at +30°C (curve C). Curves A and B were recorded with 100 and 250 Torr, respectively, of dimethyl ether-d_6 at +30°C in a 10 cm. long cell in the reference beam.

bands which are evident in curves B of Figures 19 and 20 have half-widths of about 100 cm^{-1} and their absorption maxima at 1850 cm^{-1} but display considerably different features. In $(CH_3)_2O$---DCl (Figure 19) this band has shoulders at 1905, 1810 and 1785 cm^{-1} in addition to weak absorptions at 1700 and 1580 cm^{-1}. In $(CD_3)_2O$---DCl (Figure 20) the band has shoulders at 1900, 1800 and 1680 cm^{-1}. Curves A of Figures 19 and 20 show that, although at the lower temperature the absorption bands shift to lower frequency by about 5 cm^{-1}, all of the features present at +30°C are also present at -30°C. These features are, however, less intense relative to the absorption maximum at -30°C than at +30°C. Curve A in Figure 20 also shows that the band in $(CD_3)_2O$---DCl at -30°C has an additional shoulder at about 1870 cm^{-1}.

The absorptions between 1700 and 2000 cm^{-1} in the spectra of mixtures of deuterium chloride and ethers have been assigned by Bertie and Millen (25) to the DCl stretching mode, ν_s, in the 1:1 complex of deuterium chloride with the appropriate ether. These authors noted that the ν_s bands of several ether-deuterium chloride hydrogen-bonded molecules are similar to those of the ether-hydrogen chloride molecules, with the side bands due to combinations of ν_s with ν_σ weaker for the deuterated acid. However, the details of these bands in $(CH_3)_2O$---DCl and $(CD_3)_2O$---DCl cannot be entirely explained in this way and there are differences between these two bands which must be explained. The feature at 1870 cm^{-1} is present only in the spectrum of $(CD_3)_2O$---DCl (Figure 20) and must, therefore, arise from an ethereal mode. It can be attributed to the summation transition due to the combination of the symmetric C-O stretching mode at 816 cm^{-1} with a CD_3 deformation mode at 1057 cm^{-1} (Table 1). This transition absorbs weakly in the spectrum of the pure ether and is, therefore, probably enhanced in intensity in the spectrum of $(CD_3)_2O$---DCl by a Fermi resonance interaction (Section 1.6) with the ν_s mode. The shoulder close to 1800 cm^{-1} appears as a single feature in the spectrum of $(CD_3)_2O$---DCl but as a doublet in the spectrum of $(CH_3)_2O$---DCl. This doublet may be due to a Fermi resonance type of interaction between the first overtone of the symmetric C-O stretching mode at 912 cm^{-1} (Table 1), and the mode giving rise to the absorption close to 1800 cm^{-1}, causing the single shoulder to split into two. No overtone or combination transition in $(CD_3)_2O$---DCl is available for such an interaction close to 1800 cm^{-1} and thus no splitting of this shoulder occurs in the spectrum of this molecule. The final difference between the spectra of $(CH_3)_2O$---DCl and $(CD_3)_2O$---DCl is the presence of a feature at 1580 cm^{-1} in the spectrum of the former molecule. A band at this frequency is also evident in the spectrum of $(CH_3)_2O$---HCl and undoubtedly corresponds to a weak band at essentially the same frequency in the spectrum of dimethyl ether-h_6 (Figure 19, curve C). This band must also have enhanced intensity in the spectra of the hydrogen-bonded molecules as it would otherwise not have been observed because of the ether in the reference beam.

It is clear that the ν_s bands in the spectra of the deuterium chloride complexes differ significantly from those in the spectra of the hydrogen chloride complexes in a way which is not simply due to the combination bands, $\nu_s \pm n\nu_\sigma$, being weaker for the deuterated acids (25). The absorption maximum in the spectrum of $(CH_3)_2O{-}{-}{-}DCl$ or $(CD_3)_2O{-}{-}{-}DCl$ is accompanied by shoulders about 50 cm^{-1} to either side and, in view of the assignment of the ν_β modes at about 50 cm^{-1} (Section 3.3), it is natural to assign the maximum to ν_s and the shoulders to sum and difference transitions of the type $\nu_s \pm \nu_\beta$. The observed decrease in intensity with decreasing temperature of the feature at 1900 cm^{-1}, assigned to $\nu_s + \nu_\beta$, is explained by assuming that transitions of the type $\nu_s + (n+1)\nu_\beta - n\nu_\beta$ contribute significantly to this intensity through the vibrational Franck-Condon effect. The assignment of ν_s at 1850 cm^{-1} yields 1.340 for the ratio of the frequencies of ν_s in the hydrogen chloride and deuterium chloride complexes. This value indicates that the anharmonicity of ν_s in these complexes is greater than that of the corresponding mode in the ices, where the ratio is 1.354 (108), but is not extraordinarily large.

It is noteworthy that 1:1 mixtures of ether and hydrogen chloride at -30°C, with a total pressure of 200 Torr, and at +35°C, with a total pressure of 500 Torr, gave rise to ν_s bands with approximately the same integrated absorbances but identical mixtures of ether with deuterium chloride always gave rise to ν_s bands which were more intense at the lower temperature. This suggests that there is a slight increase in the temperature dependence of the equilibrium constant for formation of the hydrogen-bonded molecule when deuterium chloride is used in place of hydrogen chloride in the mixtures, and therefore, that ΔH, the enthalpy change for formation of the hydrogen bond, is larger for $(CH_3)_2O{-}{-}{-}DCl$ than for $(CH_3)_2O{-}{-}{-}HCl$. Unfortunately, no accurate computations of the heats of formation of these molecules are possible from the spectra presented above since neither the amounts of the free components in the mixtures nor the intensities are known accurately.

3.6 Relative Intensities of the Bands

In Table 2 the frequencies and approximate relative intensities of the bands in the spectrum of $(CH_3)_2O{-}{-}{-}HCl$ are presented. Since the most intense band is that due to ν_s, its intensity is given an arbitrary value of 100, so that the values for the intensities of the other bands

TABLE 2

Frequencies and Relative Intensities of Absorption Bands in $(CH_3)_2O...HCl$

ν/cm^{-1}	Assignment	Intensity (Arbitrary Units)
2675	HCl stretch, ν_s	100.0
2574		
2480		
~2360		
1465	CH_3 deformation	5.8
1248	CH_3 rock	0.5
1171	CH_3 rock + asym. CO stretch	18.0
1097		13.0
912	Symm. CO stretch	10.0
790	$2\nu_b$, $2\nu_t$.	0.5
570	O---H-Cl deformation ν_b, ν_t.	3.0[a]
525		
470		
415	C-O-C deformation	
119	O--H stretch ν_σ	0.3

a) The intensity was measured for $(CD_3)_2O---HCl$

can be regarded as percentages of this intensity. The relative intensities of the bands above 850 cm^{-1} should be quite reliable because they were all measured, with aid of a planimeter, from a single absorbance spectrum of a mixture of 20 Torr of dimethyl ether-h$_6$ with 5850 Torr of hydrogen chloride at 10°C. However, the relative intensities of the bands below 850 cm^{-1} must be regarded as approximate as they were determined by calculating the integrated absorbance per atmosphere of complex (25) for each of these bands and comparing this value with that calculated for the ν_s band. The equilibrium constant used to calculate the amount of complex present was computed from the mean enthalpy and entropy of formation reported by Govil, Clague and Bernstein (84). However, the errors on their values of the enthalpy and entropy of formation allow the equilibrium constant at 0°C to lie between 0.15 and 9.5, standard state 1 atmosphere. Thus, the relative intensities quoted for the bands below 850 cm^{-1} may be considerably in error because widely differing pressures and temperatures of the component gases were required for the different bands and the intensities obtained markedly reflect the value of the equilibrium constant that was used. It should be noted that the relative intensity of the O---H-Cl deformation modes was determined for $(CD_3)_2O$---HCl. The limited portion of the band that was observable in $(CH_3)_2O$---HCl indicated that the intensity was approximately the same in the two systems.

3.7 Summary

The most significant results of this study are that: 1) the assignment of the ν_σ mode of $(CH_3)_2O$---HCl near to 120 cm^{-1} is confirmed by the observation of absorption in this region in the spectra of $(CH_3)_2O$---DCl and $(CD_3)_2O$---HCl; 2) the ν_b and ν_t modes give rise to absorption near to 470 cm^{-1} for the HCl complexes and near to 360 cm^{-1} for the DCl complexes. These absorptions are complicated, probably due to interaction with the ν_β modes, which are deduced to be at about 50 cm^{-1}; 3) an analysis of the shape of the band due to the C-O symmetric stretching mode of $(CH_3)_2O$---HCl does not indicate the geometry of the molecule, as previously suggested; 4) the fundamental ν_s absorption by $(CH_3)_2O$---HCl is at 2480 cm^{-1} and not at 2574 cm^{-1} as previously postulated; and 5) combination transitions of the type $\nu_s \pm n\nu_\beta$ cause shoulders 50 cm^{-1} away from the peak due to ν_s in the DCl complexes.

CHAPTER 4

VIBRATIONAL ASSIGNMENT AND NORMAL COORDINATE CALCULATIONS FOR FOUR ISOTOPIC MODIFICATIONS OF ETHYLENE SULPHIDE

4.1 General Introduction

The infrared spectra of ethylene sulphide-h_4, ethylene sulphide-d_4, *cis*-1,2-dideuterioethylene sulphide and *trans*-1,2-dideuterioethylene sulphide have been measured in this laboratory by D. A. Othen (109). Hereafter in this thesis these compounds will be referred to as C_2H_4S, C_2D_4S, *cis*-$C_2D_2H_2S$ and *trans*-$C_2D_2H_2S$, respectively. Raman spectra of liquid C_2H_4S and C_2D_4S were also recorded by D. A. Othen (109).

These spectra were assigned as part of the present work and normal coordinate calculations were carried out to determine how well a harmonic valence-force field containing selected force constants could reproduce the frequencies of the fundamental vibrations of all four isotopic modifications of ethylene sulphide. The calculations were also desired to assist the assignment of the spectrum of *trans*-$C_2D_2H_2S$, to check the mutual compatibility of the assignments of the four molecules, and to determine the form of the methylenic vibrations for the HCD groups.

The structure, symmetry and vibrational coordinates of ethylene sulphide are given in Section 4.2 and the previous studies of the vibrations of ethylene sulfide are reviewed in Section 4.3. The frequencies of the features observed in the spectra of the four isotopic molecules are presented and assigned in Section 4.4. The computer programs used in the normal coordinate calculations and various input data are described in Section 4.5 and the development of the force field is summarized in Section 4.6. The results of the calculations are discussed in Section 4.7.

4.2 Structure, Symmetry and Vibrational Coordinates of Ethylene Sulphide

The structure of C_2H_4S has been investigated by Cunningham *et al*(110) by means of microwave spectroscopy. This molecule was found to have C_{2v} symmetry and the structure shown in Figure 21. In this work the atomic sites are referred to by the numbers which appear in Figure 21 as subscripts to the atomic symbols, and the bonds are referred to by the numbers which appear in parentheses beside them. In each of the four isotopic modifications of ethylene sulphide discussed in this chapter, atoms 1, 2 and 3 refer to ^{32}S, ^{12}C and ^{12}C atoms, respectively. In C_2D_4S, which has C_{2v} symmetry, atoms 4, 5, 6 and 7 are deuterium atoms. In *cis*-$C_2D_2H_2S$, which is assumed to have C_s symmetry, atoms 5 and 7 are deuterium atoms, and in *trans*-$C_2D_2H_2S$, which is assumed to have C_2 symmetry, atoms 4 and 7 are deuterium atoms.

Also shown in Figure 21 is the orientation of the

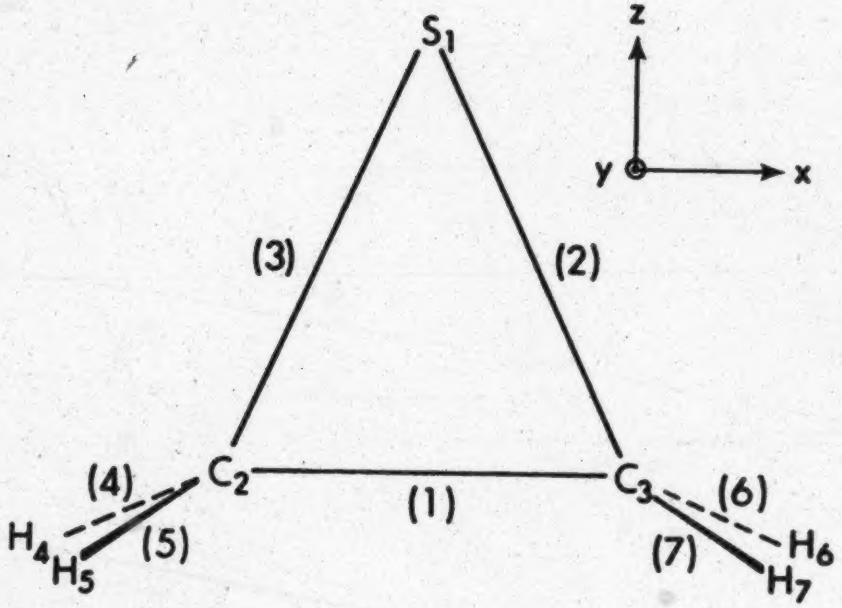
S_1
z
y
x
(3)
(2)
C_2
C_3
(1)
(4)
(5)
(6)
(7)
H_4
H_5
H_6
H_7

FIGURE 21. The structure of ethylene sulphide. In this drawing H_4 and H_6, which should lie directly under H_5 and H_7, respectively, have been offset for clarity. The number in parentheses beside each bond is used to designate that bond.

ethylene sulphide molecule with respect to the three Cartesian axes, and this orientation is the same for all four isotopic modifications. The x-Cartesian axis is parallel to the C-C bond, and the plane formed by atoms 1, 2 and 3 is the zx plane.

The bond angles and bond lengths in C_2D_4S, cis-$C_2D_2H_2S$ and trans-$C_2D_2H_2S$ are assumed to be the same as those in C_2H_4S (110), and are shown in Table 3. The rotational constants, A, B and C (Section 3.4), were calculated for each isotopic modification using these parameters and the appropriate atomic masses (101), and are presented in Table 4. The rotational constants are used in Section 4.4 to predict the rotational envelopes of the various vibrational transitions.

The fifteen fundamental vibrations of C_2H_4S form the representation (111) $5A_1 + 3A_2 + 4B_1 + 3B_2$ under the point group C_{2v}, and since C_2D_4S also has C_{2v} symmetry, its vibrations also form this representation. The vibrations of cis-$C_2D_2H_2S$ form the representation 8A' + 7A" under the point group C_s and those of trans-$C_2D_2H_2S$ form the representation 8A + 7B under the point group C_2. In this work, the fundamental vibrations are numbered in the order of decreasing frequency within each symmetry class, following the convention introduced by Herzberg (112). Thus in C_2H_4S and C_2D_4S, ν_1 through ν_5 refer to the five A_1 vibrations, ν_6 through ν_8 refer to the three A_2 vibrations, ν_9 through ν_{12}

TABLE 3

Molecular Parameters[a] of Ethylene Sulphide

d_{C-C}	1.4716 Å
d_{C-S}	1.8155 Å
d_{C-H}	1.0771 Å
$C-\hat{C}-S$	66.091°
$C-\hat{S}-C$	47.818°
$H-\hat{C}-H$	115.900°
$H-\hat{C}-C$	117.835°
$H-\hat{C}-S$	119.570°
α^b	106.567°

---

a) From reference 110.

b) α is the angle between the $C\hat{C}H$ and $C\hat{S}C$ planes.

TABLE 4

Rotational Constants[a] of Four Isotopic Modifications of Ethylene Sulphide

Molecule	A	B	C
C_2H_4S	0.7479	0.3608	0.2696
C_2D_4S	0.5256	0.3068	0.2291
cis-$C_2D_2H_2S$	0.6209	0.3314	0.2470
trans-$C_2D_2H_2S$	0.6174	0.3330	0.2463

---

a) Units are cm^{-1}.

refer to the four B_1 vibrations and ν_{13} through ν_{15} refer to the three B_2 vibrations. In cis-$C_2D_2H_2S$ or trans-$C_2D_2H_2S$, ν_1 through ν_8 refer to the eight A' or A vibrations, respectively, and ν_9 through ν_{15} refer to the seven A" or B vibrations, respectively.

The internal coordinates (100) of ethylene sulphide, which are used in the normal coordinate calculations (Section 4.6), are listed in Table 5 and are defined with respect to Figure 21. The coordinates which describe the stretching of valence bonds are denoted R_i, where i refers to the bond number shown in Figure 21. Thus R_4 is the coordinate which describes the stretching of a C-H bond at carbon atom 2 in C_2H_4S and cis-$C_2D_2H_2S$. In C_2D_4S and trans-$C_2D_2H_2S$, R_4 describes the stretching of a C-D bond at carbon atom 2. The coordinates which describe changes in valence angles are denoted α_{jk}, where j and k indicate the two bonds forming the angle. Thus α_{45} is the coordinate which describes the change in the $H\hat{C}H$ angle at carbon atom 2 in C_2H_4S and the changes in the $D\hat{C}D$ and $H\hat{C}D$ angles at carbon atom 2 in C_2D_4S and cis- or trans-$C_2D_2H_2S$, respectively.

Five of the twenty internal coordinates defined in Table 5 must be redundant since there are only fifteen genuine vibrations in each isotopic modification of ethylene sulphide. Three of these redundancies arise since six internal coordinates, R_1, R_2, R_3, α_{13}, α_{12} and α_{23}, are defined in the CSC ring, which has only three degrees of vibrational

TABLE 5

Internal Coordinates[a] for Ethylene Sulphide

Coordinate Number	Notation	Description	
1	R_1	C_2-C_3	Stretch
2	R_2	C_3-S_1	Stretch
3	R_3	C_2-S_1	Stretch
4	R_4	C_2-H_4	Stretch
5	R_5	C_2-H_5	Stretch
6	R_6	C_3-H_6	Stretch
7	R_7	C_3-H_7	Stretch
8	α_{45}	$H_4-\hat{C}_2-H_5$	Bend
9	α_{67}	$H_6-\hat{C}_3-H_7$	Bend
10	α_{34}	$S_1-\hat{C}_2-H_4$	Bend
11	α_{35}	$S_1-\hat{C}_2-H_5$	Bend
12	α_{26}	$S_1-\hat{C}_3-H_6$	Bend
13	α_{27}	$S_1-\hat{C}_3-H_7$	Bend
14	α_{14}	$C_3-\hat{C}_2-H_4$	Bend
15	α_{15}	$C_3-\hat{C}_2-H_5$	Bend
16	α_{16}	$C_2-\hat{C}_3-H_6$	Bend
17	α_{17}	$C_2-\hat{C}_3-H_7$	Bend
18	α_{13}	$S_1-\hat{C}_2-C_3$	Bend
19	α_{12}	$S_1-\hat{C}_3-C_2$	Bend
20	α_{23}	$C_2-\hat{S}_1-C_3$	Bend

---

a) Defined with respect to Figure 1.

freedom. The other two redundancies arise since only five of the six angle bending coordinates defined about each carbon atom are independent. In order to take full advantage of the symmetry of each isotopic modification, it was necessary to use all twenty internal coordinates to construct symmetry coordinates (111). The symmetry coordinates for C_2H_4S are the same as those for C_2D_4S and are presented in Table 6. These coordinates form the representation $8A_1 + 3A_2 + 6B_1 + 3B_2$ under the point group C_{2v}, and a comparison of this representation with the vibrational representation of C_2H_4S or C_2D_4S shows that three A_1 and two B_1 symmetry coordinates are redundant. The symmetry coordinates for cis-$C_2D_2H_2S$, which are presented in Table 7, form the representation 11A' + 9A" under the point group C_s and, thus, three A' and two A" symmetry coordinates are redundant. The symmetry coordinates for trans-$C_2D_2H_2S$, which are presented in Table 8, form the representation 11A + 9B under the point group C_2 and, thus, three A and two B symmetry coordinates are redundant. All redundant coordinates were included in the calculations and yielded zero roots upon solving the secular equation (100).

It is usual (113-116) to describe the vibrations of C_2H_4S as either 1) a C-H stretching mode, 2) a ring deformation mode, or 3) a methylenic angle bending mode. In certain cases the description (or form, or normal coordinate) of the vibrations is approximately given by the appropriate

TABLE 6

Symmetry Coordinates[a] for C_2H_4S and C_2D_4S

Coordinate Number	Description	Symmetry
S_1	R_1	A_1
S_2	$\frac{1}{\sqrt{2}}\left\{R_2 + R_3\right\}$	A_1
S_3	$\frac{1}{2}\left\{R_4 + R_5 + R_6 + R_7\right\}$	A_1
S_4	$\frac{1}{\sqrt{2}}\left\{\alpha_{45} + \alpha_{67}\right\}$	A_1
S_5	$\frac{1}{2}\left\{\alpha_{34} + \alpha_{35} + \alpha_{26} + \alpha_{27}\right\}$	A_1
S_6	$\frac{1}{2}\left\{\alpha_{14} + \alpha_{15} + \alpha_{16} + \alpha_{17}\right\}$	A_1
S_7	$\frac{1}{\sqrt{2}}\left\{\alpha_{13} + \alpha_{12}\right\}$	A_1
S_8	α_{23}	A_1
S_9	$\frac{1}{2}\left\{R_4 - R_5 - R_6 + R_7\right\}$	A_2
S_{10}	$\frac{1}{2}\left\{\alpha_{34} - \alpha_{35} - \alpha_{26} + \alpha_{27}\right\}$	A_2
S_{11}	$\frac{1}{2}\left\{\alpha_{14} - \alpha_{15} - \alpha_{16} + \alpha_{17}\right\}$	A_2
S_{12}	$\frac{1}{\sqrt{2}}\left\{R_2 - R_3\right\}$	B_1
S_{13}	$\frac{1}{2}\left\{R_4 + R_5 - R_6 - R_7\right\}$	B_1
S_{14}	$\frac{1}{\sqrt{2}}\left\{\alpha_{45} - \alpha_{67}\right\}$	B_1
S_{15}	$\frac{1}{2}\left\{\alpha_{34} + \alpha_{35} - \alpha_{26} - \alpha_{27}\right\}$	B_1

TABLE 6 (continued)

Coordinate Number	Description	Symmetry
S_{16}	$\frac{1}{2}\left\{\alpha_{14} + \alpha_{15} - \alpha_{16} - \alpha_{17}\right\}$	B_1
S_{17}	$\frac{1}{\sqrt{2}}\left\{\alpha_{13} - \alpha_{12}\right\}$	B_1
S_{18}	$\frac{1}{2}\left\{R_4 - R_5 + R_6 - R_7\right\}$	B_2
S_{19}	$\frac{1}{2}\left\{\alpha_{34} - \alpha_{35} + \alpha_{26} - \alpha_{27}\right\}$	B_2
S_{20}	$\frac{1}{2}\left\{\alpha_{14} - \alpha_{15} + \alpha_{16} - \alpha_{17}\right\}$	B_2

---

a) Defined with respect to the internal coordinates in Table 5.

TABLE 7

Symmetry Coordinates[a] for cis-$C_2D_2H_2S$

Coordinate Number	Description	Symmetry
S_1	R_1	A'
S_2	$\frac{1}{\sqrt{2}}\left\{R_2 + R_3\right\}$	A'
S_3	$\frac{1}{\sqrt{2}}\left\{R_4 + R_6\right\}$	A'
S_4	$\frac{1}{\sqrt{2}}\left\{R_5 + R_7\right\}$	A'
S_5	$\frac{1}{\sqrt{2}}\left\{\alpha_{45} + \alpha_{67}\right\}$	A'
S_6	$\frac{1}{\sqrt{2}}\left\{\alpha_{34} + \alpha_{26}\right\}$	A'
S_7	$\frac{1}{\sqrt{2}}\left\{\alpha_{35} + \alpha_{27}\right\}$	A'
S_8	$\frac{1}{\sqrt{2}}\left\{\alpha_{14} + \alpha_{16}\right\}$	A'
S_9	$\frac{1}{\sqrt{2}}\left\{\alpha_{15} + \alpha_{17}\right\}$	A'
S_{10}	$\frac{1}{\sqrt{2}}\left\{\alpha_{13} + \alpha_{12}\right\}$	A'
S_{11}	α_{23}	A'
S_{12}	$\frac{1}{\sqrt{2}}\left\{R_2 - R_3\right\}$	A"
S_{13}	$\frac{1}{\sqrt{2}}\left\{R_4 - R_6\right\}$	A"
S_{14}	$\frac{1}{\sqrt{2}}\left\{R_5 - R_7\right\}$	A"
S_{15}	$\frac{1}{\sqrt{2}}\left\{\alpha_{45} - \alpha_{67}\right\}$	A"

Table 7 (continued)

Coordinate Number	Description	Symmetry
S_{16}	$\frac{1}{\sqrt{2}}\left\{\alpha_{34} - \alpha_{26}\right\}$	A"
S_{17}	$\frac{1}{\sqrt{2}}\left\{\alpha_{35} - \alpha_{27}\right\}$	A"
S_{18}	$\frac{1}{\sqrt{2}}\left\{\alpha_{14} - \alpha_{16}\right\}$	A"
S_{19}	$\frac{1}{\sqrt{2}}\left\{\alpha_{15} - \alpha_{17}\right\}$	A"
S_{20}	$\frac{1}{\sqrt{2}}\left\{\alpha_{13} - \alpha_{12}\right\}$	A"

---

a) Defined with respect to the internal coordinates in Table 5.

TABLE 8

Symmetry Coordinates[a] for trans-$C_2D_2H_2S$

Coordinate Number	Description	Symmetry
S_1	R_1	A
S_2	$\frac{1}{\sqrt{2}}\left\{R_2 + R_3\right\}$	A
S_3	$\frac{1}{\sqrt{2}}\left\{R_4 + R_7\right\}$	A
S_4	$\frac{1}{\sqrt{2}}\left\{R_5 + R_6\right\}$	A
S_5	$\frac{1}{\sqrt{2}}\left\{\alpha_{45} + \alpha_{67}\right\}$	A
S_6	$\frac{1}{\sqrt{2}}\left\{\alpha_{34} + \alpha_{27}\right\}$	A
S_7	$\frac{1}{\sqrt{2}}\left\{\alpha_{35} + \alpha_{26}\right\}$	A
S_8	$\frac{1}{\sqrt{2}}\left\{\alpha_{14} + \alpha_{17}\right\}$	A
S_9	$\frac{1}{\sqrt{2}}\left\{\alpha_{15} + \alpha_{16}\right\}$	A
S_{10}	$\frac{1}{\sqrt{2}}\left\{\alpha_{13} + \alpha_{12}\right\}$	A
S_{11}	α_{23}	A
S_{12}	$\frac{1}{\sqrt{2}}\left\{R_2 - R_3\right\}$	B
S_{13}	$\frac{1}{\sqrt{2}}\left\{R_4 - R_7\right\}$	B
S_{14}	$\frac{1}{\sqrt{2}}\left\{R_5 - R_6\right\}$	B
S_{15}	$\frac{1}{\sqrt{2}}\left\{\alpha_{45} - \alpha_{67}\right\}$	B

TABLE 8 (continued)

Coordinate Number	Description	Symmetry
S_{16}	$\frac{1}{\sqrt{2}}\left\{\alpha_{34} - \alpha_{27}\right\}$	B
S_{17}	$\frac{1}{\sqrt{2}}\left\{\alpha_{35} - \alpha_{26}\right\}$	B
S_{18}	$\frac{1}{\sqrt{2}}\left\{\alpha_{14} - \alpha_{17}\right\}$	B
S_{19}	$\frac{1}{\sqrt{2}}\left\{\alpha_{15} - \alpha_{16}\right\}$	B
S_{20}	$\frac{1}{\sqrt{2}}\left\{\alpha_{13} - \alpha_{12}\right\}$	B

---

a) Defined with respect to the internal coordinates in Table 5.

symmetry coordinate. Thus, because the C-H stretching vibrations have much different frequencies from those of the other modes, their forms can be expected to be closely approximated by the symmetry coordinates S_3, S_9, S_{13} and S_{18} (Table 6). Those vibrations approximated by S_3 and S_{13} are called symmetric CH_2 stretching modes while the other two are called asymmetric (or antisymmetric) CH_2 stretching modes. There are three vibrational modes which involve deformation of the CSC ring. Since there are six symmetry coordinates in Table 6 which describe ring deformations (S_1, S_2, S_7, S_8, S_{12} and S_{17}), three of these coordinates must be redundant. Although all coordinates are included in the calculation, the ring deformation modes will be qualitatively described by the symmetry coordinates, S_1, S_2 and S_{12}, which correspond to the C-C stretching mode, the symmetric C-S stretching mode and the asymmetric C-S stretching mode, respectively.

The remaining eight vibrations in C_2H_4S are usually classified as deformations, wags, twists and rocks (117) of the methylenic groups. Each of these terms describes displacements which are defined by linear combinations of the symmetry coordinates in Table 6 which involve the $S\hat{C}H$ and $C\hat{C}H$ angle bending coordinates. The methylenic deformations are described by $S_5 + S_6$ and $S_{15} + S_{16}$ and refer to the symmetrical 'scissors-like' bending of the $H\hat{C}H$ angles. Because of redundancies, the methylenic deformations can also be described by the symmetry coordinates S_4 and S_{14} of Table 6. The term 'methylenic wags' refers to the 'fan-like' motions of the methylenic groups perpendicular to their own planes, and are defined by $S_5 - S_6$ and $S_{15} - S_{16}$. The methylenic twists are defined by $S_{10} - S_{11}$ and $S_{19} - S_{20}$, and refer to restricted rotation of the hydrogen atoms about the bisector of each $H\hat{C}H$ angle. The methylenic rocks are defined by $S_{10} + S_{11}$ and $S_{19} + S_{20}$, and refer to the rotary motion of each methylenic group about an axis perpendicular to its plane. It must be emphasized that these terms are only approximate descriptions of the vibrations and normal coordinate calculations indicate that many vibrations are much more complicated than these simple terms imply. Nevertheless, this terminology is useful, and has been applied by others (113-116) to ethylene sulphide, and is used in this work.

The terminology given above can also be used to describe the vibrations of C_2D_4S. There is, however, no analogous terminology to describe the methylenic vibrations of cis- and trans-$C_2D_2H_2S$. For simplicity, the vibrations which involve changes in the $C\hat{C}H$ and $S\hat{C}H$ angles (or $C\hat{C}D$ and $S\hat{C}D$ angles) will be referred to as $C\hat{C}H$ (or $C\hat{C}D$) deformations until the calculated form of these vibrations is presented.

4.3 Previous Studies of the Vibrations of Ethylene Sulphide

The vibrational spectra of ethylene sulphide-h_4 have been studied several times. In 1940, Thompson and Dupré (113) reported the infrared spectrum of the gas and the Raman spectrum of the liquid, with the unavoidably low frequency accuracy and resolution available at that time. In 1951, Thompson and Cave (114) repeated the work of Thompson and Dupré with better resolution and frequency accuracy, and showed that the earlier work was suspect. The following year, Guthrie, Scott and Waddington (115) reported the infrared spectrum of the liquid for the first time. More recently, LeBrumant (116) has studied the infrared and Raman spectra of the liquid and the infrared spectrum of the solid, and Aleksanyan and Kuz'yants (118) have reported the infrared spectra of the gas, liquid and solid and the Raman spectrum of the liquid.

The assignments of the fundamental frequencies which have resulted from these studies are shown in Tables 9 and 10 for the liquid and the gas, respectively. The assignment of the fundamental frequencies of the liquid (Table 9) by LeBrumant (116) was not modified from that of Guthrie, Scott and Waddington (115) apart from a more precise determination of the frequencies, but Aleksanyan and Kuz'yants (118,119) have assigned the A_1 CH_2 wag at a higher frequency than either of the A_1 ring deformation modes. There has been no experimental evidence to indicate the relative frequencies of the CH_2 wag and the C-C stretching mode, and the isotopic derivatives studied in the present work should resolve this problem. The A_2 modes appear very weakly in

TABLE 9

Previous Assignments of the Fundamental Frequencies[a] of Liquid C_2H_4S

	Description	Guthrie et al	LeBrumant[b]	Aleksanyan et al	Othen
ν_1	A_1 C-H stretch	3000	2994	2993	2995
ν_2	A_1 CH_2 deformation	1446	1446	1445	1450
ν_3	A_1 ring mode	1112	1111	1024	1112
ν_4	A_1 CH_2 wag	1025	1024	1112	1025
ν_5	A_1 ring mode	625	616	613	611
ν_6	A_2 C-H stretch	3080[c]	3071	3071	3072
ν_7	A_2 CH_2 twist	1100[c]	1172	——	——
ν_8	A_2 CH_2 rock	875[c]	900	895	(895)[d]
ν_9	B_1 C-H stretch	(3000)[e]	(2994)[e]	(2993)[e]	(2995)[e]
ν_{10}	B_1 CH_2 deformation	1427	1426	1425	1431
ν_{11}	B_1 CH_2 wag	1051	1050	1052	——
ν_{12}	B_1 ring mode	660	657	650	(651)[d]
ν_{13}	B_2 C-H stretch	3080	3071	3071	3072
ν_{14}	B_2 CH_2 twist	943	942	943	944
ν_{15}	B_2 CH_2 rock	824	823	823	822

---

a) In cm^{-1}

b) LeBrumant accepted the assignment of Guthrie et al.

c) Values calculated from the frequencies of the corresponding B_2 modes.

d) Assignment of these features is not certain.

e) Assumed to be nearly degenerate with ν_1.

TABLE 10

Previous Assignments of the Fundamental Frequencies[a] of Gaseous C_2H_4S

	Description	Thompson and Cave	Aleksanyan and Kuz'yants	Othen
ν_1	A_1 C-H stretch	3017	3013.5	3013.5
ν_2	A_1 CH_2 deformation	1471	1456	1456.8
ν_3	A_1 ring mode	——	1033	1109.9
ν_4	A_1 CH_2 wag	1107	1109.5	1024.0
ν_5	A_1 ring mode	626	627.4	627.3
ν_6	A_2 C-H stretch	——	——	——
ν_7	A_2 CH_2 twist	——	——	——
ν_8	A_2 CH_2 rock	——	——	——
ν_9	B_1 C-H stretch	(3017)[b]	(3013.5)[b]	(3013)[b]
ν_{10}	B_1 CH_2 deformation	1440	1435	1435.9
ν_{11}	B_1 CH_2 wag	1050	1050	1050.8
ν_{12}	B_1 ring mode	685	668	——
ν_{13}	B_2 C-H stretch	3089	3084	3088.0
ν_{14}	B_2 CH_2 twist	825	944.0	945.2
ν_{15}	B_2 CH_2 rock	945	824.0	824.3

---

a) In cm^{-1}

b) Assumed to be nearly degenerate with ν_1.

the Raman spectrum and are inactive in the infrared spectrum, and their frequencies cannot be regarded as well determined. For completeness, the fundamental frequencies, obtained by Othen (109) from the Raman spectrum of the liquid, which are used in this work, are also presented in Table 9. These frequencies do not differ significantly from those reported by Le Brumant (116) and by Aleksanyan and Kuz'yants (118).

For the gas (Table 10), the fundamental frequencies of Aleksanyan and Kuz'yants (118) are consistent with those of Thompson and Cave (114) apart from the addition of 1033 cm^{-1} as the frequency of an A_1 fundamental and the improved precision with which the frequencies were determined. Aleksanyan and Kuz'yants have assigned (118,119) their frequencies of the gas following their assignment of the frequencies of the liquid (Table 9). This assignment disagrees with the earlier one of Thompson and Cave (114) in that the latter authors assigned the methylenic rocking mode to high frequency of the methylenic twisting mode. In recent years it has become accepted that methylenic twisting modes lie to high frequency of the rocking modes. This conclusion is based on the spectra of cyclobutane (120), cyclopropane (117,121-123), and hexamethylene tetramine (124-127), in which at least one methylenic twisting mode has a different symmetry from a methylenic rocking mode. In all cases, the methylenic twist was assigned a frequency comparable with that of the methylenic wag and considerably higher than that of the rock. Consequently, this order has been accepted for ethylene oxide (128) and methylene cyclopropane (129,130), and is adopted in this work. For completeness, the fundamental frequencies of gaseous C_2H_4S which are used in this work (109) are included in Table 10; their assignment is discussed in Section 4.4. The vibrational spectra of C_2D_4S and cis- and trans-$C_2D_2H_2S$ have not been previously reported.

The observed frequencies listed in Tables 9 and 10 have been used (131-133) to calculate various force constants of C_2H_4S. In each case, however, the number of force constants required to reasonably reproduce the observed frequencies exceeded the number of frequencies, so these calculations are suspect. Further, Venkateswarlu et al (131,132) included frequencies from Thompson and Dupré's (113) early work which have since been shown to arise from impurities.

4.4 The Assignment of the Spectra of C_2H_4S, C_2D_4S and cis- and trans-$C_2D_2H_2S$

The infrared spectra of gaseous C_2D_4S, cis-$C_2D_2H_2S$ and trans-$C_2D_2H_2S$ are presented in Appendix IV. The vibrational spectra of C_2H_4S are published (116,118) so those recorded by Othen (109) are not reproduced in this thesis. The frequencies of the features observed between 200 and 1500 cm^{-1} and between 2000 and 4000 cm^{-1} in the infrared spectrum of the gas and the Raman spectrum of the liquid are presented in Table 11 for C_2H_4S and Table 12 for C_2D_4S. Tables 13 and 14 present the frequencies of all features consistently observed between 200 and 4000 cm^{-1} in the infrared spectra of gaseous cis-$C_2D_2H_2S$ and trans-$C_2D_2H_2S$, respectively. In Tables 11-14, the infrared absorption band associated with each frequency is described by the letters 'PR' if only P and R branches (134) were observed and by the letters 'PQR' if P, Q and R branches (134) were observed. The letter 'P' beside a frequency in Tables 11 and 12 indicates that the Raman band at this frequency has a depolarization ratio (135) which is less than 0.75. The assignments presented in Tables 11-14 were determined as part of the present work and are discussed below.

The first stage in the assignment of the peaks observed in the spectra to particular vibrations is to determine, as far as possible, the symmetry of the transition causing each peak. Two pieces of evidence give this information: 1) a Raman depolarization ratio of less than 0.75 can only arise from a totally symmetric mode (135), so the frequencies marked P in Tables 11 and 12 must arise from A_1 transitions; 2) the shapes of the infrared absorption bands of gaseous molecules vary with the symmetry of the transition causing the absorption.

The shapes of the infrared absorption bands of the gaseous ethylene sulphide molecules can be predicted using the method outlined in Section 3.4. In both C_2H_4S and C_2D_4S,

TABLE 11

Frequencies[a] and Assignment of Features Observed in the Infrared and Raman Spectra of C_2H_4S

Infrared (gas)[b]	Raman (liquid)[b]	Assignment
3088.0 m, PQR	3071.7 m	ν_{13} B_2 C-H stretch
3084.2 w, Q		hot band
3013.5 vs, PQR	2994.7 vs,P	ν_1 A_1 C-H stretch ν_9 B_1 C-H stretch
2903.6 w, PQR		$2\nu_2$ A_1
2863.5 w, PQR		$2\nu_{10}$ A_1
1456.8 m, PQR	1450 m,P	ν_2 A_1 CH_2 deformation
1435.9 m, PR	1431 m	ν_{10} B_1 CH_2 deformation
1255 vw, PQR	1230 vw	$2\nu_5$ A_1
1173.3 vw, Q		
1109.9 m, PQR	1112 s,P	ν_3 A_1 C–C stretch
1050.8 s, PR		ν_{11} B_1 CH_2 wag
1024.0 m, PQR	1025 s, P	ν_4 A_1 CH_2 wag
945.2 m, PQR	944 w	ν_{14} B_2 CH_2 twist
	895 vw	A_2?
824.3 w, PQR	822 w	ν_{15} B_2 CH_2 rock
688.1 m, bd		
	650.8 m	ν_{12}? B_1 C-S stretch
627.3 vs, PQR	611.3 vs, P	ν_5 A_1 C-S stretch
623.0 w		hot band

a) In cm^{-1}

b) Abbreviations: w = weak; m = medium; s = strong; v = very; bd = broad; P = polarized; Q = Q branch; PQR = P,Q and R branches were visible; PR = P and R branches only were visible.

TABLE 12

Frequencies[a] and Assignment of Features Observed in the Infrared and Raman Spectra of C_2D_4S

Infrared (gas)[b]	Raman (liquid)[b]	Assignment
	2385 w	
2331.3 m, PQR	2320 m	ν_{13} B_2 C-D stretch
2215 w, Q		hot band
2212.5 m, PQR	2201 s, P	ν_1 A_1 C-D stretch
2209 w, Q		hot band
2185.2 m, PR	2177 w	ν_9 B_1 C-D stretch
2125 w, PQR	2111 w,P	$2\nu_{10}$ A_1
1241.3 vw	1222 m,P	
	1180 m,P	
	1168 m,P	
1064.2 m, PR	1055 w	ν_{10} B_1 CD_2 deformation
1027.8 w		
946.4 m, PQR	940 s, P	ν_3 A_1 C-C stretch
830.7 s, PR	829 w	ν_{11} B_1 CD_2 wag
766.5 m, PQR	762 s,P	ν_4 A_1 CD_2 wag
746.8 w		
710.8 m, PQR	708 w	ν_{14} B_2 CD_2 twist
654 w, bd		
	618 m	ν_{12}? B_1 C-S stretch
613.3 vs, PQR	603 s, P	ν_5 A_1 C-S stretch
578.1 m, PQR	579 w	ν_{15} B_2 CD_2 rock

a) In cm^{-1}

b) The abbreviations are explained in Table 11.

TABLE 13

Frequencies and Assignment of Features Observed in the Infrared Spectrum of Gaseous *cis*-$C_2D_2H_2S$

ν/cm^{-1} [a]			Assignment
3052.0	s,	PQR	ν_1 A' C-H stretch
2272.4	m,	PQR	ν_2 A' C-D stretch
1332.6	w,	PQR	ν_3 A' $\mathrm{H\hat{C}D}$ deformation
1310.0	w,	PR	ν_{11} A" $\mathrm{H\hat{C}D}$ deformation
1083.7	m,	PQR?	
1068.5	m,	PR?	
971.9	m,	PQR	ν_5 A' $\mathrm{C\hat{C}H}$ or $\mathrm{C\hat{C}D}$ bend
921.3	m,	PR	ν_{13} A" $\mathrm{C\hat{C}H}$ or $\mathrm{C\hat{C}D}$ bend
756.8	m,	PQR	ν_6 A' $\mathrm{C\hat{C}H}$ or $\mathrm{C\hat{C}D}$ bend
654.7	m,	PQR	ν_7 A' $\mathrm{C\hat{C}H}$ or $\mathrm{C\hat{C}D}$ bend
614.8	s,	PQR	ν_8 A' C-S stretch

---

a) The abbreviations are explained in Table 11

TABLE 14

Frequencies and Assignment of Features Observed in the Infrared Spectrum of Gaseous *trans*-$C_2D_2H_2S$

ν/cm^{-1} [a]			Assignment
3051.0	m,	PQR	C-H stretches
3044.2	m,	PQR	
2272.2	m,	PQR	C-D stretches
2262.6	w,	PQR	
1315.2	vw,	Q	$\mathrm{H\hat{C}D}$ deformation
1293.1	vw,	Q	
1113.4	m,	PQR	ν_4 A C-C stretch
1002.8	s,	PQR	
867.7	m,	PQR	$\mathrm{C\hat{C}H}$ or $\mathrm{C\hat{C}D}$ bends
773.4	m,	PQR	
704.5	m,	PQR	
668.2	m,	PQR	
617.5	vs,	PQR	ν_8 A C-S stretch
610	shoulder		

---

a) The abbreviations are explained in Table 11.

the principal axes of inertia, a-, b- and c-, are parallel to the z-, x- and y- Cartesian axes, respectively, which are defined in Figure 21. It can therefore be seen from the character table for the point group C_{2v} (136) that, in both C_2H_4S and C_2D_4S, A_1 vibrations cause dipole moment changes parallel to the a-axis, and therefore yield A-type (104,105) infrared absorption bands; B_1 vibrations cause dipole moment changes parallel to the b-axis, and therefore yield B-type (104,105) infrared absorption bands; and B_2 vibrations cause dipole moment changes parallel to the c-axis, and therefore yield C-type (104,105) infrared absorption bands. It is found, by substituting the values of the rotational constants of C_2H_4S and C_2D_4S given in Table 4 into equations 1 and 2 of Section 3.4, that $X = 1.494$ and $Y = -0.108$ for C_2H_4S and $X = 1.493$ and $Y = -0.183$ for C_2D_4S. These parameters indicate that C_2H_4S closely approximates rotor number 16 of reference 105 and C_2D_4S closely approximates rotor number 25. Therefore, for each molecule, a B-type band is predicted to have only P and R branches while A- and C- type bands are predicted to have P, Q and R branches (105).

The assignment of the A_1 modes in C_2H_4S at 3013.5, 1456.8, 1109.9, 1024.0 and 627.3 cm^{-1}, the B_1 modes at 3013, 1435.9, and 1050.8 cm^{-1}, and the B_2 modes at 3088.0, 945.2 and 824.3 cm^{-1} is consistent with previous assignments (Tables 9 and 10). The fourth B_1 mode (ν_{12}) has been assigned between 650 and 685 cm^{-1} by all previous authors

(113-116,118). The only band which is observed in this region in the infrared spectrum of gaseous C_2H_4S is a broad, featureless absorption at 688.1 cm^{-1} whose shape is unlike any band shape predicted for C_2H_4S from reference 105. Since there is a band at 650.8 cm^{-1} in the Raman spectrum of liquid C_2H_4S it has been argued (118) that the feature at 688.1 cm^{-1} is the R branch of a band with PR structure whose P branch is hidden under the strong absorption at 627.3 cm^{-1}. This implies that the separation between the P and R branches is at least 35 cm^{-1}. However, the method of reference 105 (Section 3.4) predicts that the separation between the P and R branches of a B-type band in the infrared spectrum of gaseous C_2H_4S is about 17 cm^{-1}. Because of this discrepancy between calculated and observed PR separations, the possibility that the 688.1 cm^{-1} feature arises from an impurity cannot be ruled out, and the frequency of the fourth B_1 mode of the gaseous molecule is left unassigned. In the liquid, this mode is probably at 650.8 cm^{-1}.

The weak features with PQR structures at 2903.6, 2863.5 and 1255 cm^{-1} in the infrared spectrum of C_2H_4S are assigned to the first overtones of the fundamental transitions at 1456.8, 1435.9 and 627.3 cm^{-1}, respectively. The proximity of 1255 cm^{-1} to twice 627.3 cm^{-1} implies that this vibration is almost harmonic. The weak absorption at 3084.2 cm^{-1} undoubtedly arises from a hot transition (42) associated with the B_2 mode assigned at 3088.0 cm^{-1}. A very weak feature at 1173.3 cm^{-1} cannot be assigned to an overtone or combination transition and its origin is not obvious. It does not have the characteristic PR structure of a B_1 fundamental absorption, nor does it have a corresponding polarized Raman band which is characteristic of an A_1 mode. Its assignment to a B_2 mode would require that it shifts to 710.8 cm^{-1} or lower in C_2D_4S, which is most unlikely.

The assignment of the Raman spectrum of the liquid follows from the above assignment of the infrared spectrum of the gas. As is usual, the Raman spectrum does not provide good evidence of the location of the three A_2 modes (ν_6, ν_7 and ν_8) and, thus, they are not assigned in Table 11. The weak feature at 895 cm^{-1} has been assigned by Le Brumant (116) to an A_2 mode but was considered to be too weak to be confidently assigned in this work.

As is the case for C_2H_4S, the Raman spectrum of C_2D_4S (Table 12) does not provide a clear-cut indication of the frequencies of ν_6, ν_7 and ν_8, so these modes are not assigned. Four strong Raman bands have depolarization ratios of less than 0.75. The corresponding infrared absorption bands, at 2212.5, 946.4, 766.5 and 613.3 cm^{-1}, show PQR structures and can be assigned to A_1 modes. The product rule (137) can be used to predict the frequency of the fifth A_1 mode. The theoretical value of the product of the A_1 frequencies of C_2D_4S divided by the product of the A_1 frequencies of

C_2H_4S is given by:

$$\prod_{k=1}^{5}\left(\frac{\nu_k'}{\nu_k}\right) = \left(\frac{m_H}{m_D}\right)^{3/2}\left(\frac{M'}{M}\right)^{1/2} = 0.3657 \qquad (1)$$

where the primed symbols refer to properties of C_2D_4S and the corresponding unprimed ones refer to properties of C_2H_4S, M is the molecular weight, the ν_k are the frequencies and m_H and m_D are the masses (101) of the hydrogen and deuterium atoms, respectively. From the five A_1 frequencies of C_2H_4S (Table 11) and the four A_1 frequencies of C_2D_4S assigned above, the missing frequency is calculated to be 1168 cm^{-1}, which indicates that ν_2 is the missing fundamental. ν_2 of the gaseous molecule is left unassigned at present. There are three medium, polarized Raman bands of the liquid near to 1168 cm^{-1}, one of which could be due to ν_2, or they could all be due to combination or overtone transitions.

The three strongest infrared bands with PQR structures which have corresponding depolarized Raman bands are assigned to the three B_2 fundamentals. Thus ν_{13} is assigned at 2331.3 cm^{-1}, ν_{14} at 710.8 cm^{-1} and ν_{15} at 578.1 cm^{-1}. The theoretical value of the product rule for the B_2 modes is given by:

$$\prod_{k=13}^{15}\left(\frac{\nu_k'}{\nu_k}\right) = \left(\frac{m_H}{m_D}\right)^{3/2}\left(\frac{M'}{M}\right)^{1/2}\left(\frac{C}{C'}\right)^{1/2} = 0.3967 \qquad (2)$$

where C is the smallest rotational constant (Table 4), and the other symbols have been defined in equation 1. The value obtained from the three frequencies assigned above with those of C_2H_4S is 0.3988, which agrees well with the theoretical value.

Three of the B_1 fundamentals can be readily assigned to the medium or strong bands at 2185.2, 1064.2 and 830.7 cm^{-1}. These all have the PR structures expected for a B_1 mode and corresponding depolarized bands appear weakly in the Raman spectrum. The situation concerning the fourth B_1 mode is identical to that for C_2H_4S. The feature at 654 cm^{-1} is too far away from the absorption at 613.3 cm^{-1} for it to be the R branch of a B-type band whose P branch is buried under the absorption centered at 613.3 cm^{-1}. ν_{12} is, therefore, left unassigned for the gaseous molecule, although it probably appears as the medium band at 618 cm^{-1} in the Raman spectrum of the liquid. The description of the fundamental vibrations of C_2D_4S given in Table 12 follows from the descriptions of the vibrations of C_2H_4S and the approximate frequency shifts expected to occur upon deuteration.

The weak features in the infrared spectrum of the gas at 654, 746.8, and 1027.8 cm^{-1} cannot be assigned to combination or overtone transitions and they must be tentatively attributed to impurities. The weaker bands left unassigned above 1100 cm^{-1} could all arise from hot, overtone, or combination transitions. The only one whose specific assignment is clear from this data is at 2125 cm^{-1}, which is assigned to $2\nu_{10}$.

The assignment of the infrared spectrum of cis-$C_2D_2H_2S$ (Table 13) is also aided by considering the band shapes predicted for vibrational modes of the two symmetry classes, A' and A". Figure 22 shows the relationship between the Cartesian axes, as defined in Figure 21, and the principal axes of inertia of cis-$C_2D_2H_2S$. It can be seen that both z- and y-Cartesian axes lie in the ac plane of the molecule. The eight A' modes of cis-$C_2D_2H_2S$ cause dipole moment changes in this plane and, thus, lead to AC hybrid bands (104,105). The seven A" modes of cis-$C_2D_2H_2S$ cause dipole moment changes along the b-axis of inertia and give rise to B-type infrared absorption bands. It is found, by substituting the values of the rotational constants of cis-$C_2D_2H_2S$ (Table 4) into equations 1 and 2 of Section 3.4, that $X = 1.491$ and $Y = -0.143$, which indicates that this molecule closely approximates the rotors numbered 16 and 25 in reference 105. The A- and C- type bands calculated for these rotors both have distinct P, Q and R branches, and therefore an AC hybrid band also has PQR structure. A B-type band, on the other hand, is predicted to have PR structure. Thus, the seven bands which clearly have PQR structures, at 3052.0, 2272.4, 1332.6, 971.9, 756.8, 654.7, and 614.8 cm^{-1} can confidently be assigned to A' modes, and the two bands which clearly have PR structures, at 1310.0 and 921.3 cm^{-1} can confidently

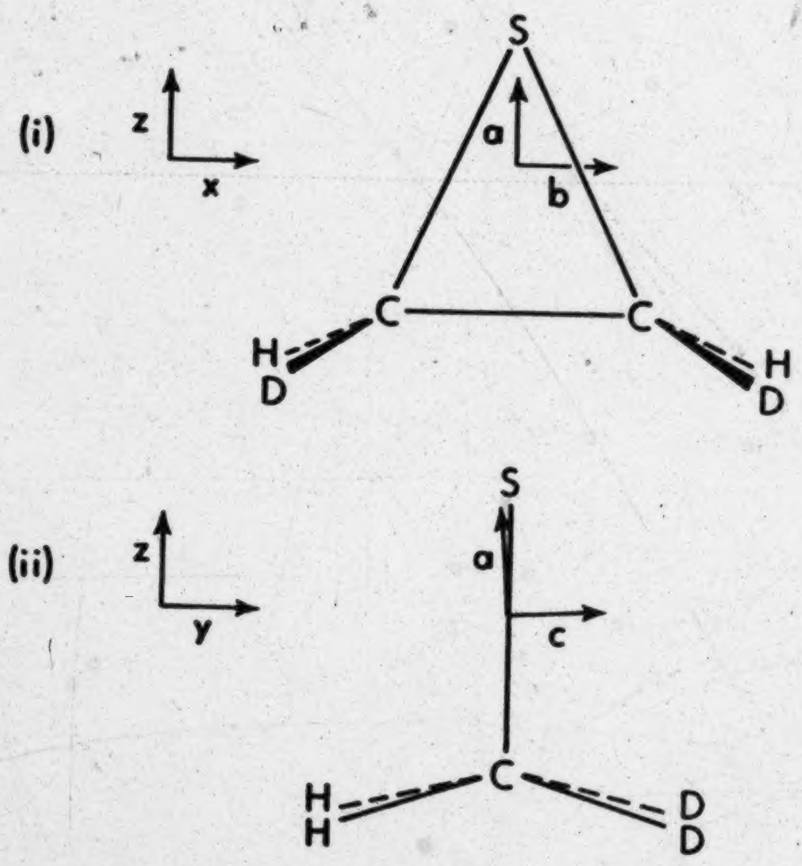
(i)
z
x
S
a
b
C
C
H
D
H
D
(ii)
z
y
S
a
c
C
H
H
D
D

FIGURE 22. Projection of cis-$C_2D_2H_2S$ on the zx (i) and zy (ii) Cartesian planes, showing the relationship between the Cartesian axes and the a-, b- and c- principal axes of inertia.

be assigned to A" modes. The absorption close to 1075 cm^{-1} may be due to the superposition of absorptions by the eighth A' mode and a third A" mode, but, at this stage these modes cannot be confidently assigned.

The vibrations must be numbered in the order of decreasing frequency within each symmetry class. For the A' vibrations this is trivial since only one vibration is not assigned and that one undoubtedly is the A' C-C stretching mode, ν_4, which should absorb somewhere between the A' frequencies 971.9 and 1332.6 cm^{-1}. In addition, the bands at 3052.0, 2272.4, 1332.6 and 614.8 cm^{-1} can be assigned to the A' C-H stretching vibration, the A' C-D stretching vibration, The A' $H\hat{C}D$ deformation, and the A' C-S stretching vibration, respectively. The other A' modes must be $C\hat{C}H$ or $C\hat{C}D$ deformations. The A" C-H and C-D stretching modes, ν_9 and ν_{10}, must absorb above 2000 cm^{-1} and are probably accidentally degenerate with the A' modes at 3052.0 and 2272.4 cm^{-1}, respectively. The A" mode at 1310 cm^{-1} is undoubtedly the $H\hat{C}D$ deformation ν_{11}. ν_{12} is probably at about 1075 cm^{-1}, so 921.3 cm^{-1} is probably due to ν_{13}. ν_{14} and ν_{15} are not observed, but ν_{15} is probably the A" C-S stretching mode and is, most likely, nearly coincident with the A' C-S stretching mode at 614.8 cm^{-1}. Thus, ν_{12} to ν_{14} must be described as $C\hat{C}H$ or $C\hat{C}D$ bends.

Figure 23 shows the relationship between the Cartesian axes, as defined in Figure 21, and the principal axes of inertia of trans-$C_2D_2H_2S$. It is seen that the x- and y-

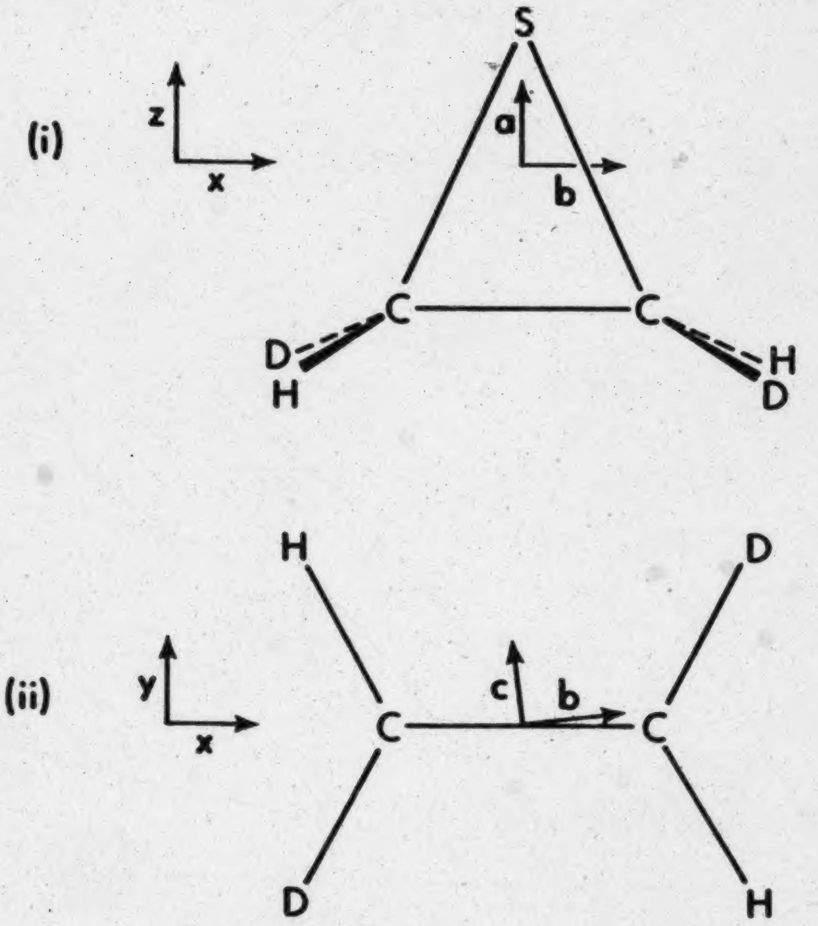
S
(i)
z
x
a
b
C
C
D
H
H
D
H
D
(ii)
y
x
c
b
C
C
D
H

FIGURE 23. Projection of trans-$C_2D_2H_2S$ on the zx (i) and yx (ii) Cartesian planes, showing the relationship between the Cartesian axes and the a-, b- and c- principal axes of inertia.

Cartesian axes both lie in the bc plane of the molecule and the eight A vibrations give rise to A-type bands and the seven B vibrations give rise to BC hybrid bands (104, 105). The values of the rotational constants of trans-$C_2D_2H_2S$ substituted into equations 1 and 2 of Section 3.4 yield X = 1.479 and Y =-0.139, which indicates that this molecule closely approximates the rotors numbered 16 and 25 of reference 105. Both A-type and BC hybrid bands for these rotors are predicted to have PQR structures, so no distinction between modes of A and B symmetry can be made on the basis of band shape alone.

Several frequencies in the spectrum of trans-$C_2D_2H_2S$ (Table 14) can be assigned in view of the assignments presented in Tables 11, 12 and 13. The bands at 1113.4 and 617.5 cm^{-1} most probably arise from the A C-C stretching mode (ν_4) and the A C-S stretching mode (ν_8), respectively, and are assigned as such in Table 14. The bands at 3051.0 and 3044.2 cm^{-1} obviously arise from C-H streching modes and those at 2272.2 and 2262.6 cm^{-1} from C-D stretching modes, although it is not known whether the A or B modes have the higher frequencies. Also, the two $H\hat{C}D$ deformations are expected to absorb close in frequency to the very weak features observed at 1315.2 and 1293.1 cm^{-1}.

The assignment of the frequencies of the gaseous molecules which have been made in this section were used as data for the calculations which are described in the next two sections. These calculations allowed further assignments to be made, as discussed later.

4.5 Computer Programs and the $\underset{\sim}{G}$ and $\underset{\sim}{F}$ Matrices

The normal coordinate analysis was carried out with the aid of the programs VSEC and FPERT (138) which were written by Schachtschneider. These programs use the well-documented $\underset{\sim}{G}\,\underset{\sim}{F}$ matrix method (100) to calculate the vibrational frequencies, ν_k, and the elements, ℓ_{ik}, of the eigenvectors. The normal coordinates, Q_k, are related to the n internal coordinates, I_i, by n expressions of the type

$$I_i = \sum_{k=1}^{3N-6} \ell_{ik}\, Q_k \qquad (1)$$

where N is the number of atoms in the molecule. Therefore the elements ℓ_{ik} with k constant provide a description of the k^{th} normal vibration. VSEC and FPERT calculate the frequencies from the $\underset{\sim}{G}$ and $\underset{\sim}{F}$ matrices supplied and, in addition, FPERT compares the calculated frequencies with the observed ones, adjusts the force constants to improve the fit, and continues until a satisfactory solution is reached. If the $\underset{\sim}{G}$ matrices and observed frequencies of two or more isotopic molecules are supplied, the same force field can be refined to simultaneously fit the frequencies of all the molecules. VSEC, which does not refine the force constants, was only used in the latter stages of the analysis to calculate the forms of the vibrations in terms of methylenic deformations, wags, etc.

The $\underset{\sim}{G}$ matrix elements were calculated for each isotopic modification of ethylene sulphide from the molecular parameters listed in Table 3 and the atomic masses (101), using the programs CART and GMAT (103). The non-zero $\underset{\sim}{G}$ matrix elements for each molecule are presented in Appendix I, where each element is identified by two integers, i and j, which refer to the internal coordinates, I_i and I_j, respectively, as defined in Table 5. Only the elements for which $i \leq j$ are listed in Appendix I since the $\underset{\sim}{G}$ matrices are symmetric.

The force constants which are described in this work are defined as the coefficients f_{ij} in the expression

$$V = \frac{1}{2} \sum_{i,j=1}^{n} f_{ij} I_i I_j \qquad (2)$$

where V is the potential energy of a molecule in terms of the n internal coordinates under the harmonic approximation. The matrix formed by these coefficients is termed the $\underset{\sim}{F}$ matrix. When $i=j$ the coefficients, f_{ii}, are referred to as the diagonal force constants, and when $i \neq j$ the coefficients, f_{ij}, are referred to as the interaction constants.

The potential energy, V_k, of a particular vibration with normal coordinate Q_k and frequency ν_k is given by (100):

$$V_k = 1/2\ \lambda_k\ Q_k^{\ 2} \tag{3}$$

where $\lambda_k = 4\Pi^2\ \nu_k^{\ 2}$, and is also given by

$$V_k = \sum_{i,j}^{n} (PED)_{ijk} \tag{4}$$

where

$$(PED)_{ijk} = \frac{f_{ij}}{\lambda_k}\ \ell_{ik}\ \ell_{jk} \tag{5}$$

Thus each term $(PED)_{ijk}$ with k constant describes the contribution to the potential energy of the k^{th} vibration from the force constant f_{ij}. The complete set of these terms with k constant is called the potential energy distribution for the k^{th} vibration, and provides a description of the vibration which supplements that given by the eigenvectors.

The general harmonic force field for C_2H_4S or C_2D_4S contains eight independent diagonal force constants and sixty-one independent interaction constants, and it is assumed that this force field is also valid for cis- and trans-$C_2D_2H_2S$. The eight diagonal force constants in the general harmonic force field will be denoted by F(CC), F(CS), F(CH), F(HCH), F(SCH), F(CCH), F(CCS) and F(CSC). The first three force constants are due to the forces which oppose the extension or contraction of the C-C, C-S and C-H bonds, respectively, and have units of mdyne / Å. The latter five constants have units of mdyne-Å, and are due to the forces which oppose the distortion of the $H\hat{C}H$, $S\hat{C}H$, $C\hat{C}H$, $C\hat{C}S$ and $C\hat{S}C$ bond angles, respectively.

The interaction constants account for the change in stiffness of a bond or bond angle as a result of the distortion of another bond or bond angle. The interaction constant between two bond-stretching coordinates, R_i and R_j (Table 5), is denoted by $f(R_i,R_j)$ and has units of mdyne / Å. The interaction constant between a bond-stretching coordinate, R_i, and an angle-bending coordinate, α_{jk}, is denoted by $f(R_i,\alpha_{jk})$ and has units of mdyne, while the interaction constant between two angle-bending coordinates, α_{ij} and α_{kl}, is denoted by $f(\alpha_{ij},\alpha_{kl})$ and has units of mdyne-Å.

Because of symmetry, many of the force constants defined in equation 2 are equivalent and, for the sake of simplicity in this work, a reference to a particular force constant in an equivalent set will also implicitly refer to the other members of the set. Thus, for example, the diagonal constant F(HCH) refers to both $F(H_4\hat{C}_2H_5)$ and $F(H_6\hat{C}_3H_7)$ (Figure 21), and reference to $f(\alpha_{14},\alpha_{34})$, which describes the interaction between the $C_3\hat{C}_2H_4$ and $S_1\hat{C}_2H_4$ angle-bending coordinates, also implies reference to $f(\alpha_{15},\alpha_{35})$, $f(\alpha_{16},\alpha_{26})$ and $f(\alpha_{17},\alpha_{27})$.

4.6 Development of the Force Field

Initially only the observed frequencies for C_2H_4S (Table 11) were used in the calculation. The initial values of the diagonal force constants are shown in column #1 of Table 15, the values of F(CC), F(CS), F(CCH) and F(SCH) having been taken from the force field for C_2H_4S reported by Freeman and Henshall (133). The values of F(CH), F(HCH), F(CCS) and F(CSC) are close to the values of analogous force constants in the force field of methylene cyclopropane reported by Bertie and Norton (130). The frequencies of C_2H_4S calculated with this initial force field are shown in column #1 of Table 16, which also contains the experimental frequencies. The differences between the calculated and observed frequencies are, on the average, 84.0 cm^{-1} or 6.99%, and were too large to allow FPERT to refine this force field. The potential energy distributions (Section 4.5) revealed that F(CCS) and F(CSC) did not contribute significantly to any of the normal modes. Thus these two diagonal force constants were constrained to zero and FPERT did then refine the remaining six constants. The fit between the eleven observed frequencies of C_2H_4S and the calculated ones did not im-

TABLE 15

Force Constants for Ethylene Sulphide[a,b]

Constant	#1	#2	#3	#4	Final	Error[c]
F(CC)	4.5	4.382	4.548	4.650	4.777	0.122
F(CS)	2.8	2.937	2.399	2.404	2.492	0.107
F(CH)	5.0	5.102	5.109	5.101	5.104	0.012
F(HCH)	0.41	0.391	0.467	0.264	0.772	0.074
F(SCH)	0.47	0.583	0.544	0.585	0.576	0.008
F(CCH)	0.77	0.504	0.599	0.746	0.344	0.054
F(CCS)	0.50	0.0	0.0	0.0	0.301	0.094
F(CSC)	0.70	0.0	0.0	0.0	0.0	——
$F(R_4,R_5)^d$	——	0.014	0.019	0.029	0.019	0.014
$F(\alpha_{14},\alpha_{34})^d$	——	−0.182	−0.252	−0.193	−0.348	0.035
$F(R_1,\alpha_{14})^d$	——	——	0.275	0.254	0.293	0.046
$F(R_2,\alpha_{26})^d$	——	——	0.227	0.243	0.373	0.065
$F(\alpha_{45},\alpha_{67})$	——	——	0.016	0.058	0.0	——
$F(\alpha_{14},\alpha_{15})^d$	——	——	——	0.190	−0.236	0.048
$F(\alpha_{34},\alpha_{35})^d$	——	——	——	0.004	0.0	——
$F(\alpha_{14},\alpha_{16})^d$	——	——	——	−0.045	−0.008	0.007
$F(\alpha_{14},\alpha_{17})^d$	——	——	——	——	0.072	0.008
$F(\alpha_{14},\alpha_{35})^d$	——	——	——	——	−0.180	0.043
$F(R_1,\alpha_{34})^d$	——	——	——	——	−0.159	0.040

---

a) The units are mdyne/Å for bond-stretching force constants and stretch-stretch interaction constants, mdyne for bond stretch-angle bend interaction constants, and mdyne-Å for angle-bending force constants and angle bend-angle bend interaction constants.

b) Force constants which are shown as zero were constrained to zero during the refinement of that stage.

c) Statistical error calculated by program (138) from relationship between force constants and frequencies.

d) All force constants which are equivalent to this under C_{2v} symmetry had the same value.

TABLE 16

Observed Frequencies for Gaseous C_2H_4S and those Calculated with the Force Fields Shown in Table 15[a]

	OBS	#1	#2	#3	#4	Final
ν_1	3013.5	2985.5	3017.8	3018.8	3019.6	3018.5
ν_2	1456.8	1684.6	1486.7	1452.1	1463.9	1466.0
ν_3	1109.9	1101.5	1115.1	1106.3	1124.3	1107.1
ν_4	1024.0	916.1	952.7	979.6	999.1	1023.5
ν_5	627.3	651.5	657.2	640.1	640.8	633.3
ν_6		3088.8	3107.0	3107.9	3103.8	3109.2
ν_7		1364.3	992.4	1051.9	1083.4	1160.3
ν_8		765.1	894.5	847.2	896.5	890.2
ν_9	3013	2975.3	3008.5	3011.2	3011.2	3010.4
ν_{10}	1435.9	1616.2	1409.7	1440.2	1432.3	1431.9
ν_{11}	1050.8	975.0	1052.4	1063.4	1057.6	1060.2
ν_{12}		653.3	616.1	586.8	583.9	645.9
ν_{13}	3088.0	3075.4	3101.6	3101.9	3096.7	3100.6
ν_{14}	945.2	1143.5	951.3	962.6	950.5	947.1
ν_{15}	824.3	801.6	817.4	811.1	817.0	820.5
Average Error[b]		84.0 cm^{-1} 6.99%	18.1 cm^{-1} 1.68%	12.2 cm^{-1} 1.15%	9.1 cm^{-1} 0.84%	5.3 cm^{-1} 0.40%

---

a) Observed and calculated frequencies in cm^{-1}

b) Error in cm^{-1} calculated from $\left[\sum_k \left| \nu_k(\text{obs}) - \nu_k(\text{calc}) \right| \right] \Big/ n$ where n is the number of observed frequencies. Percent error calculated from $\left[\sum_k \left| \frac{\nu_k(\text{obs}) - \nu_k(\text{calc})}{\nu_k(\text{obs})} \right| \times 100\% \right] \Big/ n$.

prove after ten refinements by FPERT. At this point interaction constants were introduced into the force field and all constants, except F(CCS) and F(CSC) which were both constrained to zero, were refined after each addition.

The first interaction constant which was added to the diagonal field was $f(R_4,R_5)$, which takes into account the interaction between the two C-H stretching displacements on carbon atom 2 (Figure 21). Because of the symmetry of C_2H_4S, the interaction constant $f(R_6,R_7)$ is equivalent to $f(R_4,R_5)$. These two equivalent constants improved the agreement between the observed and calculated C-H stretching frequencies, ν_1, ν_9 and ν_{13}. A second interaction constant, $f(\alpha_{14}, \alpha_{34})$, which is equivalent to $f(\alpha_{15}, \alpha_{35})$, $f(\alpha_{16}, \alpha_{26})$ and $f(\alpha_{17}, \alpha_{27})$, takes into account the interaction between the $C\hat{C}H$ and $S\hat{C}H$ angle-bending coordinates which involve a common hydrogen atom, and improved the agreement between the observed and calculated methylenic frequencies, ν_2, ν_4, ν_{10}, ν_{11}, ν_{14} and ν_{15}.

The frequencies of the ten fundamental vibrations assigned for C_2D_4S (Table 12) were then included in the calculation and the force field was refined to fit the frequencies of both C_2H_4S and C_2D_4S. The force constants and frequencies so obtained are shown in columns headed #2 in Tables 15, 16 and 17. Table 17 also contains the

TABLE 17

Observed Frequencies for Gaseous C_2D_4S and Those Calculated with the Force Fields Shown in Table 15[a]

	OBS	#2	#3	#4	Final
ν_1	2212.5	2214.1	2207.9	2209.5	2210.5
ν_2		1257.3	1151.1	1178.9	1186.8
ν_3	946.4	943.6	961.5	951.0	949.4
ν_4	766.5	796.8	766.4	783.1	764.3
ν_5	613.3	547.3	593.8	599.9	610.1
ν_6		2326.1	2327.3	2326.5	2333.4
ν_7		791.3	822.2	861.0	922.0
ν_8		632.8	611.3	635.6	630.3
ν_9	2185.2	2183.8	2184.1	2182.9	2184.8
ν_{10}	1064.2	1056.4	1059.5	1076.8	1066.6
ν_{11}	830.7	865.6	849.4	818.3	827.9
ν_{12}		546.3	546.2	549.3	607.0
ν_{13}	2331.3	2312.7	2312.3	2309.1	2312.1
ν_{14}	710.8	709.0	698.4	706.8	707.5
ν_{15}	578.1	583.4	594.8	584.5	584.3
Average Error[b]		16.9 cm^{-1} 2.19%	11.6 cm^{-1} 1.37%	10.2 cm^{-1} 1.08%	4.9 cm^{-1} 0.46%

---

a) Observed and calculated frequencies in cm^{-1}.

b) Defined in Table 16.

experimental frequencies for C_2D_4S. The frequencies of C_2H_4S were reproduced with an average error of 18.1 cm^{-1} or 1.68% and those of C_2D_4S with an average error of 16.9 cm^{-1} or 2.19%. The largest percent error occurred for the A_1 C-S stretching vibration, ν_5, in C_2D_4S, which was calculated at 547.3 cm^{-1} but assigned at 613.3 cm^{-1}. Attempts were made to improve this fit by allowing F(CCS) and F(CSC) to be refined but these attempts led to an unstable solution, no doubt due to the redundancies involved. Thus, these two force constants were reconstrained to zero.

No improvement in the overall fit was obtained by introducing any of the following interaction constants, one equivalent set at a time: $f(R_1,R_2) = f(R_1,R_3)$; $f(R_2,R_3)$; $f(R_2,\alpha_{26}) = f(R_2,\alpha_{27}) = f(R_3,\alpha_{34}) = f(R_3,\alpha_{35})$; $f(R_2,\alpha_{16}) = f(R_2,\alpha_{17}) = f(R_3,\alpha_{14}) = f(R_3,\alpha_{15})$; or $f(R_1,\alpha_{14}) = f(R_1,\alpha_{15}) = f(R_1,\alpha_{16}) = f(R_1,\alpha_{17})$. However, when $f(R_1,\alpha_{14})$ and $f(R_2,\alpha_{26})$ and their equivalents were added to the force field together, a solution was found which reproduced the observed frequencies of C_2H_4S and C_2D_4S with an average error of 1.30% in each case. However, the B_1 CH_2 deformation, ν_{10}, was calculated at a higher frequency than the A_1 CH_2 deformation, ν_2, in C_2H_4S. Thus the constant $f(\alpha_{45},\alpha_{67})$ was added to the force field and all force constants except F(CCS) and F(CSC) were refined to the values shown in column #3 of Table 15. The frequencies which were calculated for C_2H_4S and C_2D_4S with this force field are shown in the columns headed #3 in Tables 16 and 17, respectively, and the average difference between these frequencies and the experimental ones is 12.2 cm^{-1} (1.15%) for C_2H_4S and 11.6 cm^{-1} (1.37%) for C_2D_4S.

At this point, the frequencies of the normal modes of cis-$C_2D_2H_2S$ and trans-$C_2D_2H_2S$ were calculated using force field #3 and are shown in the columns headed #3 in Tables 18 and 19, respectively. The frequencies of the nine fundamentals of cis-$C_2D_2H_2S$ (ν_1, ν_2, ν_3, ν_5, ν_6, ν_7, ν_8, ν_{11}, ν_{13}) and the two fundamentals of trans-$C_2D_2H_2S$ (ν_4 and ν_8) which were assigned with confidence in Section 4.4 are also shown in these tables and the average difference between these frequencies and those calculated with force field #3 is 17.1 cm^{-1} (1.57%) for cis-$C_2D_2H_2S$ and 22.6 cm^{-1} (2.58%) for trans-$C_2D_2H_2S$. However, this force field could not be further refined to a stable solution when these nine observed frequencies for cis-$C_2D_2H_2S$ and two observed frequencies for trans-$C_2D_2H_2S$ were included in the refinement process. Since the largest errors between the observed and calculated frequencies occurred for the methylenic modes, the interaction constants which involve the $C\hat{C}H$ and $S\hat{C}H$ angle-bending coordinates, $f(\alpha_{14},\alpha_{15}) = f(\alpha_{16},\alpha_{17})$, $f(\alpha_{34},\alpha_{35}) = f(\alpha_{26},\alpha_{27})$ and $f(\alpha_{14},\alpha_{16}) = f(\alpha_{15},\alpha_{17})$, were added to the

TABLE 18

Observed Frequencies for Gaseous cis-$C_2D_2H_2S$ and Those Calculated with the Force Fields Shown in Table 15[a]

	OBS[b]	#3	#4	Final
ν_1	3052.0	3063.0	3060.6	3062.2
ν_2	2272.4	2257.5	2257.0	2259.1
ν_3	1332.6	1303.3	1320.4	1329.2
ν_4	(1083.7)	1078.3	1090.9	1080.0
ν_5	971.9	969.4	969.1	967.5
ν_6	756.8	741.0	753.2	760.2
ν_7	654.7	659.4	660.1	657.6
ν_8	614.8	610.8	609.4	608.2
ν_9		3063.3	3061.0	3063.7
ν_{10}		2253.4	2252.8	2257.4
ν_{11}	1310.0	1292.3	1305.7	1302.7
ν_{12}	(1068.5)	1028.5	1001.8	1068.1
ν_{13}	921.3	867.5	920.3	917.8
ν_{14}		698.1	712.1	719.2
ν_{15}		556.7	560.5	615.8
Average Error[c]		17.1 cm^{-1}	6.5 cm^{-1}	5.4 cm^{-1}
		1.57%	0.53%	0.45%

a) Observed and calculated frequencies in cm^{-1}

b) The frequencies in brackets could not be confidently assigned from the experimental data and were only included in the later stages of the refinement.

c) Defined in Table 16. Frequencies in brackets were included in error calculations with final force field only.

TABLE 19

Observed Frequencies for Gaseous trans-$C_2D_2H_2S$ and Those Calculated with the Force Fields Shown in Table 15[a]

	OBS[b]	#3	#4	Final
ν_1	[3051.0]	3066.5	3064.5	3067.0
ν_2	[2272.2]	2265.2	2266.2	2270.2
ν_3	[1315.2]	1306.1	1330.2	1338.3
ν_4	1113.4	1083.4	1104.1	1118.8
ν_5		995.4	984.8	1026.1
ν_6	[867.7]	814.2	874.7	876.5
ν_7	[704.5]	695.5	711.1	698.7
ν_8	617.5	602.3	608.2	616.7
ν_9	[3044.2]	3059.9	3057.0	3058.8
ν_{10}	[2262.6]	2245.5	2243.5	2245.9
ν_{11}	[1293.1]	1287.2	1289.2	1288.7
ν_{12}	(1002.8)	1023.8	1012.6	1001.0
ν_{13}	[773.4]	765.2	759.6	784.8
ν_{14}	[668.2]	673.1	666.4	659.1
ν_{15}	(618)	560.0	563.1	618.2
Average Error[c]		22.6 cm^{-1} 2.58%	9.3 cm^{-1} 1.17%	2.1 cm^{-1} 0.21%

---

a) Observed and calculated frequencies in cm^{-1}

b) The frequencies in brackets could not be confidently assigned from the experimental data. Those in round brackets were included in the late stages of the refinement, and those in square brackets were not included in the refinement.

c) Defined in Table 16. Frequencies in round brackets were included in error calculation with final force field only.

force field, one equivalent set at a time, and all force constants except F(CCS) and F(CSC) were refined after each addition. The force field and the calculated frequencies so obtained are presented in the columns headed #4 in Tables 15, 16, 17, 18 and 19. At this point in the calculation the average error between the observed and calculated frequencies of all four isotopic molecules was 8.7 cm^{-1} or 0.85%.

The calculations with force field #4 predicted that cis-$C_2D_2H_2S$ should have an A' mode (ν_4) at 1090.9 cm^{-1} and an A" mode (ν_{12}) at 1001.8 cm^{-1}. When the infrared spectrum of cis-$C_2D_2H_2S$ which was recorded by Othen (Table 13) was examined in greater detail, it was found that the broad, complicated absorption close to 1075 cm^{-1} could be reproduced by superimposing a band with PQR structure at 1083.7 cm^{-1} and a band with PR structure at 1068.5 cm^{-1}. In view of the band shapes (Section 4.4) and the predicted frequencies, 1083.7 cm^{-1} was assigned to ν_4 and 1068.5 cm^{-1} was assigned to ν_{12}.

The shape of the absorption at 1002.8 cm^{-1} in the infrared spectrum of trans-$C_2D_2H_2S$ which was recorded by Othen (Table 14) was also examined in greater detail at this point. In Section 4.4 it was shown that modes of A symmetry in trans-$C_2D_2H_2S$ should give rise to A-type infrared absorption bands and modes of B symmetry should give rise to BC hybrid bands, and that the shapes of these bands can be predicted by considering the shapes of the A-, B- and C-type bands for rotors numbered 16 or 25 of reference 105. It is found that a pure A-type band has PQR structure with the Q branch being more intense than either the P or R branches. A BC hybrid band also has PQR structure but whether or not the Q branch is more intense than the P and R branches depends upon the amount of C-type character (105). Since the Q branch of the band at 1002.8 cm^{-1} in the infrared spectrum of trans-$C_2D_2H_2S$ is less intense than the P and R branches, this band cannot arise from a mode of A symmetry and therefore it was assigned to a B mode. The calculations using force field #4 predict that the B mode ν_{12} should absorb at 1012.6 cm^{-1} and thus ν_{12} was assigned at 1002.8 cm^{-1}.

The inclusion of the two extra frequencies of cis-$C_2D_2H_2S$ and the extra one of trans-$C_2D_2H_2S$ in the calculations worsened the overall fit between the observed frequencies and those calculated with force field #4 and, even after several refinements of this force field, the average error was greater than 1.0%. Since force field #4 contained the interaction constants, $f(\alpha_{14},\alpha_{16}) = f(\alpha_{15},\alpha_{17})$, which take into account the interaction between $C\hat{C}H$ angle-bending coordinates which are 'cis' to each other, it seemed logical to add the 'trans' interaction constants, $f(\alpha_{14},\alpha_{17}) = f(\alpha_{15},\alpha_{16})$. However, when these force constants were added to the force field, an oscillatory solution was obtained. Since $f(\alpha_{45},\alpha_{67})$ oscillated about zero, this constant was constrained to zero and the subsequent refinement of the remaining force constants gave a great improvement in the overall fit of the observed frequencies.

The frequencies which were most in error at this point were the symmetric C-S stretching frequencies, ν_5 in C_2H_4S and C_2D_4S, and ν_8 in cis and trans-$C_2D_2H_2S$. Also, all of the asymmetric C-S stretching frequencies, ν_{12} in C_2H_4S and C_2D_4S, and ν_{15} in cis- and trans-$C_2D_2H_2S$, were calculated below 600 cm^{-1}. However, the only band observed below 600 cm^{-1} in the spectra of the various isotopic modifications was at 578.1 cm^{-1} in the spectrum of C_2D_4S, and this band was clearly due to a B_2 mode (Table 12). A closer inspection of the band at 617.5 cm^{-1} in the spectrum of trans-$C_2D_2H_2S$ revealed a shoulder at about 610 cm^{-1} which can be assigned to the P branch of a weak band centered close to 618 cm^{-1}. Thus the B C-S stretching mode was assigned at 618 cm^{-1} in trans-$C_2D_2H_2S$ and this frequency was included in the refinement. A stable solution was obtained only after the diagonal force constant F(CCS) was again included in the refinement. Then all asymmetric C-S stretching modes were calculated to absorb within 6 cm^{-1} of the symmetric C-S stretching mode in the same molecule. This suggests that these modes are nearly degenerate in all four isotopic modifications.

The constraint on F(CSC) was then released but a wildly oscillating solution was obtained so this constant was reconstrained to zero. The introduction of two additional sets of interaction constants, $f(\alpha_{14},\alpha_{35}) = f(\alpha_{15},\alpha_{34}) = f(\alpha_{16},\alpha_{27}) = f(\alpha_{17},\alpha_{26})$ and $f(R_1,\alpha_{34}) = f(R_1,\alpha_{35}) = F(R_1,\alpha_{26}) = f(R_1,\alpha_{27})$, improved the overall fit of the frequencies to an average error of about 0.41%. The interaction constant, $f(\alpha_{34},\alpha_{35}) = f(\alpha_{26},\alpha_{27})$, was constrained to zero because the calculated uncertainty in this constant was larger than its value, but this caused no significant change in the fit of the observed frequencies. At this point no further improvement in the fit of the calculated frequencies to observed frequencies was considered justified since errors of 1% can easily arise from anharmonicity in the observed frequencies (139). The final force field is shown in Table 15 and the frequencies calculated with this force field are shown in Tables 16-19.

4.7 Discussion

The comparison of the observed frequencies (Tables 11-14) with those calculated with the final force field (Tables 16-19) allows many of the remaining active fundamentals to be recognized in the spectra and assigned, as is summarized in Tables 20 to 23. In particular, the bands at 3051.0, 2272.2, 1315.2, 867.7 and 704.5 cm^{-1} in

TABLE 20

The Assignment of the Fundamental Frequencies of C_2H_4S

Mode	Frequencies/cm^{-1} Observed	Frequencies/cm^{-1} Calculated	Description[a]
A_1 ν_1	3013.5	3018.5	Symmetric CH_2 stretch
A_1 ν_2	1456.8	1466.0	90% CH_2 deformation + 10% C-C stretch
A_1 ν_3	1109.9	1107.1	90% C-C stretch + 10% C-S stretch
A_1 ν_4	1024.0	1023.5	CH_2 wag
A_1 ν_5	627.3	633.3	90% C-S stretch + 10% C-C stretch
A_2 ν_6	——	3109.2	Asymmetric CH_2 stretch
A_2 ν_7	——	1160.2	75% CH_2 rock + 25% CH_2 twist
A_2 ν_8	——	890.2	75% CH_2 twist + 25% CH_2 rock
B_1 ν_9	3013	3010.4	Symmetric CH_2 stretch
B_1 ν_{10}	1435.9	1431.9	CH_2 deformation
B_1 ν_{11}	1050.8	1060.2	CH_2 wag
B_1 ν_{12}	——	645.9	85% C-S stretch + 15% $C\hat{C}S$ bend
B_2 ν_{13}	3088.0	3100.6	Asymmetric CH_2 stretch
B_2 ν_{14}	945.2	947.1	55% CH_2 twist + 45% CH_2 rock
B_2 ν_{15}	824.3	820.5	55% CH_2 rock + 45% CH_2 twist

---

a) Determined from the potential energy distribution in Appendix III.

TABLE 21

The Assignment of the Fundamental Frequencies of C_2D_4S

Mode	Frequencies/cm^{-1} Observed	Frequencies/cm^{-1} Calculated	Description[a]
A_1 ν_1	2212.5	2210.5	Symmetric CD_2 stretch
A_1 ν_2	———	1186.8	60% C-C stretch + 40% CD_2 deformation
A_1 ν_3	946.4	949.4	45% C-C stretch + 45% CD_2 deformation + 10% CD_2 wag
A_1 ν_4	766.5	764.3	80% CD_2 wag + 20% C-S stretch
A_1 ν_5	613.3	610.1	90% C-S stretch + 10% C-C stretch
A_2 ν_6	———	2333.4	Asymmetric CD_2 stretch
A_2 ν_7	———	922.0	80% CD_2 rock + 20% CD_2 twist
A_2 ν_8	———	630.3	80% CD_2 twist + 20% CD_2 rock
B_1 ν_9	2185.2	2184.8	Symmetric CD_2 stretch
B_1 ν_{10}	1064.2	1066.6	80% CD_2 deformation + 10% CD_2 wag + 10% C-S stretch
B_1 ν_{11}	830.7	827.9	90% CD_2 wag + 10% CD_2 deformation
B_1 ν_{12}	———	607.0	85% C-S stretch + 15% $C\hat{C}S$ bend
B_2 ν_{13}	2331.3	2312.1	Asymmetric CD_2 stretch

TABLE 21 (continued)

B_2 ν_{14}	710.8	707.5	50% CD_2 twist + 50% CD_2 rock
B_2 ν_{15}	578.1	584.3	50% CD_2 rock + 50% CD_2 twist

a) Determined from the potential energy distribution in Appendix III.

TABLE 22

The Assignment of the Fundamental Frequencies of *cis*-$C_2D_2H_2S$

Mode	Frequencies/cm^{-1}		Description[a]
	Observed	Calculated	
$A'\ \nu_1$	3052.0	3062.2	C-H stretch
$A'\ \nu_2$	2272.4	2259.1	C-D stretch
$A'\ \nu_3$	1332.6	1329.2	65% $H\hat{C}D$ bend + 15% $S\hat{C}H$ bend + 10% $C\hat{C}H$ bend + 10% C-C stretch
$A'\ \nu_4$	1083.7	1080.1	80% C-C stretch + 15% $S\hat{C}H$ bend + 5% C-S stretch
$A'\ \nu_5$	971.9	967.5	40% $C\hat{C}H$ bend + 40% $S\hat{C}H$ bend + 20% $H\hat{C}D$ bend
$A'\ \nu_6$	756.8	760.2	85% $S\hat{C}D$ bend + 15% $S\hat{C}H$ bend
$A'\ \nu_7$	654.7	657.7	50% C-S stretch + 35% $C\hat{C}D$ bend + 15% $C\hat{C}H$ bend
$A'\ \nu_8$	614.8	608.2	75% C-S stretch + 25% $C\hat{C}D$ bend
$A''\ \nu_9$	3052	3063.7	C-H stretch
$A''\ \nu_{10}$	2272	2257.4	C-D stretch
$A''\ \nu_{11}$	1310	1302.7	65% $H\hat{C}D$ bend + 25% $S\hat{C}H$ bend + 10% $C\hat{C}H$ bend

TABLE 22 (continued)

A" ν_{12}	1068.5	1068.1	60% C$\hat{C}$H bend + 20% S$\hat{C}$D bend + 10% S$\hat{C}$H bend + 10% C$\hat{C}$D bend
A" ν_{13}	921.3	917.8	40% C$\hat{C}$D bend + 35% H$\hat{C}$D bend + 25% S$\hat{C}$H bend
A" ν_{14}	——	719.2	60% S$\hat{C}$D bend + 15% S$\hat{C}$H bend + 15% C-S stretch + 10% C$\hat{C}$D bend
A" ν_{15}	——	615.8	70% C-S stretch + 15% C$\hat{C}$S bend + 15% S$\hat{C}$D bend

a) Determined from the potential energy distributions and eigenvectors in Appendices II and III.

TABLE 23

The Assignment of the Fundamental Frequencies of trans-$C_2D_2H_2S$

	Frequencies/cm^{-1}		
Mode	Observed	Calculated	Description[a]
A ν_1	3051.0	3067.0	C-H stretch
A ν_2	2272.2	2270.2	C-D stretch
A ν_3	1315.2	1338.4	65% $H\hat{C}D$ bend + 15% $S\hat{C}H$ bend + 10% $C\hat{C}H$ bend + 10% C-C stretch
A ν_4	1113.4	1118.8	60% C-C stretch + 20% $C\hat{C}H$ bend + 10% $C\hat{C}D$ bend + 10% C-S stretch
A ν_5	——	1026.2	35% C-C stretch + 30% $C\hat{C}H$ bend + 25% $S\hat{C}H$ bend + 10% $S\hat{C}D$ bend
A ν_6	867.7	876.5	40% $C\hat{C}D$ bend + 25% $S\hat{C}H$ bend + 25% $H\hat{C}D$ bend + 10% $S\hat{C}D$ bend
A ν_7	704.5	698.7	70% $S\hat{C}D$ bend + 20% C-S stretch + 10% $S\hat{C}H$ bend
A ν_8	617.5	616.7	80% C-S stretch + 10% C-C stretch + 10% $S\hat{C}H$ bend
B ν_9	3044.2	3058.8	C-H stretch

TABLE 23 (continued)

B ν_{10}	2262.2	2245.9	C-D stretch
B ν_{11}	1293.1	1288.7	75% H$\hat{C}$D bend + 25% S$\hat{C}$H bend
B ν_{12}	1002.8	1000.9	40% C$\hat{C}$H bend + 30% H$\hat{C}$D bend + 30% S$\hat{C}$H bend
B ν_{13}	773.4	784.8	70% S$\hat{C}$D bend + 20% S$\hat{C}$H bend + 10% C-S stretch
B ν_{14}	668.2	659.1	65% C$\hat{C}$D bend + 25% C$\hat{C}$H bend + 10% H$\hat{C}$D bend
B ν_{15}	618	618.2	70% C-S stretch + 15% C$\hat{C}$S bend + 15% C$\hat{C}$D,S$\hat{C}$D bends

a) Determined from the potential energy distributions and eigenvectors in Appendices II and III the infrared spectrum of trans-$C_2D_2H_2S$ can be assigned to modes of A symmetry and those at 3044.2, 2262.2, 1293.1, 773.4 and 668.2 cm^{-1} can be assigned to modes of B symmetry. In addition, ν_2 of C_2D_4S is calculated to absorb at 1186.8 cm^{-1}, which confirms its assignment in this region in the Raman spectrum of the liquid. The calculations also revealed several near-degeneracies which undoubtedly account for the failure to observe certain fundamentals in the spectra. First, for cis-$C_2D_2H_2S$, the A' and A" C-H stretching modes are calculated at 3062.2 and 3063.7 cm^{-1}, respectively, and the A' and A" C-D stretching modes are calculated at 2259.1 and 2257.4 cm^{-1}, respectively. Second, the frequencies calculated for the symmetric and asymmetric C-S stretching modes differ by only 1.5 cm^{-1} for trans-$C_2D_2H_2S$, 3.1 cm^{-1} for C_2D_4S, 7.6 cm^{-1} for cis-$C_2D_2H_2S$ and 12.6 cm^{-1} for C_2H_4S.

The forms of the normal vibrations in terms of the internal coordinates listed in Table 5 are given by the potential energy distributions and the eigenvectors (Section 4.5) which are presented in Appendix II for each isotopic molecule. In this Appendix, the elements of the potential energy distributions are listed, under each frequency, in the order of the sixteen non-zero force constants in the 'final' column of Table 15. The elements of the eigenvectors are listed, under each frequency, in the order of the internal coordinates in Table 5. From

Appendix II it is not easy to see which of the vibrations of C_2H_4S and C_2D_4S correspond to methylenic wags, deformations, rocks and twists. In order to describe the vibrations in terms of these motions, the calculations were repeated with the final force field for C_2H_4S and C_2D_4S, using VSEC (138). This program gives the potential energy distributions among the diagonal elements of the symmetrized force constant matrix, $\underset{\sim}{F}_s$, which is defined (138) as

$$\underset{\sim}{F}_s = \underset{\sim}{U}\,\underset{\sim}{F}\,\underset{\sim}{U}^t \tag{1}$$

where the elements of the $\underset{\sim}{U}$ matrix, U_{ij}, relate the symmetry coordinates, S_i, to the internal coordinates, I_j, through the matrix equation

$$\underset{\sim}{S} = \underset{\sim}{U}\,\underset{\sim}{I} \tag{2}$$

For the calculation by VSEC, the symmetry coordinates shown in Table 6 were used, except for S_4, S_5, S_6, S_{10}, S_{11}, S_{14}, S_{15}, S_{16}, S_{19} and S_{20}, which were rewritten as the linear combinations shown in Appendix III to describe the methylenic deformations, wags, rocks and twists. Appendix III also shows the potential energy distribution among the diagonal elements of the $\underset{\sim}{F}_s$ matrix which results from this calculation for C_2H_4S and C_2D_4S.

The calculated assignments of the normal modes of C_2H_4S and C_2D_4S as determined from Appendix III are summarized in Tables 20 and 21, respectively, along with the observed and calculated frequencies. Most of the vibrations of C_2H_4S can be reasonably well described by a single type of displacement, e.g. methylenic wag, C-H stretch, etc. However, a significant amount of mixing occurs between the methylenic twisting and rocking vibrations. For C_2D_4S, all of the vibrations below 2000 cm^{-1} involve several types of displacements, so the descriptions of the vibrations as twists, rocks, deformations or wags are less meaningful than for C_2H_4S. The calculations also show that, for both C_2H_4S and C_2D_4S, the A_2 mode with the greater methylenic twisting character is to low frequency of the A_2 mode with the greater methylenic rocking character, which is the reverse of the order accepted for other molecules (Section 4.3). This may indicate that the relative order of these modes depends upon the substituent in the ring, or might reflect a deficiency in the final force field, although the frequencies calculated for the A_2 modes of C_2H_4S with this force field agree well with those reported by LeBrumant (Table 9). It is not surprising that these two modes mix since they have the same symmetry. The A_1 methylenic wag of C_2H_4S is calculated at lower frequency than the C-C stretch, which suggests that the reverse order proposed by Aleksanyan and Kuz'yants (Tables 9 and 10) is wrong.

The vibrations of cis-$C_2D_2H_2S$ and trans-$C_2D_2H_2S$ cannot be conveniently described in the same way as those of C_2H_4S and C_2D_4S, so the potential energy distributions and eigenvectors shown in Appendix II were used to indicate the form of these vibrations. It is more apparent which vibrations are $S\hat{C}H$, $C\hat{C}H$ bends and which are $S\hat{C}D$, $C\hat{C}D$ bends from the potential energy distribution among the diagonal elements of the $\underset{\sim}{F}$ matrix symmetrized using the symmetry coordinates in Tables 7 and 8. Accordingly, these distributions are included in Appendix III. The information given in Appendices II and III is summarized in Tables 22 and 23 for cis-$C_2D_2H_2S$ and trans-$C_2D_2H_2S$, respectively, by indicating the percentage contribution to the potential energy from the diagonal force constants for each equivalent set of internal coordinates. Except for the C-D and C-H stretching modes, most of the vibrations involve more than one type of displacement. Tables 22 and 23 also include the observed and calculated frequencies and, along with Tables 20 and 21, summarize the assignment of the fundamental frequencies in the spectra of the four molecules in the gas phase.

No further refinement of the force field shown in the 'final' column of Table 15 was attempted using all of the assigned frequencies in Tables 20-23. The sixteen force constants in this force field reproduced the thirty-six frequencies which were included in the final refinement with an average error of 0.41% and, thus, the force field appears to be quite reliable. The uncertainty in each force constant is calculated by FPERT from the relationship between the frequencies and the force constants (138), and is given in Table 15. It can be seen that most of the force constants are well determined. It should be borne in mind, however, that many force constants in the general valence force field were not considered at all in this work. Further, those force constants that were tried and rejected because they did not improve the fit may well have had an influence if they had been tried at a different stage of the calculation. Therefore it is probable that the physical significance of the force constants obtained is not great, and further, that they should only be compared with those obtained for other molecules if the force fields for the other molecules contain similar interaction constants to those used in this work.

The most significant results obtained in this study are believed to be 1) that the potential energy distribution and the eigenvectors yielded descriptions of the various normal vibrations which were not greatly dependent on the force field, and 2) that the calculations indicate that the fundamental frequencies selected for the four isotopic modifications of ethylene sulphide are mutually consistent. It is believed, therefore, that the fundamental frequencies listed in Tables 20 - 23 and the descriptions of the vibrations in terms of the intramolecular displacements are reliable.

REFERENCES

1. W. M. Latimer and W. H. Rodebush. J. Amer. Chem. Soc. 42, 1419 (1920).
2. G. C. Pimentel and A. L. McClellan. The Hydrogen Bond. W. H. Freeman and Co., San Francisco, 1960.
3. S. N. Vinogradov and R. H. Linnel. Hydrogen Bonding. D. Van Nostrand Reinhold Co., New York, 1971.
4. W. C. Hamilton and J. A. Ibers. Hydrogen Bonding in Solids. W. A. Benjamin Inc., New York, 1968.
5. D. Hadẑi and H. W. Thompson, editors. Hydrogen Bonding. Pergamon Press, London, 1959.
6. A. S. N. Murthy and C. N. R. Rao. Appl. Spec. Rev. 2, 69 (1968).
7. L. Pauling. The Nature of the Chemical Bond. Cornell University Press, Ithaca, N.Y., 1960, p.260.
8. Reference 3. Chapter 6.
9. C. A. Coulson. In reference 5. p.339.
10. D. A. K. Jones and J. G. Watkinson. Chem. Ind. 661 (1960).
11. Reference 2. Chapter 2.
12. Reference 3. Chapter 2.
13. Reference 2. Chapter 3.
14. Reference 3. Chapter 3.
15. Reference 3. Chapter 4.
16. Reference 4. Chapter 2.

17. R. Freymann. Comptes rendues Acad. Sci. 195, 39 (1932).

18. M. Holzbecher, O. Knop, and M. Falk. Can. J. Chem. 49, 1413 (1971).

19. G. V. Yukhonevich. Opt. Spect. 2, 223 (1963).

20. R. M. Badger and S. H. Bauer. J. Chem. Phys. 5, 839 (1937).

21. M. D. Joesten and R. S. Drago. J. Amer. Chem. Soc. 84, 3817 (1962).

22. R. S. Drago, N. O'Bryan, and G. C. Vogel. J. Amer. Chem. Soc. 92, 3924 (1970).

23. Reference 3. P.65.

24. W. A. P. Luck and W. Ditter. J. Mole. Struct. 1, 261 (1967-68).

25. J. E. Bertie and D. J. Millen. J. Chem. Soc. 514 (1965).

26. A. V. Stuart and G. B. B. M. Sutherland. J. Chem. Phys. 24, 559 (1956).

27. P. V. Huong, M. Couzi, and J. Lascombe. J. Chim. Phys. 64, 1056 (1967).

28. E. Greinacher, W. Lüttke, and R. Mecke. Z. Elektrochem. 59, 23 (1955).

29. T. Miyazawa, T. Shimanouchi, and S. Mizushima. J. Chem. Phys. 24, 408 (1956).

30. J. W. Brasch, Y. Mikawa, and R. J. Jakobsen. Appl. Spec. Rev. 1, 187 (1968).

31. Reference 3. P.74.

32. G. L. Carlson, R. E. Witkowski, and W. G. Fateley. Spectrochim. Acta. 22, 1117 (1966).

33. J. W. Brasch, R. J. Jakobsen, W. G. Fateley, and N. T. McDevitt. Spectrochim. Acta. 24A, 203 (1968).

34. K. B. Whetsel and R. E. Kagarise. Spectrochim. Acta. 18, 315 (1962).

35. H. Takahashi, K. Mamola, and E. K. Plyler. J. Mole. Spec. 21, 217 (1966).

36. E. B. Wilson, J. C. Decius, and P. C. Cross. Molecular Vibrations. McGraw Hill Book Co., New York, 1955. P.41

37. G. Herzberg, Molecular Spectra and Molecular Structure II. Infrared and Raman Spectra of Polyatomic Molecules. D. Van Nostrand Co. Inc., Princeton, N. J., 1945. Chapter II. Section 5.

38. A. Foldes and C. Sandorfy. J. Mole. Spec. 20, 62 (1966).

39. M. Asselin and C. Sandorfy. J. Mole. Struct. 8, 145 (1971).

40. T. DiPaolo, C. Bourderon, and C. Sandorfy. Can. J. Chem. 50, 3161 (1972).

41. M. Huggins and G. C. Pimentel. J. Phys. Chem. 60, 1615 (1956).

42. Reference 37. Chapter III. Section 2.

43. Reference 2. Section 3.3.8.

44. S. Bratoẑ and D. Hadẑi. J. Chem. Phys. 27, 991 (1957).

45. N. Sheppard. In reference 5. P.85.

46. M. I. Batuev. Zhurn. Fiz. Khim. 23, 1399 (1949).

47. M. I. Batuev. Izvest. Akad. Nauk. SSSR. ser. Fiz. 14, 429 (1950).

48. B. I. Stepanov. Nature. 157, 808 (1946).

49. L. Pauling and E. B. Wilson. Introduction to Quantum Mechanics. McGraw-Hill Book Co., New York, 1935. Chapter 10.

50. G. Herzberg. Molecular Spectra and Molecular Structure I. Spectra of Diatomic Molecules. D. Van Nostrand Co. Inc., Princeton, N.J., 1950. P.77.

51. Reference 50. Chapter 7.

52. J. C. Evans and G. Y-S. Lo. J. Chem. Phys. 71, 3942 (1967).

53. J. C. Evans and G. Y-S. Lo. J. Chem. Phys. 73, 448 (1969).

54. R. K. Thomas and H. Thompson. Proc. Roy. Soc. Lond. 316A, 303 (1970).

55. R. K. Thomas. Proc. Roy. Soc. Lond. 325A, 133 (1971).

56. S. Bratoẑ, D. Hadẑi, and N. Sheppard. Spectrochim. Acta. 8, 249 (1956).

57. M. Haurie and A. Novak. J. Chim. Phys. 62, 146 (1965).

58. A. Witkowski. J. Chem. Phys. 47, 3645 (1967).

59. Y. Marechal and A. Witkowski. J. Chem. Phys. 48, 3697 (1968).

60. J.-L. Leviel and Y. Marechal. J. Chem. Phys. 54, 1104 (1971).

61. J. Bournay and Y. Marechal. J. Chem. Phys. 55, 1230 (1971).

62. P. Excoffon and Y. Marechal. Spectrochim. Acta. 28A, 269 (1972).

63. R. J. Jakobsen, Y. Mikawa, and J. W. Brasch. Spectrochim. Acta. 25A, 839 (1968).

64. D. J. Millen and J. Zabicky. Nature. 196, 889 (1962).

65. D. J. Millen and J. Zabicky. J. Chem. Soc. 3080 (1965).

66. S. A. Rice and J. L. Wood. J. Chem. Soc. Fara. Trans. II. 69, 87 (1973).

67. S. G. W. Ginn and J. L. Wood. Nature. 200, 467 (1963).

68. G. L. Carlson, R. E. Witkowski, and W. G. Fateley. Nature. 211, 1289 (1966).

69. D. J. Millen and O. A. Samsonov. J. Chem. Soc. 3085 (1965).

70. L. Al Adhami and D. J. Millen. Nature. 211, 1291 (1966).

71. R. M. Seel and N. Sheppard. Spectrochim. Acta. 25A, 1291 (1969).

72. J. Arnold, J. E. Bertie, and D. J. Millen. Proc. Chem. Soc. 121 (1961).

73. J. E. Bertie and D. J. Millen. J. Chem. Soc. 497 (1965).

74. D. N. Shchepkin and L. P. Belozerskaya. Optics and Spec. Suppl. 3, 101 (1968).

75. L. P. Belozerskaya and D. N. Shchepkin. Optics and Spec. Suppl. 3, 146 (1968).

76. J. LeCalvé, P. Grange, and J. Lascombe. Comptes rendues Acad. Sci. (Paris). 261, 2075 (1965).

77. J. Arnold and D. J. Millen. J. Chem. Soc. 503 (1965).

78. M. Couzi, J. LeCalvé, P. V. Huong, and J. Lascombe. J. Mole. Struct. 5, 363 (1970).

79. R. K. Thomas. Proc. Roy. Soc. Lond. 322A, 137 (1971).

80. J. Arnold and D. J. Millen. J. Chem. Soc. 510 (1965).

81. M. Couzi and P. V. Huong. Comptes rendues Acad. Sci. (Paris). 270B, 832 (1970).

82. T. Shidei. Mem. Coll. Sci. Kyoto Univ. 9A, 97 (1925).

83. A. T. Gladishev and Y. K. Syrkin. Comptes rendues Acad. Sci. URSS. 20, 45 (1938).

84. G. Govil, A. D. H. Clague, and H. J. Bernstein. J. Chem. Phys. 49, 2821 (1968).

85. G. L. Vidale and R. C. Taylor. J. Amer. Chem. Soc. 78, 294 (1956).

86. R. M. Seel and N. Sheppard. Spectrochim. Acta. 25A, 1287 (1969).

87. J. C. Lassegues, J. C. Cornut, P. V. Huong, and Y. Grenie. Spectrochim. Acta. 27A, 73 (1971).

88. Reference 37. P.428.

89. G. Herzberg. Molecular Spectra and Molecular Stucture III. Electronic Spectra and Electronic Structure of Polyatomic Molecules. D. Van Nostrand Co. Inc., Princeton, N.J., 1966. P.455.

90. G. D. Parkes and J. W. Mellor. Mellor's Modern Inorganic Chemistry. Longmans, Green and Co., New York, 1939. P.736.

91. I.U.P.A.C. Tables of Wavenumbers for the Calibration of Infrared Spectrometers. Butterworths, London, 1961.

92. R. L. Hansler and R. A. Oetjen. J. Chem. Phys. 21, 1340 (1953).

93. I.B.M. Scientific Subroutine Package.

94. Reference 36. P. 177.

95. Y. Kanazawa and K. Nukada. Bull. Chem. Soc. Japan 35, 612 (1962).

96. J. P. Perchard, M.-T. Forel, and M.-L. Josien. J. Chim. Phys. 61, 632 (1964).

97. W. S. Benedict, R. Herman, G. E. Moore and S. Silverman. J. Chem. Phys. 26, 1671 (1957).

98. Reference 50. P.92.

99. Reference 37. P.229.

100. Reference 36. Chapter 4.

101. R. C. Weast, editor. Handbook of Chemistry and Physics. The Chemical Rubber Co., Cleveland, Ohio, 1968. p.B-4.

102. U. Buikis, P. H. Kasai, and R. J. Myers. J. Chem. Phys. 48, 2753 (1963).

103. J. H. Schachtschneider. Technical Report No. 231-64. Project No. 31450. Shell Development Co., Emeryville, Cal., 1964.

104. Reference 37. Chapter IV, Section 4.

105. S. Ueda and T. Shimanouchi. J. Mole. Spec. 28, 350 (1968).

106. J. C. Lassegues, P. V. Huong, and J. Lascombe. Presented at the International Conference on Hydrogen Bonding. Ottawa, Ont., August, 1972.

107. J. C. Lassegues and P. V. Huong. Chem. Phys. Lett. 17, 444 (1972).

108. J. E. Bertie and E. Whalley. J. Chem. Phys. 40, 1646 (1964).

109. D. A. Othen and J. E. Bertie. Unpublished data.

110. G. L. Cunningham, A. W. Boyd, R. J. Myers, G. W. Gwinn, and W. J. LeVan. J. Chem. Phys. 19, 676 (1951).

111. Reference 36. Chapter 6.

112. Reference 37. p.271.

113. H. W.Thompson and J. Dupré . Trans. Fara. Soc. 36, 805 (1940).

114. H. W. Thompson and W. T. Cave. Trans. Fara. Soc. 47, 951 (1951).

115. G. B. Guthrie, D. W. Scott, and G. Waddington. J. Amer. Chem. Soc. 74, 2795 (1952).

116. J. Lebrumant. Comptes rendues (Paris) 266B, 283 (1968).

117. A. W. Baker and R. C. Lord. J. Chem. Phys. 23, 1636 (1955).

118. V. T. Aleksanyan and G. M. Kuz'yants. Zh. Strukt. Khim. 12, 266 (1971).

119. G. M. Kuz'yants and V. T. Aleksanyan. Zh. Strukt. Khim. 13, 617 (1972).

120. F. A. Miller, R. J. Capwell, R. C. Lord, and D. G. Rea. Spectrochim. Acta. 28A, 603 (1972).

121. Hs. W. Gunthard, R. C. Lord, and T. K. McCubbin Jr. J. Chem. Phys. 26, 768 (1956).

122. P. M. Mathai, G. G. Shepherd, and H. L. Welsh. Can. J. Phys. 34, 1448 (1956).

123. C. Brecher, E. Krikorian, J. Blanc, and R. S. Halford. J. Chem. Phys. 35, 1092 (1961).

124. M. Solinas. Ph.D. Thesis, University of Alberta, (1973).

125. R. Mecke and H. Spiesecke. Spectrochim. Acta. 7, 387 (1957).

126. A. Cheutin and J. P. Mathieu. J. Chim. Phys. 53, 106 (1956).

127. L. Couture-Mathieu, J. P. Mathieu, J. Cramer, and H. Poulet. J. Chim. Phys. 48, 1 (1951).

128. J. E. Bertie and D. A. Othen. Can. J. Chem. 51, 1155 (1973).

129. J. E. Bertie and M. G. Norton. Can. J. Chem. 48, 3889 (1970).

130. J. E. Bertie and M. G. Norton. Can. J. Chem. 49, 2229 (1971).

131. K. Venkateswarlu, S. Mariam, and M. P. Mathew. Proc. Ind. Acad. Sci. 62A, 159 (1965).

132. K. Venkateswarlu and P. A. Joseph. J. Mole. Struct. 6, 145 (1970).

133. J. M. Freeman and T. Henshall. Can. J. Chem. 46, 2135 (1968).

134. Reference 37. P.380.

135. Reference 36. Section 3.7.

136. Reference 36. Appendix X.

137. Reference 36. P.183.

138. J. H. Schachtschneider. Technical Report No. 57-65. Project No. 31450. Shell Development Co., Emeryville, Cal., 1965.

139. Reference 36. P.196.

APPENDIX I

$\underset{\sim}{G}$ MATRIX ELEMENTS[a] FOR C_2H_4S, C_2D_4S, *cis*-$C_2D_2H_2S$ and *trans*-$C_2D_2H_2S$

(i) C_2H_4S

1	1	0.166667	1	2	0.033774	1	3	0.033774	1	4	-0.038911
1	5	-0.038911	1	6	-0.038910	1	7	-0.038910	1	8	0.115402
1	9	0.115402	1	10	-0.002830	1	11	-0.002830	1	12	-0.002831
1	13	-0.002831	1	14	-0.068417	1	15	-0.068417	1	16	-0.068417
1	17	-0.068417	1	18	-0.041962	1	19	-0.041962	1	20	0.083925
2	2	0.114611	2	3	0.021002	2	6	-0.034979	2	7	-0.034979
2	9	0.103741	2	10	-0.004567	2	11	-0.004567	2	12	-0.070223
2	13	-0.070223	2	14	-0.014761	2	15	-0.014761	2	16	-0.003551
2	17	-0.003551	2	18	0.064535	2	19	-0.051769	2	20	-0.012766
3	3	0.114611	3	4	-0.034979	3	5	-0.034979	3	8	0.103741
3	10	-0.070223	3	11	-0.070223	3	12	-0.004567	3	13	-0.004567
3	14	-0.003550	3	15	-0.003550	3	16	-0.014761	3	17	-0.014761
3	18	-0.051769	3	19	0.064535	3	20	-0.012766	4	4	1.075427
4	5	-0.036401	4	8	-0.069597	4	10	-0.0-1662	4	11	0.082409
4	14	-0.050076	4	15	0.100630	4	16	0.050076	4	17	-0.041933
4	18	0.029181	4	19	-0.014278	4	20	-0.014903	5	5	1.075427
5	8	-0.069597	5	10	0.082409	5	11	-0.041662	5	14	0.100630
5	15	-0.050076	5	16	-0.041933	5	17	0.050076	5	18	0.029181
5	19	-0.014278	5	20	-0.014903	6	6	1.075427	6	7	-0.036401
6	9	-0.069597	6	12	-0.041662	6	13	0.082409	6	14	0.050076
6	15	-0.041933	6	16	-0.050076	6	17	0.100630	6	18	-0.014278
6	19	0.029181	6	20	-0.014903	7	7	1.075427	7	9	-0.069597
7	12	0.082409	7	13	-0.041662	7	14	-0.041933	7	15	0.050076
7	16	0.100630	7	17	-0.050076	7	18	-0.014278	7	19	0.029181
7	20	-0.014903	8	8	1.916708	8	10	-0.692087	8	11	-0.692087
8	14	-0.796177	8	15	-0.796177	8	16	-0.012075	8	17	-0.012075
8	18	-0.086546	8	19	0.042347	8	20	0.044199	9	9	1.916713
9	12	-0.692089	9	13	-0.692089	9	14	-0.012075	9	15	-0.012075
9	16	-0.796181	9	17	-0.796181	9	18	0.042347	9	19	-0.086545
9	20	0.044199	10	10	0.997526	10	11	-0.002737	10	12	0.007460
10	13	-0.009091	10	14	0.279417	10	15	-0.099738	10	16	-0.033031
10	17	0.062311	10	18	0.032508	10	19	-0.049056	10	20	0.016558
11	11	0.997526	11	12	-0.009091	11	13	0.007460	11	14	-0.099738
11	15	0.279417	11	16	0.062311	11	17	-0.033031	11	18	0.032508
11	19	-0.049066	11	20	0.016558	12	12	0.997528	12	13	-0.002736
12	14	-0.033030	12	15	0.062311	12	16	0.279422	12	17	-0.099736
12	18	-0.049066	12	19	0.032508	12	20	0.016557	13	13	0.997528
13	14	0.062311	13	15	-0.033030	13	16	-0.099738	13	17	0.279422
13	18	-0.049066	13	19	0.032508	13	20	0.016557	14	14	1.053038
14	15	-0.062504	14	16	-0.126058	14	17	0.105560	14	18	0.011411
14	19	0.025339	14	20	-0.036751	15	15	1.053038	15	16	0.105560
15	17	-0.126058	15	18	0.011411	15	19	0.025339	15	20	-0.036751
16	16	1.053039	16	17	-0.062504	16	18	0.025339	16	19	0.011411
16	20	-0.036750	17	17	1.053039	17	18	0.025339	17	19	0.011411
17	20	-0.036750	18	18	0.086450	18	19	-0.058050	18	20	-0.028400
19	19	0.086450	19	20	-0.028400	20	20	0.056001	-1		

(a) The integers before each entry refer to the internal coordinates in Table 5.

APPENDIX I (continued)

(ii) C_2D_4S

```
 1  1   0.166667   1  2   0.033774   1  3   0.033774   1  4  -0.038911
 1  5  -0.038911   1  6  -0.038910   1  7  -0.038910   1  8   0.115402
 1  9   0.115402   1 10  -0.002830   1 11  -0.002830   1 12  -0.002831
 1 13  -0.002831   1 14  -0.068417   1 15  -0.068417   1 16  -0.068417
 1 17  -0.068417   1 18  -0.041962   1 19  -0.041962   1 20   0.083925
 2  2   0.114611   2  3   0.021002   2  6  -0.034979   2  7  -0.034979
 2  9   0.103741   2 10  -0.004567   2 11  -0.004567   2 12  -0.070223
 2 13  -0.070223   2 14  -0.014761   2 15  -0.014761   2 16  -0.003551
 2 17  -0.003551   2 18   0.064535   2 19  -0.051769   2 20  -0.012766
 3  3   0.114611   3  4  -0.034979   3  5  -0.034979   3  8   0.103741
 3 10  -0.070223   3 11  -0.070223   3 12  -0.004567   3 13  -0.004567
 3 14  -0.003550   3 15  -0.003550   3 16  -0.014761   3 17  -0.014761
 3 18  -0.051769   3 19   0.064535   3 20  -0.012766   4  4   0.579833
 4  5  -0.036401   4  8  -0.069597   4 10  -0.041662   4 11   0.082409
 4 14  -0.050076   4 15   0.100630   4 16   0.050076   4 17  -0.041933
 4 18   0.029181   4 19  -0.014278   4 20  -0.014903   5  5   0.579833
 5  8  -0.069597   5 10   0.082409   5 11  -0.041662   5 14   0.100630
 5 15  -0.050076   5 16  -0.041933   5 17   0.050076   5 18   0.029181
 5 19  -0.014278   5 20  -0.014903   6  6   0.579833   6  7  -0.036401
 6  9  -0.069597   6 12  -0.041662   6 13   0.082409   6 14   0.050076
 6 15  -0.041933   6 16  -0.050076   6 17   0.100630   6 18  -0.014278
 6 19   0.029181   6 20  -0.014903   7  7   0.579833   7  9  -0.069597
 7 12   0.082409   7 13  -0.041662   7 14  -0.041933   7 15   0.050076
 7 16   0.100630   7 17  -0.050076   7 18  -0.014278   7 19   0.029181
 7 20  -0.014903   8  8   1.062343   8 10  -0.376544   8 11  -0.376544
 8 14  -0.435901   8 15  -0.435901   8 16  -0.012075   8 17  -0.012075
 8 18  -0.086546   8 19   0.042347   8 20   0.044159   9  9   1.062345
 9 12  -0.376545   9 13  -0.376545   9 14  -0.012075   9 15  -0.012075
 9 16  -0.435904   9 17  -0.435904   9 18   0.042347   9 19  -0.086545
 9 20   0.044199  10 10   0.570343  10 11  -0.002737  10 12   0.007460
10 13  -0.009091  10 14   0.168023  10 15  -0.099738  10 16  -0.033031
10 17   0.062311  10 18   0.032508  10 19  -0.049066  10 20   0.016558
11 11   0.570343  11 12  -0.009091  11 13   0.007460  11 14  -0.099738
11 15   0.168023  11 16   0.062311  11 17  -0.033031  11 18   0.032508
11 19  -0.049066  11 20   0.016558  12 12   0.570344  12 13  -0.002736
12 14  -0.033030  12 15   0.062311  12 16   0.168026  12 17  -0.099738
12 18  -0.049066  12 19   0.032508  12 20   0.016557  13 13   0.570344
13 14   0.062311  13 15  -0.033030  13 16  -0.099738  13 17   0.168026
13 18  -0.049066  13 19   0.032508  13 20   0.016557  14 14   0.625854
14 15  -0.062504  14 16  -0.126058  14 17   0.105560  14 18   0.011411
14 19   0.025339  14 20  -0.036751  15 15   0.625854  15 16   0.105560
15 17  -0.126058  15 18   0.011411  15 19   0.025339  15 20  -0.036751
16 16   0.625854  16 17  -0.062504  16 18   0.025339  16 19   0.011411
16 20  -0.036750  17 17   0.625854  17 18   0.025339  17 19   0.011411
17 20  -0.036750  18 18   0.086450  18 19  -0.058050  18 20  -0.028400
19 19   0.086450  19 20  -0.028400  20 20   0.056801  -1
```

APPENDIX I (continued)

(iii) cis-$C_2D_2H_2S$

```
 1  1   0.166667  1  2   0.033774  1  3   0.033774  1  4  -0.038911
 1  5  -0.038911  1  6  -0.038910  1  7  -0.038910  1  8   0.115402
 1  9   0.115402  1 10  -0.002830  1 11  -0.002830  1 12  -0.002831
 1 13  -0.002831  1 14  -0.068417  1 15  -0.068417  1 16  -0.068417
 1 17  -0.068417  1 18  -0.041962  1 19  -0.041962  1 20   0.083925
 2  2   0.114611  2  3   0.021002  2  6  -0.034979  2  7  -0.034979
 2  9   0.103741  2 10  -0.004567  2 11  -0.004567  2 12  -0.070223
 2 13  -0.070223  2 14  -0.014761  2 15  -0.014761  2 16  -0.003551
 2 17  -0.003551  2 18   0.064535  2 19  -0.051769  2 20  -0.012766
 3  3   0.114611  3  4  -0.034979  3  5  -0.034979  3  8   0.103741
 3 10  -0.070223  3 11  -0.070223  3 12  -0.004567  3 13  -0.004567
 3 14  -0.003550  3 15  -0.003550  3 16  -0.014761  3 17  -0.014761
 3 18  -0.051769  3 19   0.064535  3 20  -0.012766  4  4   1.075427
 4  5  -0.036401  4  8  -0.069597  4 10  -0.041662  4 11   0.082409
 4 14  -0.050076  4 15   0.100630  4 16   0.050076  4 17  -0.041933
 4 18   0.029181  4 19  -0.014278  4 20  -0.014903  5  5   0.579833
 5  8  -0.069597  5 10   0.082409  5 11  -0.041662  5 14   0.100630
 5 15  -0.050076  5 16  -0.041933  5 17   0.050076  5 18   0.029181
 5 19  -0.014278  5 20  -0.014903  6  6   1.075427  6  7  -0.036401
 6  9  -0.069597  6 12  -0.041662  6 13   0.082409  6 14   0.050076
 6 15  -0.041933  6 16  -0.050076  6 17   0.100630  6 18  -0.014278
 6 19   0.029181  6 20  -0.014903  7  7   0.579833  7  9  -0.069597
 7 12   0.082409  7 13  -0.041662  7 14  -0.041933  7 15   0.050076
 7 16   0.100630  7 17  -0.050076  7 18  -0.014278  7 19   0.029181
 7 20  -0.014903  8  8   1.489525  8 10  -0.692087  8 11  -0.376544
 8 14  -0.796177  8 15  -0.435901  8 16  -0.012075  8 17  -0.012075
 8 18  -0.086546  8 19   0.042347  8 20   0.044199  9  9   1.489529
 9 12  -0.692089  9 13  -0.376545  9 14  -0.012075  9 15  -0.012075
 9 16  -0.796181  9 17  -0.435904  9 18   0.042347  9 19  -0.086545
 9 20   0.044199 10 10   0.997526 10 11  -0.002737 10 12   0.007460
10 13  -0.009091 10 14   0.279417 10 15  -0.099738 10 16  -0.033031
10 17   0.062311 10 18   0.032508 10 19  -0.049066 10 20   0.016558
11 11   0.570343 11 12  -0.009091 11 13   0.007460 11 14  -0.099738
11 15   0.168023 11 16   0.062311 11 17  -0.033031 11 18   0.032508
11 19  -0.049066 11 20   0.016558 12 12   0.997528 12 13  -0.002736
12 14  -0.033030 12 15   0.062311 12 16   0.279422 12 17  -0.099738
12 18  -0.049066 12 19   0.032508 12 20   0.016557 13 13   0.570344
13 14   0.062311 13 15  -0.033030 13 16  -0.099738 13 17   0.168026
13 18  -0.049066 13 19   0.032508 13 20   0.016557 14 14   1.053038
14 15  -0.062504 14 16  -0.126058 14 17   0.105560 14 18   0.011411
14 19   0.025339 14 20  -0.036751 15 15   0.625854 15 16   0.105560
15 17  -0.126058 15 18   0.011411 15 19   0.025339 15 20  -0.036751
16 16   1.053039 16 17  -0.062504 16 18   0.025339 16 19   0.011411
16 20  -0.036750 17 17   0.625854 17 18   0.025339 17 19   0.011411
17 20  -0.036750 18 18   0.086450 18 19  -0.058050 18 20  -0.028400
19 19   0.086450 19 20  -0.028400 20 20   0.056801 -1
```

APPENDIX I (continued)

(iv) trans-$C_2D_2H_2S$

```
 1  1   0.166667  1  2   0.033774  1  3   0.033774  1  4  -0.038911
 1  5  -0.038911  1  6  -0.038910  1  7  -0.038910  1  8   0.115402
 1  9   0.115402  1 10  -0.002830  1 11  -0.002830  1 12  -0.002831
 1 13  -0.002831  1 14  -0.068417  1 15  -0.068417  1 16  -0.068417
 1 17  -0.068417  1 18  -0.041962  1 19  -0.041962  1 20   0.083925
 2  2   0.114611  2  3   0.021002  2  6  -0.034979  2  7  -0.034979
 2  9   0.103741  2 10  -0.004567  2 11  -0.004567  2 12  -0.070223
 2 13  -0.070223  2 14  -0.014761  2 15  -0.014761  2 16  -0.003551
 2 17  -0.003551  2 18   0.064535  2 19  -0.051769  2 20  -0.012766
 3  3   0.114611  3  4  -0.034979  3  5  -0.034979  3  8   0.103741
 3 10  -0.070223  3 11  -0.070223  3 12  -0.004567  3 13  -0.004567
 3 14  -0.003550  3 15  -0.003550  3 16  -0.014761  3 17  -0.014761
 3 18  -0.051769  3 19   0.064535  3 20  -0.012766  4  4   0.579833
 4  5  -0.036401  4  8  -0.069597  4 10  -0.041662  4 11   0.082409
 4 14  -0.050076  4 15   0.100630  4 16   0.050076  4 17  -0.041933
 4 18   0.029181  4 19  -0.014278  4 20  -0.014903  5  5   1.075427
 5  8  -0.069597  5 10   0.082409  5 11  -0.041662  5 14   0.100630
 5 15  -0.050076  5 16  -0.041933  5 17   0.050076  5 18   0.029181
 5 19  -0.014278  5 20  -0.014903  6  6   1.075427  6  7  -0.036401
 6  9  -0.069597  6 12  -0.041662  6 13   0.082409  6 14   0.050076
 6 15  -0.041933  6 16  -0.050076  6 17   0.100630  6 18  -0.014278
 6 19   0.029181  6 20  -0.014903  7  7   0.579833  7  9  -0.069597
 7 12   0.082409  7 13  -0.041662  7 14  -0.041933  7 15   0.050076
 7 16   0.100630  7 17  -0.050076  7 18  -0.014278  7 19   0.029181
 7 20  -0.014903  8  8   1.489525  8 10  -0.376544  8 11  -0.692087
 8 14  -0.435901  8 15  -0.796177  8 16  -0.012075  8 17  -0.012075
 8 18  -0.086546  8 19   0.042347  8 20   0.044199  9  9   1.489529
 9 12  -0.692089  9 13  -0.376545  9 14  -0.012075  9 15  -0.012075
 9 16  -0.796181  9 17  -0.435904  9 18   0.042347  9 19  -0.086545
 9 20   0.044199 10 10   0.570343 10 11  -0.002737 10 12   0.007460
10 13  -0.009091 10 14   0.168023 10 15  -0.099738 10 16  -0.033031
10 17   0.062311 10 18   0.032508 10 19  -0.049066 10 20   0.016558
11 11   0.997526 11 12  -0.009091 11 13   0.007460 11 14  -0.099738
11 15   0.279417 11 16   0.062311 11 17  -0.033031 11 18   0.032508
11 19  -0.049066 11 20   0.016558 12 12   0.997528 12 13  -0.002736
12 14  -0.033030 12 15   0.062311 12 16   0.279422 12 17  -0.099738
12 18  -0.049066 12 19   0.032508 12 20   0.016557 13 13   0.570344
13 14   0.062311 13 15  -0.033030 13 16  -0.099738 13 17   0.168026
13 18  -0.049066 13 19   0.032508 13 20   0.016557 14 14   0.625854
14 15  -0.062504 14 16  -0.126058 14 17   0.105560 14 18   0.011411
14 19   0.025339 14 20  -0.036751 15 15   1.053038 15 16   0.105560
15 17  -0.126058 15 18   0.011411 15 19   0.025339 15 20  -0.036751
16 16   1.053039 16 17  -0.062504 16 18   0.025339 16 19   0.011411
16 20  -0.036750 17 17   0.625854 17 18   0.025339 17 19   0.011411
17 20  -0.036750 18 18   0.086450 18 19  -0.058050 18 20  -0.028400
19 19   0.086450 19 20  -0.028400 20 20   0.056801 -1
```

A P P E N D I X   I I

POTENTIAL ENERGY DISTRIBUTIONS[a] AND EIGENVECTORS[b] FOR C_2H_4S, C_2D_4S, cis-$C_2D_2H_2S$ and trans-$C_2D_2H_2S$

(i) C_2H_4S : Potential Energy Distribution[a]

```
FREQUENCY =3018.5 CM-1
 0.0073  0.0015  0.9868  0.0024  0.0003  0.0004  0.0000  0.0038 -0.0006
-0.0015 -0.0006 -0.0003 -0.0000  0.0001 -0.0003  0.0006
FREQUENCY =1466.0 CM-1
 0.0828  0.0111  0.0032  1.1071  0.2846  0.1377  0.0005  0.0000 -0.3095
-0.0976 -0.0494 -0.0946 -0.0033  0.0290 -0.1604  0.0590
FREQUENCY =1107.1 CM-1
 0.8562  0.0904  0.0060  0.0178  0.0487  0.0002  0.0054  0.0000  0.0049
-0.0120  0.0584 -0.0001 -0.0000  0.0000  0.0025 -0.0785
FREQUENCY =1023.5 CM-1
 0.0059  0.0150  0.0000  0.0877  0.2590  0.2551  0.0003  0.0000  0.4019
-0.0356 -0.0549 -0.1752 -0.0062  0.0537  0.2083 -0.0151
FREQUENCY = 633.3 CM-1
 0.1296  1.0231  0.0001  0.0363  0.0658  0.0006  0.0155  0.0000 -0.0096
 0.0079 -0.2284 -0.0004 -0.0000  0.0001 -0.0050 -0.0355
FREQUENCY =3109.2 CM-1
 0.0     0.0     0.9958  0.0     0.0019  0.0043  0.0    -0.0038 -0.0044
 0.0     0.0     0.0030  0.0001  0.0009  0.0023  0.0
FREQUENCY =1160.2 CM-1
 0.0     0.0     0.0080  0.0     0.1639  0.5488  0.0    -0.0000 -0.4688
 0.0     0.0     0.3768  0.0133  0.1154  0.2430  0.0
FREQUENCY = 890.2 CM-1
 0.0     0.0     0.0000  0.0     0.9140  0.0091  0.0    -0.0000  0.1423
 0.0     0.0     0.0062  0.0002  0.0019 -0.0737  0.0
FREQUENCY =3010.4 CM-1
 0.0     0.0013  0.9933  0.0022  0 0003  0.0002  0.0002  0.0038 -0.0004
 0.0    -0.0006 -0.0001  0.0000 -0.0000 -0.0002  0.0
FREQUENCY =1431.9 CM-1
 0.0     0.0149  0.0015  1.1196  0.3698  0.0997  0.0028  0.0000 -0.3003
 0.0    -0.0653 -0.0685  0.0024 -0.0210 -0.1556  0.0
FREQUENCY =1060.2 CM-1
 0.0     0.0041  0.0002  0.1907  0.1906  0.3308  0.0008  0.0000  0.3927
 0.0    -0.0246 -0.2273  0.0080 -0.0696  0.2035  0.0
FREQUENCY = 645.9 CM-1
 0.0     0.8382  0.0012  0.0001  0.0000  0.0308  0.1565  0.0000 -0.0001
 0.0     0.0003 -0.0212  0.0007 -0.0065 -0.0001  0.0
FREQUENCY =3100.6 CM-1
 0.0     0.0     1.0023  0.0     0.0017  0.0002  0.0    -0.0038 -0.0010
 0.0     0.0     0.0002 -0.0000 -0.0000  0.0005  0.0
FREQUENCY = 947.1 CM-1
 0.0     0.0     0.0014  0.0     1.0447  0.0047  0.0    -0.0000 -0.1098
 0.0     0.0     0.0032 -0.0001 -0.0010  0.0569  0.0
FREQUENCY = 820.5 CM-1
 0.0     0.0     0.0002  0.0     0.0619  0.7581  0.0    -0.0000 -0.3387
 0.0     0.0     0.5208 -0.0184 -0.1595  0.1755  0.0
```

a) Entries under each frequency are listed in the order of the sixteen non-zero force constants in the 'final' column of Table 15.

b) Entries under each frequency are listed in the order of the internal coordinates in Table 5.

APPENDIX II (continued)

(i) C_2H_4S : Eigenvectors[b]

```
FREQUENCY =3018.5 CM-1
 0.0904  0.0395  0.0395 -0.5093 -0.5093 -0.5093 -0.5093  0.0919  0.0919 -0.0281
-0.0281 -0.0281 -0.0281 -0.0383 -0.0383 -0.0383 -0.0383 -0.0177 -0.0177  0.0353
FREQUENCY =1466.0 CM-1
 0.1491  0.0530  0.0530  0.0142  0.0142  0.0142  0.0142  0.9494  0.9494 -0.3953
-0.3953 -0.3953 -0.3953 -0.3557 -0.3557 -0.3557 -0.3557 -0.0317 -0.0317  0.0633
FREQUENCY =1107.1 CM-1
 0.3597  0.1144  0.1144  0.0146  0.0146  0.0146  0.0146 -0.0910 -0.0910  0.1234
 0.1234  0.1234  0.1234 -0.0103 -0.0103 -0.0103 -0.0103 -0.0804 -0.0804  0.1608
FREQUENCY =102[illegible].5 CM-1
 0.0277 -0.0432 -0.0432 -0.0011 -0.0011 -0.0011 -0.0011  0.1866  0.1866  0.2632
 0.2632  0.2632  0.2632 -0.3381 -0.3381 -0.3381 -0.3381 -0.0189 -0.0189  0.0378
FREQUENCY = 633.3 CM-1
-0.0890  0.2202  0.2202  0.0008  0.0008  0.0008  0.0008  0.0742  0.0742 -0.0821
-0.0821 -0.0821 -0.0821 -0.0099 -0.0099 -0.0099 -0.0099  0.0779  0.0779 -0.1557
FREQUENCY =3109.2 CM-1
 0.0     0.0     0.0     0.5269 -0.5269 -0.5269  0.5269  0.0     0.0    -0.0677
 0.0677  0.0677 -0.0677 -0.1339  0.1339  0.1339 -0.1339  0.0     0.0     0.0
FREQUENCY =1160.2 CM-1
 0.0     0.0     0.0     0.0177 -0.0177 -0.0177  0.0177  0.0     0.0     0.2374
-0.2374 -0.2374  0.2374  0.5620 -0.5620 -0.5620  0.5620  0.0     0.0     0.0
FREQUENCY = 890.2 CM-1
 0.0     0.0     0.0     0.0011 -0.0011 -0.0011  0.0011  0.0     0.0     0.4301
-0.4301 -0.4301  0.4301 -0.0554  0.0554  0.0554 -0.0554  0.0     0.0     0.0
FREQUENCY =3010.4 CM-1
 0.0     0.0368 -0.0368  0.5096  0.5096 -0.5096 -0.5096 -0.0869  0.0869  0.0270
 0.0270 -0.0270 -0.0270  0.0276  0.0276 -0.0276 -0.0276  0.0458 -0.0458  0.0
FREQUENCY =1431.9 CM-1
 0.0    -0.0600  0.0600  0.0095  0.0095 -0.0095 -0.0095  0.9325 -0.9325 -0.4401
-0.4401  0.4401  0.4401 -0.2957 -0.2957  0.2957  0.2957 -0.0746  0.0746  0.0
FREQUENCY =1060.2 CM-1
 0.0     0.0233 -0.0233  0.0024  0.0024 -0.0024 -0.0024  0.2850 -0.2850  0.2339
 0.2339 -0.2339 -0.2339 -0.3988 -0.3988  0.3988  0.3988  0.0290 -0.0290  0.0
FREQUENCY = 645.9 CM-1
 0.0     0.2032 -0.2032 -0.0038 -0.0038  0.0038  0.0038  0.0032 -0.0032 -0.0001
-0.0001  0.0001  0.0001 -0.0742 -0.0742  0.0742  0.0742  0.2525 -0.2525  0.0
FREQUENCY =3100.6 CM-1
 0.0     0.0     0.0     0.5272 -0.5272  0.5272 -0.5272  0.0     0.0    -0.0648
 0.0648 -0.0648  0.0648 -0.0301  0.0301 -0.0301  0.0301  0.0     0.0     0.0
FREQUENCY = 947.1 CM-1
 0.0     0.0     0.0     0.0060 -0.0060  0.0060 -0.0060  0.0     0.0     0.4893
-0.4893  0.4893 -0.4893  0.0425 -0.0425  0.0425 -0.0425  0.0     0.0     0.0
FREQUENCY = 820.5 CM-1
 0.0     0.0     0.0    -0.0020  0.0020 -0.0020  0.0020  0.0     0.0    -0.1032
 0.1032 -0.1032  0.1032 -0.4672  0.4672 -0.4672  0.4672  0.0     0.0     0.0
```

APPENDIX II (continued)

(ii) C_2D_4S : Potential Energy Distribution[a]

```
FREQUENCY =2210.5 CM-1
 0.0355  0.0067  0.9517  0.0112  0.0014  0.0018  0.0002  0.0036 -0.0025
-0.0073 -0.0027 -0.0012 -0.0000  0.0004 -0.0013  0.0027
FREQUENCY =1186.8 CM-1
 0.5834  0.0648  0.0397  0.5827  0.0871  0.0941  0.0036  0.0002 -0.1416
-0.2141 -0.0661 -0.0646 -0.0023  0.0198 -0.0734  0.0867
FREQUENCY = 949.4 CM-1
 0.3423  0.0203  0.0042  0.5006  0.2943  0.0270  0.0025  0.0000 -0.1395
 0.0879  0.0681 -0.0186 -0.0007  0.0057 -0.0723 -0.1220
FREQUENCY = 764.3 CM-1
 0.0166  0.1951  0.0005  0.0818  0.2675  0.2394  0.0026  0.0000  0.3957
-0.0577 -0.2011 -0.1645 -0.0058  0.0503  0.2051 -0.0256
FREQUENCY = 610.1 CM-1
 0.1039  0.8543  0.0001  0.0750  0.0081  0.0316  0.0128  0.0000 -0.0250
 0.0524 -0.0733 -0.0217 -0.0008  0.0067 -0.0130 -0.0112
FREQUENCY =2333.4 CM-1
 0.0     0.0     0.9768  0.0     0.0062  0.0145  0.0    -0.0037 -0.0148
 0.0     0.0     0.0100  0.0004  0.0030  0.0077  0.0
FREQUENCY = 922.0 CM-1
 0.0     0.0     0.0270  0.0     0.1861  0.5330  0.0    -0.0001 -0.4926
 0.0     0.0     0.3662  0.0129  0.1121  0.2553  0.0
FREQUENCY = 630.3 CM-1
 0.0     0.0     0.0001  0.0     0.8873  0.0144  0.0    -0.0000  0.1765
 0.0     0.0     0.0099  0.0003  0.0030 -0.0915  0.0
FREQUENCY =2184.8 CM-1
 0.0     0.0052  0.9847  0.0085  0.0013  0.0007  0.0010  0.0038 -0.0015
 0.0    -0.0023 -0.0005  0.0000 -0.0002 -0.0008  0.0
FREQUENCY =1066.6 CM-1
 0.0     0.0662  0.0073  1.0445  0.3826  0.0675  0.0124  0.0000 -0.2513
 0.0    -0.1401 -0.0464  0.0016 -0.0142 -0.1302  0.0
FREQUENCY = 827.9 CM-1
 0.0     0.0190  0.0006  0.2449  0.1597  0.3664  0.0035  0.0000  0.3782
 0.0    -0.0485 -0.2517  0.0089 -0.0771  0.1960  0.0
FREQUENCY = 607.0 CM-1
 0.0     0.7680  0.0036  0.0146  0.0171  0.0269  0.1434  0.0000 -0.0336
 0.0     0.1008 -0.0185  0.0007 -0.0057 -0.0174  0.0
FREQUENCY =2312.1 CM-1
 0.0     0.0     0.9987  0.0     0.0056  0.0007  0.0    -0.0038 -0.0031
 0.0     0.0     0.0005 -0.0000 -0.0002  0.0016  0.0
FREQUENCY = 707.4 CM-1
 0.0     0.0     0.0047  0.0     1.0744  0.0183  0.0    -0.0000 -0.2195
 0.0     0.0     0.0126 -0.0004 -0.0039  0.1138  0.0
FREQUENCY = 584.3 CM-1
 0.0     0.0     0.0004  0.0     0.0283  0.7440  0.0    -0.0000 -0.2268
 0.0     0.0     0.5111 -0.0181 -0.1565  0.1175  0.0
```

APPENDIX II (continued)

(ii) C_2D_4S : Eigenvectors[b]

```
FREQUENCY =2210.5 CM-1
 0.1462  0.0620  0.0620 -0.3662 -0.3662 -0.3662 -0.3662  0.1437  0.1437 -0.0415
-0.0415 -0.0415 -0.0415 -0.0616 -0.0616 -0.0616 -0.0616 -0.0289 -0.0289  0.0578
FREQUENCY =1166.8 CM-1
 0.3183  0.1038  0.1038  0.0402  0.0402  0.0402  0.0402  0.5576  0.5576 -0.1770
-0.1770 -0.1770 -0.1770 -0.2380 -0.2380 -0.2380 -0.2380 -0.0705 -0.0705  0.1411
FREQUENCY =  949.4 CM-1
 0.1950  0.0465  0.0465  0.0104  0.0104  0.0104  0.0104 -0.4134 -0.4134  0.2603
 0.2603  0.2603  0.2603  0.1021  0.1021  0.1021  0.1021 -0.0474 -0.0474  0.0948
FREQUENCY =  764.3 CM-1
 0.0346 -0.1160 -0.1160 -0.0029 -0.0029 -0.0029 -0.0029  0.1346  0.1346  0.1998
 0.1998  0.1998  0.1998 -0.2445 -0.2445 -0.2445 -0.2445 -0.0388 -0.0388  0.0775
FREQUENCY =  610.1 CM-1
-0.0691  0.1938  0.1938  0.0011  0.0011  0.0011  0.0011  0.1029  0.1029 -0.0278
-0.0278 -0.0278 -0.0278 -0.0709 -0.0709 -0.0709 -0.0709  0.0681  0.0681 -0.1363
FREQUENCY =2333.4 CM-1
 0.0     0.0     0.0     0.3917 -0.3917 -0.3917  0.3917  0.0     0.0    -0.0930
 0.0930  0.0930 -0.0930 -0.1837  0.1837  0.1837 -0.1837  0.0     0.0     0.0
FREQUENCY =  922.0 CM-1
 0.0     0.0     0.0     0.0257 -0.0257 -0.0257  0.0257  0.0     0.0     0.2011
-0.2011 -0.2011  0.2011  0.4402 -0.4402 -0.4402  0.4402  0.0     0.0     0.0
FREQUENCY =  830.3 CM-1
 0.0     0.0     0.0     0.0008 -0.0008 -0.0008  0.0008  0.0     0.0     0.3001
-0.3001 -0.3001  0.3001 -0.0494  0.0494  0.0494 -0.0494  0.0     0.0     0.0
FREQUENCY =2184.8 CM-1
 0.0     0.0542 -0.0542  0.3682  0.3682 -0.3682 -0.3682 -0.1242  0.1242  0.0395
 0.0395 -0.0395 -0.0395  0.0383  0.0383 -0.0383 -0.0383  0.0673 -0.0673  0.0
FREQUENCY =1066.6 CM-1
 0.0    -0.0943  0.0943  0.0155  0.0155 -0.0155 -0.0155  0.6709 -0.6709 -0.3335
-0.3335  0.3335  0.3335 -0.1812 -0.1812  0.1812  0.1812 -0.1172  0.1172  0.0
FREQUENCY =  827.9 CM-1
 0.0     0.0392 -0.0392  0.0033  0.0033 -0.0033 -0.0033  0.2522 -0.2522  0.1672
 0.1672 -0.1672 -0.1672 -0.3277 -0.3277  0.3277  0.3277  0.0487 -0.0487  0.0
FREQUENCY =  607.0 CM-1
 0.0     0.1828 -0.1828 -0.0062 -0.0062  0.0062  0.0062  0.0452 -0.0452 -0.0401
-0.0401  0.0401  0.0401 -0.0652 -0.0652  0.0652  0.0652  0.2272 -0.2272  0.0
FREQUENCY =2312.1 CM-1
 0.0     0.0     0.0     0.3924 -0.3924  0.3924 -0.3924  0.0     0.0    -0.0871
 0.0871 -0.0871  0.0871 -0.0404  0.0404 -0.0404  0.0404  0.0     0.0     0.0
FREQUENCY =  707.4 CM-1
 0.0     0.0     0.0     0.0082 -0.0082  0.0082 -0.0082  0.0     0.0     0.3706
-0.3706  0.3706 -0.3706  0.0627 -0.0627  0.0627 -0.0627  0.0     0.0     0.0
FREQUENCY =  584.3 CM-1
 0.0     0.0     0.0    -0.0020  0.0020 -0.0020  0.0020  0.0     0.0    -0.0497
 0.0497 -0.0497  0.0497 -0.3296  0.3296 -0.3296  0.3296  0.0     0.0     0.0
```

APPENDIX II (continued)

(iii) cis-$C_2D_2H_2S$: Potential Energy Distribution[a]

```
FREQUENCY =3062.1 CM-1
 0.0030  0.0006  0.9958  0.0009  0.0010  0.0003  0.0000 -0.0005 -0.0007
-0.0006 -0.0002 -0.0000 -0.0000  0.0000  0.0002  0.0002
FREQUENCY =2259.1 CM-1
 0.0179  0.0034  0.9730  0.0072  0.0044  0.0015  0.0001  0.0004 -0.0036
-0.0040 -0.0017 -0.0004 -0.0000  0.0001  0.0001  0.0017
FREQUENCY =1329.1 CM-1
 0.1704  0.0214  0.0162  0.9741  0.2776  0.1385  0.0010  0.0000 -0.3056
-0.1332 -0.0623 -0.0761 -0.0034  0.0233 -0.1188  0.0768
FREQUENCY =1080.0 CM-1
 0.7449  0.0697  0.0108  0.0448  0.1603  0.0118  0.0049  0.0000 -0.0357
-0.0126  0.0712  0.0077 -0.0003 -0.0024  0.0264 -0.1016
FREQUENCY = 967.5 CM-1
 0.0004  0.0233  0.0009  0.1046  0.2455  0.2695  0.0001  0.0000  0.3965
 0.0084 -0.0503 -0.0859 -0.0065  0.0263  0.0643  0.0030
FREQUENCY = 760.2 CM-1
 0.0325  0.0297  0.0026  0.0252  0.9901  0.0611  0.0012 -0.0000 -0.2574
-0.0178 -0.0566  0.0259 -0.0015 -0.0079  0.1989 -0.0259
FREQUENCY = 657.6 CM-1
 0.0317  0.4135  0.0006  0.0101  0.0788  0.4527  0.0054 -0.0000 -0.1478
-0.0262 -0.1146  0.2755 -0.0110 -0.0843  0.1294 -0.0139
FREQUENCY = 608.2 CM-1
 0.0809  0.5797  0.0000  0.0845  0.0088  0.2215  0.0090  0.0000 -0.0080
 0.0472 -0.0604  0.1070 -0.0054 -0.0328 -0.0224 -0.0099
FREQUENCY =3063.7 CM-1
 0.0     0.0005  0.9950  0.0006  0.0011  0.0025  0.0001 -0.0006 -0.0026
 0.0    -0.0002  0.0017  0.0001  0.0005  0.0013  0.0
FREQUENCY =2257.4 CM-1
 0.0     0.0026  0.9756  0.0068  0.0049  0.0094  0.0005  0.0006 -0.0104
 0.0    -0.0014  0.0055  0.0002  0.0017  0.0040  0.0
FREQUENCY =1302.7 CM-1
 0.0     0.0176  0.0122  0.9695  0.3870  0.1437  0.0033  0.0000 -0.3620
 0.0    -0.0646 -0.0233  0.0035 -0.0071 -0.0797  0.0
FREQUENCY =1068.1 CM-1
 0.0     0.0138  0.0094  0.0002  0.1698  0.3838  0.0026 -0.0000  0.1358
 0.0    -0.0422  0.1533  0.0093  0.0469  0.1173  0.0
FREQUENCY = 917.8 CM-1
 0.0     0.0034  0.0047  0.3290  0.2906  0.3919  0.0006 -0.0000 -0.2276
 0.0     0.0077 -0.0314  0.0095 -0.0096  0.2313  0.0
FREQUENCY = 719.2 CM-1
 0.0     0.1347  0.0003  0.0020  0.6578  0.0757  0.0251  0.0000  0.2529
 0.0    -0.0729 -0.0255  0.0018 -0.0078 -0.0442  0.0
FREQUENCY = 615.8 CM-1
 0.0     0.6859  0.0027  0.0045  0.1292  0.0166  0.1280  0.0000 -0.0251
 0.0     0.0836 -0.0113  0.0004 -0.0035 -0.0109  0.0
```

APPENDIX II (continued)

(iii) cis-$C_2D_2H_2S$: Eigenvectors[b]

```
FREQUENCY =3062.1 CM-1
-0.0590 -0.0258 -0.0258  0.7325 -0.0457  0.7325 -0.0457 -0.0553 -0.0553 -0.0312
 0.0631 -0.0312  0.0631  0.0018  0.0455  0.0018  0.0455  0.0115  0.0115 -0.0230
FREQUENCY =2259.1 CM-1
 0.1060  0.0450  0.0450 -0.0271 -0.5345 -0.0271 -0.5345  0.1181  0.1181 -0.1037
 0.0286 -0.1037  0.0286 -0.0797 -0.0176 -0.0797 -0.0176 -0.0209 -0.0209  0.0419
FREQUENCY =1329.1 CM-1
 0.1926  0.0668  0.0668  0.0132  0.0385  0.0132  0.0385  0.8074  0.8074 -0.4647
-0.1860 -0.4647 -0.1860 -0.4093 -0.2045 -0.4093 -0.2045 -0.0417 -0.0417  0.0834
FREQUENCY =1060.0 CM-1
 0.3273  0.0980  0.0980  0.0148  0.0225  0.0148  0.0225 -0.1406 -0.1406  0.3080
 0.0263  0.3080  0.0263  0.0645 -0.0870  0.0645 -0.0870 -0.0747 -0.0747  0.1493
FREQUENCY = 967.5 CM-1
-0.0070 -0.0507 -0.0507 -0.0003 -0.0072 -0.0003 -0.0072  0.1926  0.1926  0.3417
 0.0248  0.3417  0.0248 -0.4511 -0.1110 -0.4511 -0.1110 -0.0103 -0.0103  0.0205
FREQUENCY = 760.2 CM-1
-0.0481  0.0451  0.0451  0.0043 -0.0082  0.0043 -0.0082  0.0743  0.0743  0.2110
-0.4978  0.2110 -0.4978  0.1643 -0.0567  0.1643 -0.0567  0.0255  0.0255 -0.0510
FREQUENCY = 657.6 CM-1
-0.0411  0.1453  0.1453 -0.0003  0.0039 -0.0003  0.0039 -0.0407 -0.0407 -0.1320
-0.0027 -0.1320 -0.0027 -0.2118  0.3502 -0.2118  0.3502  0.0479  0.0479 -0.0958
FREQUENCY = 608.2 CM-1
-0.0608  0.1591  0.1591  0.0006  0.0004  0.0006  0.0004  0.1088  0.1088 -0.0357
-0.0197 -0.0357 -0.0197  0.1006 -0.2449  0.1006 -0.2449  0.0572  0.0572 -0.1143
FREQUENCY =3063.7 CM-1
 0.0    -0.0235  0.0235 -0.7320  0.0842  0.7320 -0.0842  0.0473 -0.0473  0.0354
-0.0650 -0.0354  0.0650  0.0859 -0.1133 -0.0859  0.1133 -0.0292  0.0292  0.0
FREQUENCY =2257.4 CM-1
 0.0     0.0397 -0.0397  0.0408  0.5340 -0.0408 -0.5340 -0.1148  0.1148  0.1070
-0.0346 -0.1070  0.0346  0.1770 -0.0983 -0.1770  0.0983  0.0493 -0.0493  0.0
FREQUENCY =1302.7 CM-1
 0.0     0.0594 -0.0594 -0.0013 -0.0346  0.0013  0.0346 -0.7895  0.7895  0.5515
 0.1771 -0.5515 -0.1771  0.4535  0.0543 -0.4535 -0.0543  0.0738 -0.0738  0.0
FREQUENCY =1068.1 CM-1
 0.0    -0.0431  0.0431  0.0109 -0.0223 -0.0109  0.0223 -0.0095  0.0095 -0.1922
-0.2490  0.1922  0.2490  0.5827 -0.1869 -0.5827  0.1869 -0.0535  0.0535  0.0
FREQUENCY = 917.8 CM-1
 0.0    -0.0184  0.0184  0.0112 -0.0101 -0.0112  0.0101  0.3240 -0.3240  0.3096
-0.1709 -0.3096  0.1709 -0.0311 -0.5305  0.0311  0.5305 -0.0229  0.0229  0.0
FREQUENCY = 719.2 CM-1
 0.0    -0.0907  0.0907  0.0014  0.0029 -0.0014 -0.0029 -0.0198  0.0198  0.2011
-0.3652 -0.2011  0.3652  0.0464  0.1770 -0.0464 -0.1770 -0.1127  0.1127  0.0
FREQUENCY = 615.8 CM-1
 0.0    -0.1753  0.1753  0.0026  0.0073 -0.0026 -0.0073 -0.0253  0.0253 -0.0704
 0.1417  0.0704 -0.1417  0.0502  0.0534 -0.0502 -0.0534 -0.2178  0.2178  0.0
```

APPENDIX II (continued)

(iv) trans-$C_2D_2H_2S$: Potential Energy Distribution[a]

```
FREQUENCY =3067.0 CM-1
  0.0029   0.0006   0.9923   0.0007   0.0011   0.0026   0.0000  -0.0005  -0.0026
 -0.0005  -0.0002   0.0016   0.0001   0.0005   0.0012   0.0002
FREQUENCY =2270.2 CM-1
  0.0176   0.0033   0.9601   0.0083   0.0050   0.0097   0.0001   0.0005  -0.0108
 -0.0045  -0.0017   0.0048   0.0002   0.0020   0.0036   0.0017
FREQUENCY =1338.3 CM-1
  0.1389   0.0170   0.0213   0.9521   0.2735   0.1644   0.0008   0.0000  -0.3314
 -0.1215  -0.0537  -0.0619  -0.0022   0.0346  -0.0990   0.0671
FREQUENCY =1118.8 CM-1
  0.5313   0.0668   0.0075   0.0045   0.0588   0.2006   0.0031   0.0000  -0.1697
  0.0321   0.0078   0.1346   0.0048   0.0422   0.0852  -0.0096
FREQUENCY =1026.1 CM-1
  0.2369   0.0041   0.0101   0.0097   0.2702   0.2075   0.0022  -0.0000   0.2530
 -0.1001   0.0286   0.0730   0.0026   0.0437   0.0532  -0.0946
FREQUENCY = 876.5 CM-1
  0.0196   0.0371   0.0086   0.2311   0.3244   0.3116   0.0000  -0.0000  -0.2288
  0.0529  -0.0247  -0.0206  -0.0007   0.0655   0.2163   0.0079
FREQUENCY = 698.7 CM-1
  0.0391   0.1822   0.0001   0.0046   0.7168   0.0413   0.0033   0.0000   0.2371
 -0.0302  -0.1447  -0.0099  -0.0004   0.0087  -0.0186  -0.0293
FREQUENCY = 616.7 CM-1
  0.0954   0.6301   0.0001   0.0404   0.0884   0.0181   0.0122   0.0000   0.0095
  0.0329  -0.0864  -0.0062  -0.0002   0.0038  -0.0253  -0.0126
FREQUENCY =3058.8 CM-1
  0.0      0.0000   0.9986   0.0007   0.0010   0.0002   0.0001  -0.0005  -0.0006
  0.0     -0.0002   0.0000  -0.0000  -0.0000   0.0002   0.0
FREQUENCY =2245.9 CM-1
  0.0      0.0026   0.9895   0.0058   0.0043   0.0010   0.0005   0.0005  -0.0031
  0.0     -0.0014  -0.0000   0.0000  -0.0002   0.0005   0.0
FREQUENCY =1288.7 CM-1
  0.0      0.0218   0.0063   1.0154   0.4232   0.0983   0.0041   0.0000  -0.3169
  0.0     -0.0774  -0.0441   0.0016  -0.0207  -0.1096   0.0
FREQUENCY =1000.9 CM-1
  0.0      0.0026   0.0003   0.2048   0.1975   0.3380   0.0005   0.0000   0.3929
  0.0     -0.0158  -0.1581   0.0056  -0.0711   0.1029   0.0
FREQUENCY = 784.8 CM-1
  0.0      0.0878   0.0019   0.0099   0.9440   0.0633   0.0164  -0.0000  -0.2437
  0.0     -0.0664   0.0146  -0.0005  -0.0133   0.1861   0.0
FREQUENCY = 659.1 CM-1
  0.0      0.0235   0.0003   0.0614   0.0154   0.6463   0.0044   0.0000  -0.0726
  0.0      0.0125   0.3914  -0.0138  -0.1389   0.0670   0.0
FREQUENCY = 618.2 CM-1
  0.0      0.7196   0.0031   0.0146   0.0835   0.0776   0.1343   0.0000  -0.1116
  0.0      0.0588   0.0032  -0.0001  -0.0163   0.0335   0.0
```

APPENDIX II (continued)

(iv) *trans*-$C_2D_2H_2S$: Eigenvectors[b]

```
FREQUENCY =3067.0 CM-1
-0.0583 -0.0255 -0.0255 -0.0502  0.7321  0.7321 -0.0502 -0.0513 -0.0513  0.0653
-0.0342 -0.0342  0.0653  C.1205 -0.C782 -0.0782  0.1205  0.0113  0.0113 -0.0227
FREQUENCY =2270.2 CM-1
 0.1059  0.0449  0.0449 -0.5332 -0.0341 -0.0341 -0.5332  0.1273  0.1273  0.0329
-0.1094 -0.1094  0.0329  0.0812 -0.1906 -0.1906  0.0812 -0.0209 -0.0209  0.0419
FREQUENCY =1338.3 CM-1
 0.1751  0.0599  0.0599  0.0462  0.0084  0.0084  0.0462  0.8037  0.8037 -0.1592
-0.4742 -0.4742 -0.1592 -0.1435 -0.4810 -0.4810 -0.1435 -0.0381 -0.0381  0.0762
FREQUENCY =1118.8 CM-1
 0.2863  0.0994  0.0994  0.0052  0.0227  0.0227  0.0052 -0.0462 -0.0462 -0.1162
 0.1551  0.1551 -0.1162 -0.2905  0.3611  0.3611 -0.2905 -0.0620 -0.0620  0.1240
FREQUENCY =1026.1 CM-1
-0.1753 -0.0227 -0.0227 -0.0247  0.0017  0.0017 -0.0247  0.0621  0.0621 -0.1992
-0.3250 -0.3250 -0.1992 -C.1148  0.4168  0.4168 -0.1148  0.0473  0.0473 -0.0946
FREQUENCY = 876.5 CM-1
 0.0431  0.0580  0.0580  0.0189 -0.0047 -0.0047  0.0189 -0.2593 -0.2593  0.1793
-0.3085 -0.3085  0.1793  0.4519  0.0218  0.0218  0.4519  0.0012  0.0012 -0.0024
FREQUENCY = 698.7 CM-1
-0.0485  0.1025  0.1025  0.0010  0.0008  0.0008  0.0010  0.0291  0.0291 -C.4023
 0.1302  0.1302 -0.4023  0.1292  0.0234  0.0234  0.1292  0.0396  0.0396 -0.0793
FREQUENCY = 616.7 CM-1
 0.0669 -0.1931 -0.1931 -0.0007 -0.0008 -0.0008 -0.0007 -0.0763 -0.0763 -0.0526
 0.1199  0.1199 -0.0526  0.0742  0.0199  0.0199  0.0742 -0.0673 -0.0673  0.1346
FREQUENCY =3058.8 CM-1
 0.0    -0.0238  0.0238  0.0497 -0.7324  0.7324 -0.0497  0.0512 -0.0512 -0.0628
 0.0324 -0.0324  0.0628 -0.0377  0.0054 -0.0054  0.0377 -0.0296  0.0296  0.0
FREQUENCY =2248.9 CM-1
 0.0    -0.0397  0.0397 -0.5355 -0.0337  0.0337  0.5355  0.1053 -0.1053  0.0301
-0.1011  0.1011 -0.0301 -0.0007 -0.0654  0.0654  0.0007 -0.0493  0.0493  0.0
FREQUENCY =1288.7 CM-1
 0.0    -0.0654  0.0654  0.0238  0.0060 -0.0060 -0.0238  0.7992 -0.7992 -0.2165
-0.5587  0.5587  0.2165 -C.1301 -0.3503  0.3503  0.1301 -0.0813  0.0813  0.0
FREQUENCY =1000.9 CM-1
 0.0     0.0174 -0.0174  0.0020  0.0038 -0.0038 -0.0020  0.2788 -0.2788  0.0441
 0.3148 -0.3148 -0.0441 -0.1968 -0.5009  0.5009  0.1968  0.0216 -0.0216  0.0
FREQUENCY = 784.8 CM-1
 0.0     0.0799 -0.0799  0.0055 -0.0061  0.0061 -0.0055 -0.0480  0.0480  0.4729
-0.2710  0.2710 -0.4729  0.0311 -0.1799  0.1799 -0.0311  0.0993 -0.0993  0.0
FREQUENCY = 659.1 CM-1
 0.0     0.0347 -0.0347 -0.0013 -0.0024  0.0024  0.0013 -0.1005  0.1005 -0.0033
-0.0585  0.0585  0.0033  0.4204 -0.2518  0.2518 -0.4204  0.0431 -0.0431  0.0
FREQUENCY = 618.2 CM-1
 0.0     0.1803 -0.1803 -0.0080 -0.0021  0.0021  0.0080  0.0459 -0.0459 -0.1114
 0.0624 -0.0624  0.1114 -0.1592  0.0047 -0.0047  0.1592  0.2240 -0.2240  0.0
```

APPENDIX III

POTENTIAL ENERGY DISTRIBUTIONS FOR C_2H_4S, C_2D_4S, *cis*-$C_2D_2H_2S$ AND *trans*-$C_2D_2H_2S$ AMONG THE DIAGONAL ELEMENTS OF THE SYMMETRIZED $\underset{\sim}{F}$ MATRIX

The entries in the following tables for C_2H_4S and C_2D_4S are listed, under each frequency, in the order of the symmetry coordinates listed in Table 6 with the exception that certain symmetry coordinates, S_i, were re-defined to yield the symmetry coordinates, S_i', as shown below.

$$S_4' = \frac{1}{\sqrt{6}} \left\{ 2S_4 + S_5 + S_6 \right\} \quad \text{(redundant)}$$

$$S_5' = \frac{1}{\sqrt{6}} \left\{ 2S_4 - S_5 - S_6 \right\} \quad (CH_2 \text{ deformation})$$

$$S_6' = \frac{1}{\sqrt{2}} \left\{ S_5 - S_6 \right\} \quad (CH_2 \text{ wag})$$

$$S_{10}' = \frac{1}{\sqrt{2}} \left\{ S_{10} + S_{11} \right\} \quad (CH_2 \text{ rock})$$

$$S_{11}' = \frac{1}{\sqrt{2}} \left\{ S_{10} - S_{11} \right\} \quad (CH_2 \text{ twist})$$

$$S_{14}' = \frac{1}{\sqrt{6}} \left\{ 2S_{14} + S_{15} + S_{16} \right\} \quad \text{(redundant)}$$

$$S_{15}' = \frac{1}{\sqrt{6}} \left\{ 2S_{14} - S_{15} - S_{16} \right\} \quad (CH_2 \text{ deformation})$$

$$S_{16}' = \frac{1}{\sqrt{2}} \left\{ S_{15} - S_{16} \right\} \quad (CH_2 \text{ wag})$$

$$S_{19}' = \frac{1}{\sqrt{2}} \left\{ S_{19} + S_{20} \right\} \quad (CH_2 \text{ rock})$$

$$S_{20}' = \frac{1}{\sqrt{2}} \left\{ S_{19} - S_{20} \right\} \quad (CH_2 \text{ twist})$$

Appendix III (continued)

The entries in the tables for cis-$C_2D_2H_2S$ and trans-$C_2D_2H_2S$ are listed, under each frequency, in the order of the symmetry coordinates listed in Tables 7 and 8, respectively.

(i) C_2H_4S

```
FREQUENCY =3018.5 CM-1
 0.0073  0.0015  0.9906  0.0000  0.0015  0.0000  0.0000  0.0     0.0     0.0
 0.0     0.0     0.0     0.0     0.0     0.0     0.0     0.0     0.0     0.0
FREQUENCY =1466.0 CM-1
 0.0828  0.0111  0.0032  0.0097  0.7112  0.0022  0.0005  0.0     0.0     0.0
 0.0     0.0     0.0     0.0     0.0     0.0     0.0     0.0     0.0     0.0
FREQUENCY =1107.1 CM-1
 0.8562  0.0904  0.0061  0.0002  0.0180  0.0447  0.0054  0.0     0.0     0.0
 0.0     0.0     0.0     0.0     0.0     0.0     0.0     0.0     0.0     0.0
FREQUENCY =1023.5 CM-1
 0.0059  0.0150  0.0000  0.0063  0.0348  1.0583  0.0003  0.0     0.0     0.0
 0.0     0.0     0.0     0.0     0.0     0.0     0.0     0.0     0.0     0.0
FREQUENCY = 633.3 CM-1
 0.1296  1.0231  0.0001  0.0004  0.0364  0.0398  0.0155  0.0     0.0     0.0
 0.0     0.0     0.0     0.0     0.0     0.0     0.0     0.0     0.0     0.0
FREQUENCY =3109.2 CM-1
 0.0     0.0     0.0     0.0     0.0     0.0     0.0     0.0     0.9919  0.0064
 0.0012  0.0     0.0     0.0     0.0     0.0     0.0     0.0     0.0     0.0
FREQUENCY =1160.2 CM-1
 0.0     0.0     0.0     0.0     0.0     0.0     0.0     0.0     0.0080  0.7272
 0.2091  0.0     0.0     0.0     0.0     0.0     0.0     0.0     0.0     0.0
FREQUENCY = 890.2 CM-1
 0.0     0.0     0.0     0.0     0.0     0.0     0.0     0.0     0.0000  0.2715
 0.7948  0.0     0.0     0.0     0.0     0.0     0.0     0.0     0.0     0.0
FREQUENCY =3010.4 CM-1
 0.0     0.0     0.0     0.0     0.0     0.0     0.0     0.0     0.0     0.0
 0.0     0.0013  0.9971  0.0001  0.0010  0.0000  0.0002  0.0     0.0     0.0
FREQUENCY =1431.9 CM-1
 0.0     0.0     0.0     0.0     0.0     0.0     0.0     0.0     0.0     0.0
 0.0     0.0149  0.0015  0.0090  0.6438  0.0289  0.0028  0.0     0.0     0.0
FREQUENCY =1060.2 CM-1
 0.0     0.0     0.0     0.0     0.0     0.0     0.0     0.0     0.0     0.0
 0.0     0.0041  0.0002  0.0061  0.0854  1.0147  0.0008  0.0     0.0     0.0
FREQUENCY = 645.9 CM-1
 0.0     0.0     0.0     0.0     0.0     0.0     0.0     0.0     0.0     0.0
 0.0     0.8382  0.0012  0.0058  0.0068  0.0374  0.1585  0.0     0.0     0.0
FREQUENCY =3100.6 CM-1
 0.0     0.0     0.0     0.0     0.0     0.0     0.0     0.0     0.0     0.0
 0.0     0.0     0.0     0.0     0.0     0.0     0.0     0.9984  0.0012  0.0303
FREQUENCY = 947.1 CM-1
 0.0     0.0     0.0     0.0     0.0     0.0     0.0     0.0     0.0     0.0
 0.0     0.0     0.0     0.0     0.0     0.0     0.0     0.0014  0.3966  0.5333
FREQUENCY = 820.5 CM-1
 0.0     0.0     0.0     0.0     0.0     0.0     0.0     0.0     0.0     0.0
 0.0     0.0     0.0     0.0     0.0     0.0     0.0     0.0002  0.6078  0.4720
```

APPENDIX III (continued)

(ii) C_2D_4S

```
FREQUENCY =2210.5 CM-1
 0.0385   0.0067   0.9553   0.0002   0.0066   0.0003   0.0002   0.0      0.0      0.0
 0.0      0.0      0.0      0.0      0.0      0.0      0.0      0.0      0.0      0.0
FREQUENCY =1188.8 CM-1
 0.5834   0.0648   0.0399   0.0076   0.3551   0.0081   0.0036   0.0      0.0      0.0
 0.0      0.0      0.0      0.0      0.0      0.0      0.0      0.0      0.0      0.0
FREQUENCY = 949.4 CM-1
 0.3423   0.0203   0.0042   0.0015   0.3530   0.0851   0.0025   0.0      0.0      0.0
 0.0      0.0      0.0      0.0      0.0      0.0      0.0      0.0      0.0      0.0
FREQUENCY = 764.3 CM-1
 0.0166   0.1951   0.0008   0.0073   0.0291   1.0363   0.0026   0.0      0.0      0.0
 0.0      0.0      0.0      0.0      0.0      0.0      0.0      0.0      0.0      0.0
FREQUENCY = 610.1 CM-1
 0.1039   0.8543   0.0001   0.0000   0.0577   0.0154   0.0128   0.0      0.0      0.0
 0.0      0.0      0.0      0.0      0.0      0.0      0.0      0.0      0.0      0.0
FREQUENCY =2333.4 CM-1
 0.0      0.0      0.0      0.0      0.0      0.0      0.0      0.0      0.9731   0.0216
 0.0040   0.0      0.0      0.0      0.0      0.0      0.0      0.0      0.0      0.0
FREQUENCY = 822.0 CM-1
 0.0      0.0      0.0      0.0      0.0      0.0      0.0      0.0      0.0269   0.7412
 0.1798   0.0      0.0      0.0      0.0      0.0      0.0      0.0      0.0      0.0
FREQUENCY = 630.3 CM-1
 0.0      0.0      0.0      0.0      0.0      0.0      0.0      0.0      0.0001   0.2424
 0.0213   0.0      0.0      0.0      0.0      0.0      0.0      0.0      0.0      0.0
FREQUENCY =2184.8 CM-1
 0.0      0.0      0.0      0.0      0.0      0.0      0.0      0.0      0.0      0.0
 0.0      0.0052   0.9885   0.0002   0.0041   0.0000   0.0010   0.0      0.0      0.0
FREQUENCY =1066.6 CM-1
 0.0      0.0      0.0      0.0      0.0      0.0      0.0      0.0      0.0      0.0
 0.0      0.0662   0.0073   0.0102   0.5860   0.0580   0.0124   0.0      0.0      0.0
FREQUENCY = 827.9 CM-1
 0.0      0.0      0.0      0.0      0.0      0.0      0.0      0.0      0.0      0.0
 0.0      0.0190   0.0006   0.0058   0.1179   1.0181   0.0035   0.0      0.0      0.0
FREQUENCY = 607.0 CM-1
 0.0      0.0      0.0      0.0      0.0      0.0      0.0      0.0      0.0      0.0
 0.0      0.7680   0.0037   0.0046   0.0291   0.0049   0.1436   0.0      0.0      0.0
FREQUENCY =2312.1 CM-1
 0.0      0.0      0.0      0.0      0.0      0.0      0.0      0.0      0.0      0.0
 0.0      0.0      0.0      0.0      0.0      0.0      0.0      0.9949   0.0038   0.0010
FREQUENCY = 707.4 CM-1
 0.0      0.0      0.0      0.0      0.0      0.0      0.0      0.0      0.0      0.0
 0.0      0.0      0.0      0.0      0.0      0.0      0.0      0.0047   0.4718   0.4543
FREQUENCY = 584.3 CM-1
 0.0      0.0      0.0      0.0      0.0      0.0      0.0      0.0      0.0      0.0
 0.0      0.0      0.0      0.0      0.0      0.0      0.0      0.0004   0.5300   0.5503
```

APPENDIX III (continued)

(iii) cis-$C_2D_2H_2S$

```
FREQUENCY =3062.1 CM-1
 0.0030  0.0006  0.9920  0.0039  0.0009  0.0002  0.0008  0.0000  0.0003  0.0000
 0.0     0.0     0.0     0.0     0.0     0.0     0.0     0.0     0.0     0.0
FREQUENCY =2259.1 CM-1
 0.0179  0.0034  0.0025  0.9705  0.0072  0.0041  0.0003  0.0014  0.0001  0.0001
 0.0     0.0     0.0     0.0     0.0     0.0     0.0     0.0     0.0     0.0
FREQUENCY =1329.1 CM-1
 0.1704  0.0214  0.0017  0.0145  0.9741  0.2393  0.0383  0.1082  0.0270  0.0010
 0.0     0.0     0.0     0.0     0.0     0.0     0.0     0.0     0.0     0.0
FREQUENCY =1080.0 CM-1
 0.7449  0.0697  0.0032  0.0075  0.0448  0.1592  0.0012  0.0041  0.0074  0.0049
 0.0     0.0     0.0     0.0     0.0     0.0     0.0     0.0     0.0     0.0
FREQUENCY = 967.5 CM-1
 0.0004  0.0233  0.0000  0.0009  0.1046  0.2442  0.0013  0.2479  0.0150  0.0001
 0.0     0.0     0.0     0.0     0.0     0.0     0.0     0.0     0.0     0.0
FREQUENCY = 760.2 CM-1
 0.0325  0.0297  0.0005  0.0020  0.0252  0.1508  0.8393  0.0533  0.0063  0.0012
 0.0     0.0     0.0     0.0     0.0     0.0     0.0     0.0     0.0     0.0
FREQUENCY = 657.6 CM-1
 0.0317  0.4135  0.0000  0.0006  0.0101  0.0788  0.0000  0.1184  0.3234  0.0054
 0.0     0.0     0.0     0.0     0.0     0.0     0.0     0.0     0.0     0.0
FREQUENCY = 608.2 CM-1
 0.0809  0.5797  0.0000  0.0000  0.0845  0.0067  0.0021  0.0312  0.1850  0.0090
 0.0     0.0     0.0     0.0     0.0     0.0     0.0     0.0     0.0     0.0
FREQUENCY =3063.7 CM-1
 0.0     0.0     0.0     0.0     0.0     0.0     0.0     0.0     0.0     0.0
 0.0     0.00[illegible]  0.9896  0.0054  0.0006  0.0003  0.0009  0.0009  0.0016  0.0001
FREQUENCY =2257.4 CM-1
 0.0     0.0     0.0     0.0     0.0     0.0     0.0     0.0     0.0     0.0
 0.0     0.0026  0.0057  0.9700  0.0068  0.0044  0.0005  0.0074  0.0023  0.0005
FREQUENCY =1302.7 CM-1
 0.0     0.0     0.0     0.0     0.0     0.0     0.0     0.0     0.0     0.0
 0.0     0.0176  0.0000  0.0122  0.5695  0.3508  0.0367  0.1451  0.0021  0.0033
FREQUENCY =1068.1 CM-1
 0.0     0.0     0.0     0.0     0.0     0.0     0.0     0.0     0.0     0.0
 0.0     0.0138  0.0018  0.0076  0.0002  0.0634  0.1084  0.3564  0.0367  0.0026
FREQUENCY = 917.8 CM-1
 0.0     0.0     0.0     0.0     0.0     0.0     0.0     0.0     0.0     0.0
 0.0     0.0034  0.0026  0.0021  0.3290  0.2227  0.0679  0.0014  0.4000  0.0006
FREQUENCY = 719.2 CM-1
 0.0     0.0     0.0     0.0     0.0     0.0     0.0     0.0     0.0     0.0
 0.0     0.1347  0.0001  0.0003  0.0020  0.1531  0.5048  0.0050  0.0725  0.0251
FREQUENCY = 615.8 CM-1
 0.0     0.0     0.0     0.0     0.0     0.0     0.0     0.0     0.0     0.0
 0.0     0.6859  0.0003  0.0024  0.0045  0.0255  0.1036  0.0080  0.0090  0.1280
```

APPENDIX III (continued)

(iv) trans-$C_2D_2H_2S$

```
FREQUENCY =3067.0 CM-1
 0.0029  0.0006  0.0047  0.9877  0.0007  0.0099  0.0002  0.0022  0.0009  0.0000
 0.0     0.0     0.0     0.0     0.0     0.0     0.0     0.0     0.0     0.0
FREQUENCY =2270.2 CM-1
 0.0176  0.0033  0.9562  0.0039  0.0083  0.0004  0.0045  0.0018  0.0100  0.0001
 0.0     0.0     0.0     0.0     0.0     0.0     0.0     0.0     0.0     0.0
FREQUENCY =1338.3 CM-1
 0.1389  0.0170  0.0206  0.0007  0.9521  0.0277  0.2458  0.0163  0.1027  0.0008
 0.0     0.0     0.0     0.0     0.0     0.0     0.0     0.0     0.0     0.0
FREQUENCY =1118.8 CM-1
 0.5313  0.0668  0.0004  0.0071  0.0045  0.0211  0.0376  0.0954  0.1474  0.0031
 0.0     0.0     0.0     0.0     0.0     0.0     0.0     0.0     0.0     0.0
FREQUENCY =1026.1 CM-1
 0.2369  0.0041  0.0101  0.0000  0.0097  0.0738  0.1964  0.0177  0.2335  0.0022
 0.0     0.0     0.0     0.0     0.0     0.0     0.0     0.0     0.0     0.0
FREQUENCY = 876.5 CM-1
 0.0196  0.0371  0.0081  0.0005  0.2311  0.0819  0.2425  0.3762  0.0009  0.0000
 0.0     0.0     0.0     0.0     0.0     0.0     0.0     0.0     0.0     0.0
FREQUENCY = 698.7 CM-1
 0.0391  0.1822  0.0000  0.0000  0.0046  0.6489  0.0680  0.0484  0.0016  0.0033
 0.0     0.0     0.0     0.0     0.0     0.0     0.0     0.0     0.0     0.0
FREQUENCY = 616.7 CM-1
 0.0954  0.8301  0.0000  0.0000  0.0404  0.0143  0.0740  0.0205  0.0015  0.0122
 0.0     0.0     0.0     0.0     0.0     0.0     0.0     0.0     0.0     0.0
FREQUENCY =3058.8 CM-1
 0.0     0.0     0.0     0.0     0.0     0.0     0.0     0.0     0.0     0.0
 0.0     0.0005  0.0046  0.9940  0.0007  0.0008  0.0002  0.0001  0.0000  0.0001
FREQUENCY =2245.9 CM-1
 0.0     0.0     0.0     0.0     0.0     0.0     0.0     0.0     0.0     0.0
 0.0     0.0026  0.9856  0.0039  0.0058  0.0004  0.0040  0.0000  0.0008  0.0005
FREQUENCY =1288.7 CM-1
 0.0     0.0     0.0     0.0     0.0     0.0     0.0     0.0     0.0     0.0
 0.0     0.0218  0.0059  0.0004  1.0154  0.0553  0.3679  0.0094  0.0682  0.0041
FREQUENCY =1000.9 CM-1
 0.0     0.0     0.0     0.0     0.0     0.0     0.0     0.0     0.0     0.0
 0.0     0.0026  0.0001  0.0002  0.2048  0.0038  0.1936  0.0357  0.2312  0.0005
FREQUENCY = 784.8 CM-1
 0.0     0.0     0.0     0.0     0.0     0.0     0.0     0.0     0.0     0.0
 0.0     0.0878  0.0008  0.0011  0.0099  0.7106  0.2334  0.0014  0.0485  0.0164
FREQUENCY = 659.1 CM-1
 0.0     0.0     0.0     0.0     0.0     0.0     0.0     0.0     0.0     0.0
 0.0     0.0235  0.0001  0.0002  0.0614  0.0000  0.0154  0.3756  0.1347  0.0044
FREQUENCY = 618.2 CM-1
 0.0     0.0     0.0     0.0     0.0     0.0     0.0     0.0     0.0     0.0
 0.0     0.7196  0.0029  0.0002  0.0146  0.0635  0.0199  0.0612  0.0001  0.1343
```

APPENDIX IV

INFRARED SPECTRA OF GASEOUS C_2D_4S, cis-$C_2D_2H_2S$ AND trans-$C_2D_2H_2S$

Preparation and Handling of Samples

The deuterated forms of ethylene sulphide were supplied by Dr. O. P. Strausz of this department. The C_2D_4S was prepared by the reaction of the carbonate ester of 1,1,2,2-ethylene-d_4 glycol (prepared by the method of W. H. Carothers and F. J. Van Natta, J. Amer. Chem. Soc. 52, 314 (1930)) with potassium thiocyanate (S. Searles and E. F. Lutz, J. Amer. Chem. Soc. 80, 3168 (1958)). The product was purified by gas-liquid chromatography using a 10 ft. long 20% tricresyl phosphate column at 46°C, with a helium flow rate of 60 cc/min. Mass spectroscopy of the product indicated that it contained 9% or less of C_2D_3HS.

The *cis*- and *trans*-1,2-dideuterioethylene sulphides were prepared by the photolytic reaction of *cis*- or *trans*-1,2-dideuterioethylene with carbonyl sulphide in the presence of carbon dioxide. The reaction is, with care, stereo-specific (A. Jackson and O. P. Strausz, to be published) but varying amounts of the *cis*-isomer existed as impurities in the *trans*-isomer, and *vice versa*. Except for traces of water and carbon dioxide in some samples, no other impurities were detected.

The infrared spectra were recorded by D. A. Othen of this laboratory on a Beckman IR-12 spectrophotometer, operated at a resolution of about 1 cm^{-1}. The gases were contained in a 9.5 cm. long Pyrex microcell which was fitted with cesium iodide windows and a standard taper, greaseless Teflon stop-cock. The pressure of gas within the cell was not known accurately but was probably between 10 and 60 Torr in all cases.

Appendix IV (continued)

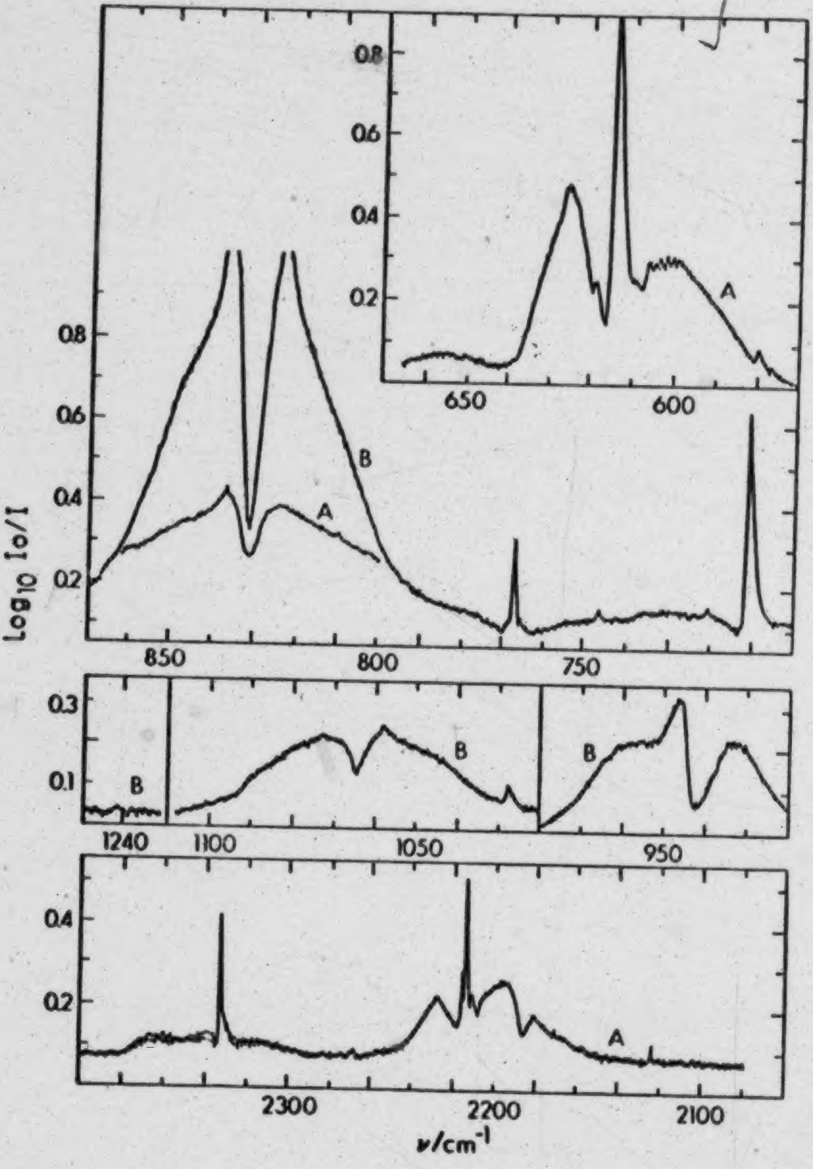

Infrared spectrum of gaseous C_2D_4S at +25°. The curves labelled A show the spectrum of one sample; those labelled B show the spectrum of a second sample. The frequency scale is the same for all spectra below 2000 cm^{-1}.

Appendix IV (continued)

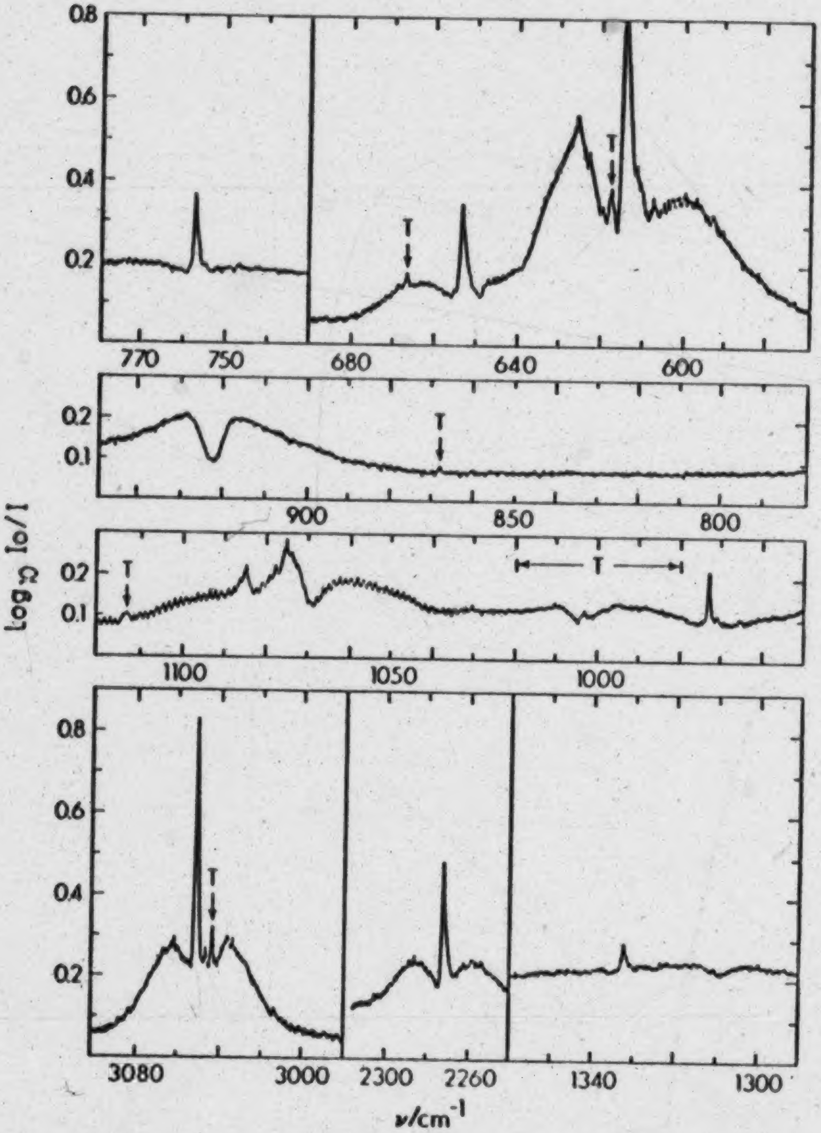

Infrared spectrum of gaseous cis-$C_2D_2H_2S$ at +25°C. All curves show the spectrum of a single sample. The features labelled T arise from trans-$C_2D_2H_2S$ which was present as an impurity.

Appendix IV (continued)

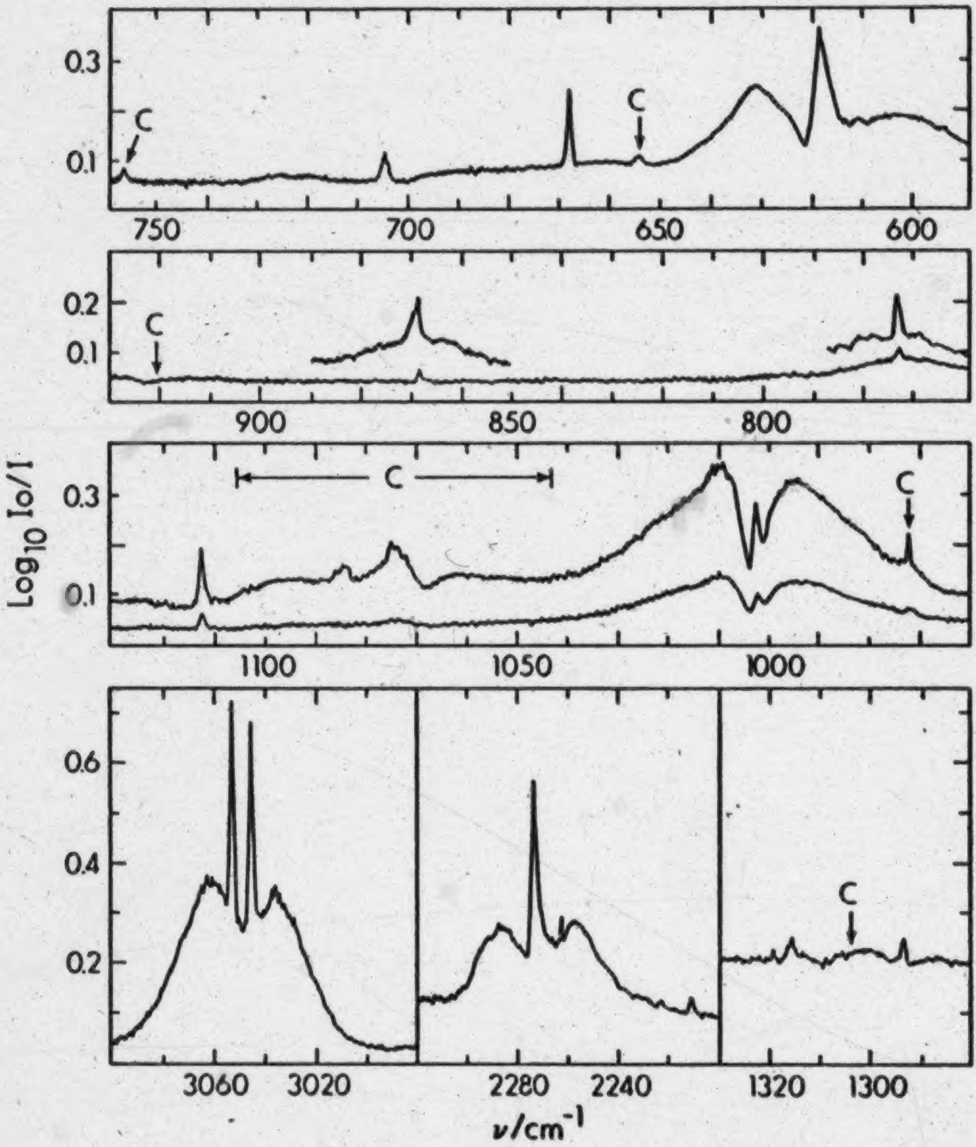

Infrared spectrum of gaseous trans-$C_2D_2H_2S$ at +25°C. The bottom curves in the upper three boxes show the spectrum of one sample and the other curves show the spectrum of a second sample. The features labelled C arise from cis-$C_2D_2H_2S$ which was present as an impurity.